UNIVERSITÀ DEGLI STUDI DI
CASSINO E DEL LAZIO MERIDIONALE

Corso di Dottorato in
Metodi, Modelli e Tecnologie per l'Ingegneria
Curriculum: Ingegneria Elettrica
Ciclo XXXVI

Design methodologies of modular active equalization circuits for lithium-ion battery packs

SSD: ING/IND-32

Supervisor
Prof. Giuseppe Tomasso

Ph.D. Student
Emanuele Di fazio

Coordinator
Prof. Fabrizio Marignetti

January 2024

UNIVERSITÀ DEGLI STUDI DI
CASSINO E DEL LAZIO MERIDIONALE

Date: **January 2024**

Author: **Emanuele Di Fazio**

Title: **Design methodologies of modular active equalization circuits for lithium-ion battery packs**

Department: **Dipartimento di Ingegneria Elettrica e dell'Informazione "M. Scarano"**

Degree: **PHILOSOPHIAE DOCTOR**

To whom support me every day.

Acknowledgements

Foremost, I would like to express my sincere gratitude to the team of the Laboratory of Industrial Automation of University of Cassino and Southern Lazio. A special mention to Prof. Giuseppe Tomasso, who has belived in my capability giving me the opportunity for a personal and professional growth. Moreover, many thanks to Dr. Mauro Di Monaco for the help, the support and the encouragement he gave me. I especially want to thank Dr. Francesco Porpora, he has represented a mentor for me during this overall experience. He has been by my side in difficult moment trying to giving me serenity by means the right words in the right moments. He represents for me not just a colleague but also a friend.

Another special mention goes to Dr. Matilde D'arpino, who gave me the opportunity to study at The Ohio State University - Center for Automotive Research. She also have supported me during my period in the USA, representing a precious guide to me, transmitting the knowledge and her enthusiasm. I would also like to thank all the people I have met on this journey, those who have helped me through difficult times and those who have brought me serenity and joy. Additional thanks go to my family who have always supported me. Last but not least, my girlfriend Lucrezia. I thank you for always trying to bring me back to the right path through your sometimes stern ways but hiding the non-acceptance of seeing me fail, you are special.

Contents

Introduction

The research activity described in this work of thesis finds its motivation in the higher and higher adoption of lithium-ion batteries, representing one of the fastest-developing technologies. Indeed, they present a great enhancement with respect to the other electrochemical system technologies available on the market nowadays, in terms of energy density, power density, charging and discharging current profiles and useful lifetime. However, lithium-ion batteries are not inherently safe if they operate outside a certain range of terminal voltage and temperature, which leads severe safety risks for the application and operator that use it. Moreover, this battery technology is characterized by degradation mechanisms which cause performance. Therefore, the battery packs based on lithium-ion technology rely on battery management systems (BMS) for ensuring safety and optimize performances, prolonging lifetime. BMS addresses safety and optimization tasks through several requirements and functionalities, which are detailed illustrated in chapter 2. Among them, two issues in particular were explored in depth in this dissertation, namely online prediction of power limits and unbalance between different cells connected in series. The first task involved the study of the methodologies currently adopted in the commercial application and in the literature for defining instant-by-instant the maximum power that a battery pack can safely deliver or receive continuously in a predefined future time horizon. Specifically, among the various methods proposed in the literature, an in-depth comparison of map-based and model-based approaches was made, highlighting the benefits and drawbacks. In addition, some experimental tests were carried out for a greater understanding of the phenomena that produce a major impact on limit estimation. On the other hand, the topic of cell imbalance has been addressed systematically and describes most of the original contribution contained in this thesis work. The causes and effects of imbalance have been described in detail. In addition, current application solutions in the literature have been reported. Two architectures for performing active balancing have been investigated. The mathematical model has been developed for both of them, including parameters related to the parasitic effects and nonlinearities that

the real system presents, in order to propose a design strategy for such architectures. In fact, a lack of design strategies directed at optimizing the balancing currents with respect to the real parameters of the architectures has been found in the literature. An experimental prototype was developed according to the proposed design strategies in order to verify the accuracy of the design strategy and evaluate the performance of the prototype for different unbalance conditions in the considered battery pack.

Therefore, this dissertation is organized in five chapters. The first one introduce the lithium-ion battery technology, including the architecture of the cell in their components, the shapes commercially available ant the working principle. A large overview of the anode and cathode materials is also reported with a brief mention of those materials which promise a further improvement in safety, lifetime and energy density. Battery pack architecture section include the principle and the best practices which are used to scale from the cell level to the pack level. The most common model approaches in lithium-ion battery and degradation mechanisms have been also included in the first chapter.

The second one, contain the description of the all requirements and functionalities the BMS implements, encompassing details related to the monitoring and measurement, safety and protection, state estimation, performance optimization and communication. Chapter 3 gives an overview on the algorithm, currently proposed in literature, for the state estimation, that is SoC, SoH and SoP. Regarding the latter more details have been included, with a mathematical description of the model based method with numerical and experimental results. The chapter 4 provides a wide description of the solution currently available for accounting the imbalance issue. Both passive and active architectures are reported highlighting the pros and cons of each architecture, in terms of energy transfer and components included.

The final chapter deal with the two case studies ofactive equalization system for whom a model-based design methodology have been proposed.

Chapter 1

Lithium-ion Battery Packs

The demand for electrical energy storage is rising across a variety of industries, contexts, and scales as a result of the expanding significance of electricity as an energy carrier in decarbonizing economies. In this contest, lithium-ion batteries has been playing the key role of enabling technology for the large adoption of energy storage systems. Several application fields are benefiting of this technology due to their improved features with respect to the other battery chemistries. Indeed, for instance, lithium-ion batteries have enabled the electrification of mobility allowing to develop electric vehicles that can compete with traditional ones on the market, at least in terms of driving range, comfort and performance. The single cell is limited in energy but it can be used as a building block, thus connecting multiple cells in series and parallel it is possible to meet the requirement of the specific application. In this chapter, all the aspect that involve this battery technology will be discussed. In particular, the first part is focused on the operating principle and the architecture of the non-reducible unit will. Then, all the concern and issues related to develop the battery pack. The last part of the chapter gives an overview of the battery modelling approaches, the degradation mechanisms and a general overview of the specific field of application of the lithium-ion batteries.

1.1 Motivation for lithium-ion batteries

Lithium-ion batteries' (LIBs) high performance in terms of energy density, power capability, cycle life, and durability have made this electrochemical storage technology particularly appealing for transportation and grid-connected applications. Lithium-ion cells, in particular, have enabled the development of electric and hybrid vehicles with significant driving

range and performance, the optimal energy usage of the production uncertainty of renewable energy sources (RESs), and the implementation of several critical grid management services, such as load leveling and backup power systems. Indeed, compared to the other chemistries available so far, lithium-ion cells offer several advantages:

- The presence of lithium ion allow the cell to operate at much higher voltage, typically about 3.7 V, with respect to 1.2 V that characterize NiMH (Nickel Metal Hydride) or NiCd (Nickel Cadmium) cells. This allows to use less electrochemical unit for the applications with a specific voltage requirements and means more energy and power density compared to the similar capacity NiCd and NiMH cells.

- Lithium-ion cells also have a lower self-discharge rate than other types of rechargeable cells. Unlike NiMH and NiCd cells, that can lose anywhere from 1-5% of their charge per day, even if they are not installed, lithium-ion cells will retain most of their charge even after months of storage.

On the other hand, lithium-ion battery are more expensive than the other electrochemical storage technology available on the market and present several safety issue. The first one is mainly due to the supply chain of raw material and the production volume of the manufacturer, and it is expected that will come down during the next few years because the large demand of lithium-ion batteries. Conversely, the second one brings to the integration of safety devices and an appropriate control board that ensure the batteries to operate in the safety operating area. The need for a Battery Management Systems (BMS) also impact on the cost and the complexity of the design for a battery pack.

1.2 Definitions

Descriptions of the main characteristics associated with electrochemical energy storage systems are outlined in this section. The terminology introduced will be used in the following paragraphs.This type of knowledge is useful for developing cells, selecting cells to utilize in an application, and understanding how to use cells correctly in an application.

- **Energy Density**

  This feature represent the amount of energy stored in a specific amount of battery material. It is possible to distinguish between gravimetric energy density (Wh/kg) and volumetric energy density (Wh/L),

depending on whether it is normalized to the mass or the volume of the battery, respectively. Considering the design of a battery pack for an electric vehicle, energy density impact on the weight and handling of the vehicle itself, in terms of driving comfort, stability, energy consumption and the design of the vehicle. moreover, this parameter gains much importance for either pure EV or PHEV because the energy density controls the vehicle range.

- **Power Density**

  The power density represent the maximum electrical power that can be supplied, in input and output, of the battery per unit of mass (W/kg). It is very important to rate the performance of EV and PHEV. However, power density is critically important in HEV because it affects the regeneration capability as well as short bursts of electric assists such as vehicle launch and passing power.

- **Terminal Voltage**

  This is the measured voltage difference between the terminals of the cell. It varies with the operating condition in terms of load applied and temperature.

- **Open Circuit Voltage**

  The open circuit voltage (OCV) is defined as the difference between the terminals of the cell when it is fully rested, namely the cell has been subjected to zero current over an extended period of time. This amount of time depends on both the cell chemistry and the charging/discharging current profile applied before the rest period. Indeed, the open circuit voltage is related to the internal electrochemical equilibrium of the cell. Moreover, it is hard to measure the actual open circuit voltage because the usual voltage meters introduce a low-amplitude current to measure the voltage. In general, the OCV depends on the charging level of the cell and temperature.

- **Internal resistance**

  This refers to the overall resistance that the battery encounter when current flows through it. Cell internal resistance includes ohmic and polarization resistance. The former follows the Ohm's law and is related to the materials that compose the cell and the contacts between them, whereas the latter is caused by the electrochemical polarization and concentration polarization to the passage of current. Hence, the internal resistance varies continuously during charging and discharging processes depending on the amplitude and sign of the current as

well as the temperature. The bigger internal resistance, the lower battery efficiency and thermal stability due to a large amount of energy is converted into heat.

- **Capacity**

  The battery capacity (C) is referred to the amount of electric energy, in Ampére-hours (Ah) or milliAmpére-hours (mAh), that a cell can provide under specific operating condition in terms of current and temperature within a certain range of terminal voltage. It is possible to make a classification between rated capacity, theoretical capacity and actual capacity:

  - *Rated capacity*: this is the capacity that suppliers indicate in the datasheets of the cell and it is referred to the total amount of charge that the cell can provide in a fully discharging process under specific condition. The value of the capacity is measured by integrating the current in time, during the process in which the terminal voltage decreases from the maximum to the minimum values defined by the manufacturer. The rated capacity is usually measured at very low constant current and an operating temperature of 25°C.
  - *Theoretical capacity*: this is referred to the value of charge considering the mass and the properties of the active material during the battery design.
  - *Actual capacity*: the actual value of the amount of electric energy that the cell can provide under specific operating conditions even considering the aging.

  Moreover, the nominal capacity can be expressed as energy (kWh) by multiplying the nominal capacity to the nominal voltage.

- **State of Charge**

  The State of Charge (SoC) represent the amount of charge at given time stored in a cell with respect to the rated capacity. It is a dimensionless parameter, usually expressed as a percentage, and it's not possible to directly measure. In laboratory condition, it is computed by integrating amount of the Coulombic charge flowing through the battery. In the real applications, the measurement uncertainties strongly affect the real value of the SoC, then state observed and filters need to be implemented for better estimating the State of Charge. More details related to the SoC estimation methods will be illustrated

in section 3.1. The depth of discharge (DoD) is the SoC's complement to the rated capacity and expresses the amount of battery capacity discharged.

- **State of Health**

  This parameter indicates indicates the condition of the battery compared to its ideal ones. The State of Health (SoH) is intrinsically related to the aging mechanisms of the battery and to the operating conditions. As the SoC, the SoH is a parameter that cannot be directly measured because it's not referred to a physical quantity. However, the assessment of SoH takes into account three parameter: battery capacity, internal resistance and self discharge. The state of the art of SoH estimation methods is reported in section 3.2.

- **C-rate**

  The C-rate is a method to normalize the rate of the imposed discharge or charge current with respect to the rated capacity of the battery. Therefore, C-rate gives an indication in time, and it represents the number of hours needed to fully discharge the battery at a certain constant current. It is possible to interpreter as the current value needed to exstract the rated capacity of the cell in a specific time. The manufacturer usually reports how the capacity of the cell varies over different C-rates.

1.3 Cell Architecture

Cell is the atomic electrochemical unit that provide a voltage between the two terminals depending on the combination of the the active material chosen to make it. In order to meet the requirement of the specific application, a certain number of the single unit can be combined together increasing power and energy. Among different chemistry, lithium-ion cells are characterized by several advantages with respect to the the other available electrochemical technology, such as more energy and power density, no memory effect, very low self-discharge and higher open circuit voltage. Lithium-ion cells include a large design flexibility in terms of design format, which allows to be suitable for a large variety of different applications. Another big advantage consist of the possibility to select several combination of materials for the cell components, giving a degree of freedom in order to meet the requirement of the specific application. To better understand what the features just mentioned result from, the following is a

detailed description of the cell's basic components, materials used, shapes, and operating principle.

1.3.1 Components

The individual electrochemical unit is composed by four main components, regardless the shape and materials: anode, cathode, separator and electrolyte.

- *Anode*: the anode is composed by a copper foil coated with the active anode material. It represent the negative electrode and generally it is made by a carbon material, while the copper foil is the negative current collector that allow the connection to the negative voltage terminal. Graphite is the most commonly utilized because of its stability and ideal capacity to retain lithium inside its structure, but graphene and carbon black are also frequent.

- *Cathode*: this is the positive electrode and it's generally realized by an aluminum foil coated with the active positive material. Similarly to the anode, the aluminum foil represents the positive current collector that allow the connection to the positive voltage terminal, whereas the active material is made by a lithium compound that is able to donate lithium ions (Li^+).

- *Separator*: this component is usually a freestanding microporous membrane or polymer that only permits lithium ions to flow through. It is not involved on the electrochemical reaction inside the cell, but it serves as a safety measure to prevent an internal short circuit between the anode and cathode. Indeed, it has characterized by holes large enough to allow the lithium ion to pass through, but small enough to avoid contact between positive and electrode particles. Besides this, a separator must guarantee several mechanical properties, such as appropriate stretching and physical strength, good puncture and compression resistance, and balanced thickness and porosity, due to its importance in avoiding safety issues within the cell.

- *Electrolyte*: the electrolyte is the substance that allow ions to pass from the negative to the positive layer and vice versa. Although solid polimer electrolyte are possible, generally, it is a liquid composed solution of lithium salts, organic solvents and some additives, which are used to improve the electrolyte properties. Since lithium reacts violently with water, the electrolyte in a lithium-ion cell is composed of nonaqueous organic solvents and the use of it is critical for increasing

the mobility of lithium ions. The potential tolerance of the electrolyte fluid is an important feature since it is exposed to the potential difference between the electrodes. The typical salt used in commercial Li-ion batteries is lithium hexafluorophosphate ($LiPF_6$). Propylene carbonate or ethylene carbonate/dimethyl carbonate mixtures are often utilized.

It's important to mention that active materials change its own volume during discharging/charging processes that can potentially cause undesired crack into the electrodes reducing the active material inside the cell. This means fast degradation of the cell and performance reduction in terms of capacity. A polymeric binder is used to improve elastic properties to the electrodes avoiding degradation mechanisms related to the mechanical stability of the active materials.

1.3.2 Manufacturing process and Shapes

The manufacturing process of the cells follows four different phases. The first one consist of the electrode processing in which both anode and cathode are cut into a appropriate sheets starting from a big mother roll. Then, they are dried thoroughly at high temperature and they are ready for the next step. In the second step involves the anode, the separator and the cathode whom are stacked together in order to create the basic structure of the cell, namely the jellyroll. The layers are then connected by tabs and welded. This assembled stack is inserted into either a metal can, a plastic enclosure or a foil-type pouch for protection. In this phase, the cell also gains its final shape. This process needs to be very accurate because a misalignment among the stacked foil may cause a short circuit or increasing the self-discharge rate of the cell. The third step consist of the electrolyte injection. In detail, the cells are moved to a room with a controlled environment where the electrolyte are injected into them. This is the stage where the lithium is introduced into the cell since the pure lithium oxide instantly when exposed to air. The entire assembly is then sealed. This process is also crucial in terms of accuracy in order to avoid loss of electrolyte through evaporation during the lifetime of the cell. During the last phase, the cells are aged to allow the cell chemistry to properly formed. Indeed, several cycle needs to force the salt to release the lithium ions enabling the correct behavior of the cell. During these formation cycles, a stable compound is formed between the electrolyte and the anode as a layer of material that cover the negative electrode surface known as Solid Electrolyte Interface (SEI). The formation of the SEI stabilizes the system and give long life to the lithium ion, even if it results in a reduction in cell

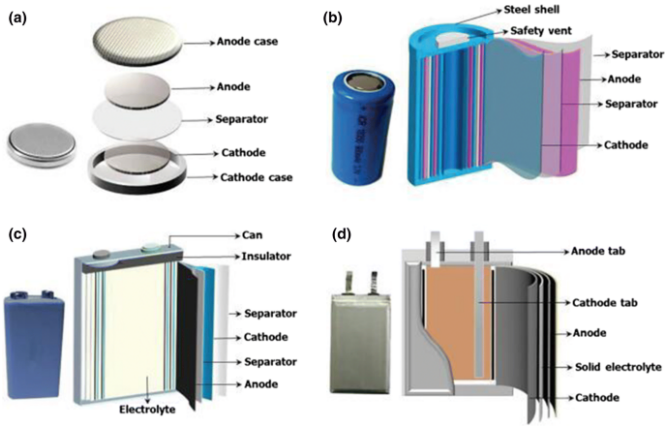

Figure 1.1: Different common shapes of lithium-ion battery cell: (a) button, (b) cylindrical, (c) prismatic and (d) pouch [1].

capacitance and an increase in internal resistance. After the aging step, the cells are charged, then tested to meet the quality standards. Depending on how the jellyroll is processed in the assemble step, four different lithium-ion cell formats are available are available on the market, as illustrated in figure 1.1.

- **Button/coin**

  The button cells, or coin cells, are very small in size and are mainly used for portable devices with limited power and energy demand. Despite being tiny and affordable to manufacture, the stacked button cell went out of popularity and was replaced by more traditional battery types. Indeed, the main drawback is swelling if they are charged too fast, needing many hours to be charged. Moreover, they do not present any safety vent to let out any gases that might be produced in the cell.

- **Cylindrical**

  Cylindrical cell are made by wound the jellyroll on itself and placed inside a cylindrical metal container. Once the liquid electrolyte is inserted, both sides of the jellyroll are sealed with plugs that allow to connect both the current collectors to the cell terminals. Therefore, the cylindrical cells present the terminals on the top and bottom sides of the cylinder. The cylindrical cell is still one of the most popular primary and secondary battery packaging types. The benefits include ease of production and mechanical stability. Without deforming, the

tubular cylinder can bear high internal pressures. A peculiarity of this cell shape with respect to the other ones consist of integrating some safety features into the cell package such as the positive temperature coefficient (PTC) device, current interrupt device (CID), and exhaust or safety vent disk. The first one is a safety device that acts as a short circuit protection increasing the resistance with the temperature rises when a high current pass trough it, whereas the current interrupt device physically and irreversibly disconnect the cell when activated to an unsafe pressure builds up. The typical nomenclature associated to the cylindrical cell is related to the dimensions of the package. Indeed, the most popular cylindrical cells are 18650, that means 18 mm diameter and 65 mm in length. Other different format available on the market include 20700, 21700, 22700 and 26650 which retain higher capacity than the 18650. Among all materials that can be selected for a lithium-ion battery, the 18650 cylindrical cell is usually characterized by a 3 Ah capacity that means a small battery capacity. There are also large-capacity cylindrical cells, however they still presents several issues in safety and aging, most related on the low data to asses the performance of them. Fore these reasons, the typical application for the 18650 cells are electric bicycle, medical equipment and power tools a well as electric vehicles involving a very large number of cells. Even though it is the most popular cell format, cylindrical cells present several issues. First of all, the wound-type architecture involves high internal stress affecting useful lifetime. Moreover, cylindrical shape offer small specific surface area that impact on the heat dissipation of the cell. For these reasons, the design of the cooling system of a cylindrical cell- battery pack is more complex with respect to the other conventional shapes of the lithium-ion batteries. On the other hand, the cylindrical geometry inherently limits the fill factor when multiple cells need to be integrated into a battery pack, regardless any type of external case.

- **Prismatic**

  Prismatic cells are characterized by a robust rectangular enclosure that is usually sealed through a laser welding process after the assembly but before electrolyte filling. The rigid case provides threaded terminal connection and a vent plug. Considering the manufacturing process, they are constructed both in a wound or flat plate configuration. The first process is the same for assembling cylindrical cells, whereas the second one includes to stack layers side by side and either pressed together or folded in a flat plate cell. Prismatic cell are usually characterized by a large capacity, that means a lower number of

parallel-connected cells need to match the capacity requirement than adopting cylindrical cells. Accordingly, a lower number of electrical interconnections is needed with advantages in terms of reliability and design complexity. Moreover, the prismatic shape offer a very big surface area that increase with capacity. This cell format offer simpler solution with respect to the cylindrical one in terms of battery pack integration and thermal management system design. As a consequence, prismatic cells are widely selected for EVs.

- **Pouch**

  The assembly process of the pouch cells consist of stack or fold individual layers, then packed under vacuum and held together by the pouch. Eliminating the metal enclosure reduces weight, but the cell needs support and allowance to expand in the battery compartment. Positive and negative terminals are made by conductive foil tabs that are also welded with the electrodes and brought to the outside in a fully sealed way. They can be placed either on the same side or opposite sides, depending on the manufacturers design. For the lithium-ion cells with terminal at both ends, an extra orientation is required during the assembly process increasing the complexity of the external structure design, wiring and assembly cost. However, terminals on opposite sides allows the tabs to be wider, lowering the total series resistance and increasing the ability to conduct heat from the package. This kind of shape offer simple, flexible and lightweight solution in terms of cell form factors. These characteristics allow the pouch cells to be suitable for a wide range of application ranging from portable electronic devices (low capacity and little space) to electric vehicles (high capacity and medium space). They represent the best battery format considering the packaging efficiency and heat exchange surface area per unit of volume. However, pouch material offer little physical protection resulting vulnerable to handle shock, vibration and nail penetration issues. Moreover, pouch cell are very sensitive to overcharging and overheating conditions because swelling due to the gas released. These gases may expanding the cell causing separation between layers, resulting in internal permanent damages. In order to overcome this, an external structure is required for the module or battery housing to support, restrain, and protect the pouch cell.

1.3.3 Working principle

The purpose of a lithium-ion cell, and battery cells in general, is to store and deliver energy at desired time. This occurs through electrochem-

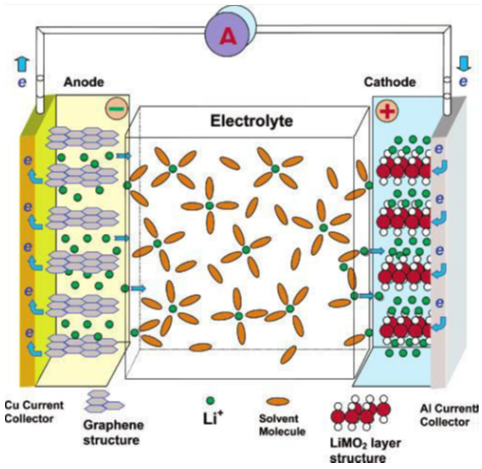

Figure 1.2: Schematic representation of lithium-ion battery cell [2].

ical reactions at the interfaces between each electrode and the electrolyte, consisting of transfer of charge and mass from and to the species involved in the reactions themselves. In particular, considering the discharge process illustrated in figure 1.2, the anode experiences an oxidation reaction which means the anode gives up an electron and a lithium ion. The electron flows to the external circuit towards the cathode whereas the lithium ion released goes to the cathode by means the electrolyte through the separator. At the cathode a reduction reaction occurs allowing the intercalation of the lithium ion in the crystal architecture of the positive electrode. Indeed, the electrolyte provides the available medium for positive-ions movement whereas the separator prevents electron movement within the cell and an external circuit must be connected between the two terminals in order to establish a current. An example of the side reactions that occur during the discharging process are showed in (1.1).

$$\begin{aligned} LiC_6 &\rightarrow Li^+ + e^- + C_6 \\ Li^+ + e^- + CoO_2 &\rightarrow LiCoO_2 \end{aligned} \tag{1.1}$$

The opposite occurs when a voltage potential difference, higher than the cell's own electrical potential, is applied leading a charging process. In this case, the cathode active material releases an electron and a positive charged lithium ion, whereas a reduction reaction involves the anode, as described by (1.2).

Cathode Material	Average potential difference	Specific Capacity
$LiCoO_2$	3.7 V	140 mAh/g
$LiMn_2O_4$	4.0 V	100 mAh/g
$LiNiO_2$	3.5 V	180 mAh/g
$LiFePO_4$	3.3 V	150 mAh/g
$LiCo_{1/3}Ni_{1/3}Mn_{1/3}O_2$	3.6 V	160 mAh/g
$Li(Li_aNi_xMn_yCo_z)O_2$	4.2 V	220 mAh/g

Table 1.1: Average voltage difference and specific capacity of the most adopted cathode materials

$$\begin{aligned} Li^+ + e^- + C_6 &\rightarrow LiC_6 \\ LiCoO_2 &\rightarrow Li^+ + e^- + CoO_2 \end{aligned} \tag{1.2}$$

These reactions describe the basic working principle that allow the cell to store and deliver electric energy to or from an external circuit. The variable that allows electrodes materials to store and release lithium is the electrochemical potential. This is the measure of the chemical amount of energy stored into the battery and it is defined in equilibrium condition that means zero current flows through the cell. Any electrode material can be paired with a reference electrode, whose potential is known and fixed, with the aim to measure the absolute potential. For lithium-ion cells, both electrode potentials are referenced to the $Li^+ + e^- \rightarrow Li$ reaction, also indicated with Li/Li^+. The open circuit voltage, is the result of the difference between the electrochemical potential of each electrodes, also called, open circuit potential. The electrochemical capacity also depends on the cathode and anode materials and it is computed by considering the molecular weights of reactants and the charge moved by reaction. Table 1.1 and table 1.2 report the average potential difference and the specific capacity for the most common materials adopted in lithium-ion cells as cathode and anode, respectively.

The specific capacity is important in the design process in order to select the correct amount of each electrode material needs to be used in the cell, whereas the average voltage difference impact on the choise of the electrolyte. Indeed, the potential tolerance of the electrolyte needs to be high to avoid electrolytic decomposition that cause several aging issue for the cell.

Anode Material	Average potential difference	Specific Capacity
LiC_6	0.1-0.2 V	372 mAh/g
$Li_4Ti_5O_12$	1-2 V	160 mAh/g
$Li_4.4Si$	0.5-1 V	4212 mAh/g
$Li_4.4Ge$	0.7-1.2 V	1624 mAh/g

Table 1.2: Average voltage difference and specific capacity of the most adopted anode materials

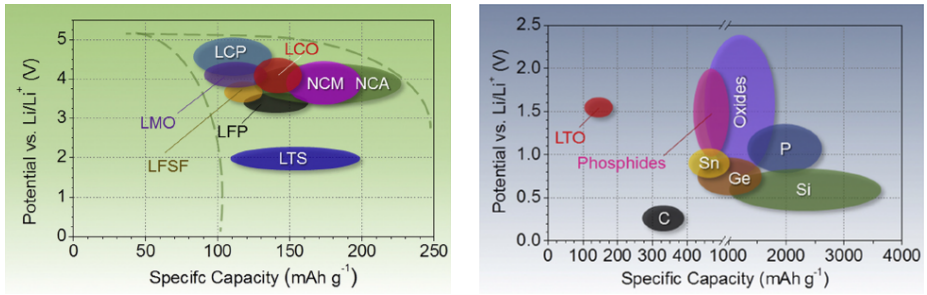

(a) (b)

Figure 1.3: Approximate range of average potential difference to Li/Li^+ and specific capacity of the most common (a) cathodes and (b) anodes materials for lithium-ion batteries [3].

1.3.4 Materials

The selection of the materials for both negative and positive electrodes, as well as the composition of the electrolyte is often referred to the battery chemistry and defines the theoretical open circuit voltage, capacity and power density. Currently, there are numerous chemistries adopted for each component within the cell architecture. Figure 1.3 show the approximate range of average discharge potentials and specific capacity of the most common active suitable materials for the electrodes of a lithium-ion cell.

Each combination of cathode and anode chemistry, electrolyte composition and additives as well as separator type provides a range of performances, safety concerns and challenges. The term "battery chemistry" is most often referred to the choice of cathode material, even because many lithium-ion batteries use a carbon-based anode. However, it is important to note that the choice of both anode and cathode materials, as well as other substances in both electrodes, has significant impact on cell behavior. To be

candidate as active cathode material, it must process the following features:

- High potential compared to the lithium metal potential
- Capability to reversibly insert and release lithium ions without changing in structure
- High lithium-ion diffusivity through its matrix
- good electrical conductivity
- Chemical resistance to solubilization into the elecrolyte

The most common cathode materials currently used are made of lithium transition metal oxides or lithium metal phosphate and their main features are illustrated as follows:

- *Lithium cobalt oxide (LCO)*

  This represent the first solution as lithium-ion cathode for a commercial cell. Introduced by Goodenough [4] in 1980, $LiCoO_2$ (LCO) is still used in the majority of commercial Li-ion batteries due to its technological maturity. Its layered structure allows intercalation and deintercalation of lithium ions when current flows and is a very attractive solution due to its high theoretical specific capacity, high discharge voltage and good cycling performances. The major drawbacks consist in limited load capabilty, low thermal stability and fast capacity fade especially for high current rates resulting in a short lifetime. In addition, the presence of cobalt in LCO increase the cost of this cathode material. LCO is commonly used in lithium-ion cells for portable electronics, such as laptop, mobile phones and digital cameras, but suffers some problems when trying to scale up to larger cells for grid storage and automotive applications

- *Lithium Nickel Cobalt Aluminum Oxide (NCA)*

  It is composed by $LiNiCoAlO_2$ as a cathode material. It is a results of several researches in replacing the cobalt in order to improve the performance of the cathode in terms of capacity fading and thermal stability as well as reducing the whole cost of the cell. Indeed, NCA battery cells gain slightly improvement in thermal stability and better performance in calendar life compared to the LCO, keeping high specific energy. However, its thermal stability is worse than other cathode solutions. NCA cathode has found relatively widespread commercial use, for example, in Panasonic batteries for Tesla EVs.

- *Lithium Manganese Oxide (LMO)*

  Among all the proposed solution to replace the cobalt as the metal in cathode, Manganese offer a good improvement in terms of specific power. Indeed, this cathode is composed by $LiMn_2O_4$ whose architecture forms a three-dimensional spinel structure that improves ion flow on the electrode, resulting in lower internal resistance and improved current handling. These characteristics enable fast charging and discharging with moderate heat buildup. Moreover, this type of cathode material is much safer, has higher open circuit voltage and is much cheaper than the cobalt-based cathode architectures. On the contrary, the major limitation on LMO is low specific energy (roughly one-third lower than lithium-cobalt) and poor calendar and cycle life due to capacity loss, especially at high temperature. Indeed, the manganese dissolution occurs into the electrolyte and destabilize the anode SEI.

- *Lithium Nickel Manganese Cobalt Oxide (NMC)*

  One of the most successful Li-ion systems is a cathode combination of nickel-manganese-cobalt (NMC) because these systems can be adjusted to serve as Energy Cells or Power Cells. The secret of NMC lies in properly mixing nickel and manganese. Since, nickel is known for its high specific energy but poor stability and manganese has the benefit of low internal resistance but low specific energy, the combination of the two metals enhances each other strengths. A cobalt is needed because it stabilizes the nichel, a very energy active material. High design flexibility of NMC allow them to be the adopted for power tools, e-bikes and other electric powertrains. The most popular cathode combination provides for one-third of each metal, alson known as 1-1-1. Since cobalt is expensive and limited in supply, lots of manufacturers provide solution with disproportion between the manganese and nickel to cobalt. Among them, the most common combination available on the market are NMC811 and NMC622.

- *Lithium Iron Phosphate (LFP)*

  Besides lithium metal transition oxide, lithium iron phosphate cathode are composed by $LiFePO_4$, a lithium metal phosphate that is arranged in an olivine crystal structure. This nano-scale phosphate cathode material offer good electrochemical performance with low resistance, resulting able to handle high current without triggering aggressive aging mechanisms. The other benefits are long cycle life and high thermal stability that enhance safety and tolerance against

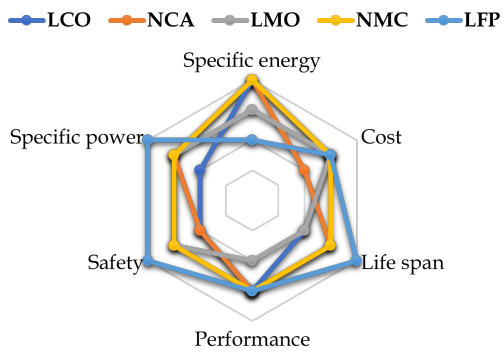

Figure 1.4: Features comparison of different type of lithium-ion cells based on cathode materials. The outer hexagon is the most desired.

abuse conditions. As a trade-off, LFP cathode are characterized by a lower voltage potential to the pure metal lithium and lower specific capacity with respect to the other active cathode materials illustrated before. In particular, the voltage characteristic presents an extremely flat discharge profile over the 20%-80% of the lithium concentration range due to the formation of a two-phase mixture during discharge rather than a continuous reduction in lithium concentration. The lower voltage difference with respect to the lithium metal means that more cells need to meet the voltage requirement for the specific application. The reduced energy density of this chemistry also implies that a LFP-based energy storage system results larger and heavier than other chemistries.

In order to improve the balance between energy and power, it is also possible to combine different cathode compound together as cathode active material. In figure 1.4, the main features of the cathode material described are summarized, in terms of *specific energy* or capacity, *specific power* that means the possibility to deliver high current, *performance* in temperature, *safety*, *life span* and *cost*.

On the other hand, the theoretical best anode material is lithium metal. It is the lightest of all metals, has the greatest electrochemical potential with very high specific capacity of 3860 mAh/g, but it is responsible to form dentrites during charging and discharging cycles, that can lead short circuit with the cathode and potentially cause the battery to catch on fire. For these safety issues, lots of secondary anode materials has been studied in order to replace lithium metal and still guarantee high voltage operation and specific capacity to the cells. For what concern the anode, the

candidate active material must be characterized by very low average difference potential with respect to the lithium metal, good electric conductivity and the capability to easy accept and release lithium-ions in its chemical architecture. In particular, conventional anodes are based on intercalation reactions, with most important materials being graphite and lithium titanate.

- *Graphite (LiC_6)*

  Graphite is the most stable form of the carbon it is heat-resistant, electrically and thermally conductive, chemically passive and lither than aluminum. As anode material it is characterized by a good specific capacity and very low voltage difference with respect to Li/Li^+ as well as its layered structure allow lithium ions to be inserted and removed easily. The maximum amount of lithium that can be stored in graphite is one atom of lithium per six atoms of carbon. In addition, its wide availability, low cost, and nontoxicity make it the most widely used material as an anode in lithium-ion batteries. Most of researches are focused on optimize this material by blending small amount of other material with higher energy density, such as silicon. However, high concentration of silicon strongly reduce the mechanical robustness of the cell due to very high volume change during charging and discharging process. SEI formation is still the major issue for graphite-based lithium-ion cell.

- *Lithium Titanate Oxide (LTO)*

  Another anode material successfully commercialized to replace graphite is the lithium titanate ($Li_4Ti_5O_12$) while the cathode can be manganese or NMC. LTO anodes offer very good performance in thermal stability for a wider range of operating temperature with respect to the other anodes, leading the cell to discharge at high C-rates at very low temperatures. A zero-strain intercalation for lithium ions in combination with high potential of lithiation are the reasons why LTO achieve stability and possibility to be charged and discharged at high C-rates. The small volume change during lithium intercalation (up to 0.2%) lead to a small voltage hysteresis between charging and discharging profiles. However, LTO anode has high voltage difference with respect to the Li/Li^+ with a small specific energy, that means more cells connected in series and in parallel need to be considered in a battery pack to meet the specific requirements. Nevertheless, the high potential avoid SEI formation that reduce the efficiency in lithium intercalation in graphite anodes. High potential to the lithium metal also prevents Li dentrite, even at high C-rates, that makes LTO

extremely safe. Another drawback is the the cost due to the presence of titanium that is expensive.

1.3.5 Future Trends

Currently, the goals of battery R&D are to address barriers which hold back EVs from matching the full driving performace, convenience and price of an internal combustion engine (ICE) vehicle. Indeed, automotive sector, or in general powertrain systems, are the most challenging application for the large scale penetration of lithium-ion batteries because they have to compete against another established technology. The leading cell chemistry technology for automotive application is based on high voltage and high energy density metal transition oxide as cathode, lithiated graphite materials as anode and lithium salt in organic liquid solvent for the electrolyte. In particular, nickel-rich layered oxide cathode materials, NMC and NCA, has been quite successful in improving the range and the cost of EVs. However, each components mentioned have some limitations:

- High voltage NMC cathode materials need to incorporate a high percentage of manganese, which reduces the specific capacitance of the cell and, consequently, also the gravimetric energy density.

- Graphite anode suffer for low energy density and is flammable that can cause safety issues. Moreover, graphite anode involves SEI formation that stores a significant amount of lithium and impact on the ionic and electronic conductivity reducing capacity and increasing internal resistance.

- The major limitations on liquid electrolytes are the low voltage tolerance and flammability as well as electrolyte decomposition as safety issues.

Therefore, a lot of effort in battery research are focusing on advanced materials with the aim of reducing weight and cost. According to *US Department of Energy Vehicle Technology Office Annual Merit Review (2022)*, future lithium-ion technology is represented by *Next-Gen* lithium-ion cells, namely chemistry based on an alloy anode and/or a high voltage cathode, and *Beyond lithium-ion (BLI)* cells in which Li metal is adopted as anode material. Both of these promising technologies offer the possibility to achieve very high energy density and reduce the cost, although they need a lot of improvement in stabilize the performance over cycles. In particular, next-gen batteries adopt conversion materials as anode electrode in which conversion reactions occur when lithium ions are accepted or removed in

and from the crystal structure. Moreover, a conversion reaction leads to a change in the anode material architecture. The most important elements that undergo reversible alloying with lithium at high capacity are tin (Sn) and silicon (Si), which can yield capacities of 900 mAh/g and 4200 mAh/g, respectively. Therefore, these materials gained a lot of attention for the negative electrode because they show much more specific capacity than graphite, about ten time considering silicon. A common phenomenon for Li-Si/Sn alloying processes is the volume expansion over conversion reactions. Electrochemical reversibility of the process apart, volume changes induces mechanical stresses that may destroy the integrity of the active material upon cycling. Silicon anodes, more than tin ones, are considered the primary candidates for the next-gen cells not only due to the high gravimetric density but also for the high availability as raw material and low cost of manufacturing. However, the major drawbacks consist in poor cycle life and high-rate capability due to the mechanical stress caused by a significant volume change of active material upon lithiation (about 300%). Moreover, some challenges need to be addressed for silicon anodes such as slow reaction kinetics, low value of diffusivity of lithium in silicon and low electronic conductivity. Other silicon based anode material for next-gen batteries are silicon monoxide (SiO) and composites of silicon and carbon. The former ones show lower swelling and shrinking during charging and discharging profiles and faster interfacial reaction kinetics at the price of significant reduction in specific capacitance and higher open-circuit potential (OCP) than silicon [5]. Si-C composites combine the best features of the two elements, namely high volumetric energy of the silicon and low volume expansion of carbon. Usually, Si nanoparticles are encased in a carbon matrix with the aim of improving the mechanical stress of the active material. Beside the improvement in terms of gravimetric capacity to the graphite, manufacturing process of the active material is very complicated due to the formation of SiC that is inactive with lithium. Moreover, a lot of empty space within the composite results in low volumetric density.

On the other hand, BLI cells are considered in the long term future as a energy storage system for EVs. BLI are the cells that adopt lithium metal as anode active material. Lithium metal is characterized by a very high specific capacity (3860 mAh/g) and the most negative reduction potential, which allow the cell to work at higher voltage and, consequently, more specific energy. The big brake on the spread of this anode material is the growth of lithium dendrites that strongly affects the cycle life of these cells and represent a serious safety risk. In detail, during charging and discharging profiles, uncontrolled deposition of lithium occurs on the surface of the anode that penetrate through the separator even causing loss of active

material for normal operation and increase of internal resistance. This phenomena is irreversible and can lead to internal short circuits and thermal runaway. For this reason, all Li-metal cells commercial available are only used as primary batteries and research effort are currently focus on stabilizing dentrite growth. Beside this, cost of extraction and raw material availability are, currently, the challenges related to lithium metal anode cells. The first solution of BLI cells involve sulfur as the cathode while lithium metal is generally employed as anode material. During discharge, lithium dissolution from the anode surface occurs, and lithium plating to the anode while charging. Sulfur-based cathode represents a conversion material for the positive electrode, and behaves just like conversion anodes, thus it suffer of high volume change during cycling. Sulfur has an extremely high theoretical capacity of 1675 mAh/g, being low cost and abundant in the Earth's crust as well. The cathode half-reaction during is the sulfur reduction tho the lithium sulphide (Li_2S), hence each sulfur atom can host two lithium ions. However, this side reaction has low potential with respect to the lithium metal reduction reaction and involves the formation of different lithium polysulfides which still exist at electrochemical equilibrium and dissolve in electrolyte. These mechanism is due to the slow reduction kinetics at Li_2S and cause a loss of active material. Moreover, some polysulfides are insoluble products and diffuse through the electrolyte to Li-metal anode leading self-discharge and anode corrosion. However, a lot of solution are investigating with the aim of improving sulfur cathode features by means either the use of carbon within the sulfur cathode architecture or electrolyte modification for mitigating polysulfide dissolution. Another type of BLI batteries consist in lithium-air (Li-air) cells in which the anode is composed by the lithium metal whereas the cathode consist of the oxygen obtained from the air. The operating principle is similar to that occurs for fuel cells in making the battery breath air and a mesoporous carbon is usually adopted as a cathode substrate with metal catalysts that enhance reduction kinetics. In this battery technology, the operating voltage and the theoretical capacity only depends on lithium metal, thus it results in the highest theoretical specific energy for a lithium-ion cell, comparable to the specific energy of gasoline. However, the overall capacity of the cell needs to consider the impact of both cathode and electrolyte of lithium-air cells. Regarding the electrolyte, several solution are presented in literature grouped in non-aqueous, aqueous, hybrid and solid state Li-air batteries, that differ from each others for the products of the cathode reaction. In particular, solid state and non-aqueous electrolytes lead the reduction of the oxygen to lithium superoxide (Li2O) and the formations of lithium peroxide (Li2O2) which is insoluble in non-aqueous electrolyte. On the other hand,

in aqueous lithium-air batteries the main discharge product is represented by the lithium hydroxide (LiOH) which shows limited solubility. Therefore, the described electrochemical reactions of each lithium-air battery solution result in loss of capacity over cycle and low coulombic efficiency. Currently, several challenges need to be addressed in order to make Li-air ready to the commercialization. First of all, elucidation of cathode-side reaction mechanisms and chemically stabilization of cell components as well as further improvement on ionic conductivity of the electrolyte. A lot of research effort for BLI batteries is also focused in electrolytes that are safer, more chemically and electrochemically stable against high voltage cells, as well as keeping low melting point, for low temperature applications, and low cost In this regard, another lithium-ion battery promising technology is represented by the solid-state batteries (SSB), in which a solid electrolyte is used instead of either liquid organic or polymer gel electrolytes, commonly used in lithium-ion and lithium polymer batteries, respectively. These batteries are considered one of the most safe type due to the replacing of flammable liquid electrolytes. Moreover, the use of lithium metal as anode and the volume reduction with respect to liquid electrolyte promise batteries with much higher specific energy than the current mature lithium-ion cells commercially available. However, solid electrolytes presents lower ionic conductivity than the liquid ones, especially at low temperatures, and poor superficial contacts. Moreover, dentrite growth remain a big problem to improve cycle life of this cell technology.

Among all the future battery technologies illustrated, the major remaining challenges to commercializing batteries for electrificated vehicles are as follows:

- The current *cost* of high energy lithium-ion batteries need to be further reduced to achieve head-to-head cost competitiveness of EV with internal combustion engine without Federal or Government subsides. The current high cost is due to the high cost of raw materials, cost associated with materials processing, the cell and module packaging, and manufacturing.

- Historically, the research was focused on increasing energy density of the cells to reduce weight and volume and, consequently, to improve the *performance* of the electric vehicles. However, weight and volume issues have been mostly addressed while the current cell chemistries that provide high energy have life and performance issues. Indeed, existing chemistries need improvement on receiving high rate current and low temperature performance to compete favorabily with gasoline-powered vehicles.

- All of the promising battery chemistries under investigation suffer cycle and calendar *life* issues.
- Basically, lithium-ion cells are not intrinsecally stable and safe when they undergo abusive conditions. Considering cell components, the reactivity of nickel-rich cathodes and flammability of electrolyte and graphite offer the possibility to think about other materials that are intrinsecally safer. Regarding lithium-ion batteries with lithium as anode, enhanced abuce tolerance strategies need to be implemented to avoid dentrite growth which can lead to internal shorts and thermal runaway.
- Nowadays, a large cost is needed to recycle end of life EV batteries. Finding solutions to reduce the cost of recycling might drastically lower the life cycle cost of EV batteries, avoid material shortages, reduce the environmental effect of new material manufacture, and potentially offer low-cost active materials for new EV battery manufacturing.

1.4 Battery Packs Architecture

The design of a battery pack inherently depends on the specific application and its requirements. Indeed, the architecture of a battery pack for automotive application is different with respect the one that needs to be suited for grid applications as well as portable electronics. Also in automotive applications, hybrid electric vehicles and battery electric vehicles have different needs. This requirements can be described in terms of voltage level, capacity and storage energy, C-rate capability, peak and continuous power and ambient temperature range as well as weight, size and available space, safety and cost. Figure 1.5 schematically resumes the main components that realize the architecture of a battery pack.

The first fundamental block is represented by the module which consist of several cells connected in series and parallel in order to meet the specific requirement in terms of voltage level and capacity at module stage. In detail, it is straightforward to understand that series connection of cells increase only the voltage whereas the parallel connection increases the capacity of the battery module. As result, the module voltage is roughly equal to the cell voltage amplified by the number of series connected units and the total capacity is equal to the cell capacity times the parallel connection and the whole energy of battery module is equal to the product of the module capacity to the module voltage level. This discussion can be extended from the module level to the pack level. Moreover, two different approaches allow

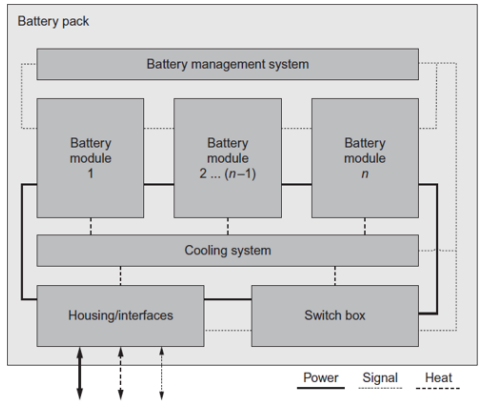

Figure 1.5: Schematic picture of the main components that realize a battery pack [6].

to meet the voltage and capacity requirement: series-parallel (SP) configuration and parallel-series (PS) configuration. Regarding the former, the cells are connected in series firstly to meet the specific voltage requirement, forming a string of cells and then several strings are connected in parallel to match the required capacity, while the opposite for the latter. Each module is provided by a monitoring and control unit which measures cell voltages and temperatures, ensure the safety of the module and communicate to the pack-level battery management system (BMS). The implementation of the BMS in lithium-ion battery packs results fundamental to guarantee safety operating condition of the cells. It has to monitor many variables such as cell terminal voltages, temperatures and pack current, estimate the state of the pack, detect any failure condition and eventually disconnect the battery system to the external load to prevent any safety risk. The switches that are used to disconnect the battery are contained in a switch box together with other components such as the isolation monitor and current sensor. A battery pack also require a cooling system because the temperature has a strong impacts on cell performance safety and lifetime, therefore the cooling system is needed to ensure the cell to operate within the optimal temperature range. All of these components are enclosed into a rigid structure with the aim of protecting every element from mechanical stresses and hard environmental conditions over the hole lifetime designed. The housing of a battery pack also provide the interfaces to the specific application, such as the high voltage (HV) plugs, communication and cooling interfaces. Further details of each component are described in the following subsections.

1.4.1 Battery Module

The simplest battery pack architecture is composed by a single battery cell that still needs its dedicated BMS, the switch box, the cooling system and a proper housing. However, large battery packs usually involve hundreds, or sometimes thousands, of cells in order to meet capacity and voltage requirement and a modular approach is used. It consists of dividing the whole battery pack in several fraction of it and each one is called module. Therefore, each module can be characterized by lower voltage level and lower capacity with respect to the entire battery pack. The terminal voltage is usually below to 60V so that production and transportation stages are simplified by eliminating additional and expensive safety precautions. The size of the module is also limited by the monitoring capability of the BMS. The modules have their own housing that ensure the mechanical stability of the cells within it. In particular, the module housing must be capable of absorbing both any mechanical stresses from the outside and the stresses caused by the change in cell volume that occurs during the charging and discharging processes and that vary with temperature, SoC, and SoH. Lastly, the module housing also contain power, signal and communication interfaces to be fully integrated to the other modules within the battery pack. In vehicle application, mechanical integration is key to optimize packaging, guarantee safety, improve serviceability and recyclability. Each module is equipped with its own BMS, usually a slave unit that is responsible to monitor the measurable variables, communicate with the master unit and take limited action as control board such as the balancing of the cells within the module. The module also contain the electrical connection between the cells as well as the wiring harness to connect the temperature sensors and voltage sense wires to the module control unit.

1.4.2 Safety and Control Unit

Lithium-ion cells are not inherently safe with respect to abnormal operating conditions, or abuse, such as overtemperature, overvoltage/overcharge, undervoltage/overdischarge, and extremely high C-rates. Such conditions cause an acceleration in the degradation mechanisms of cell components, even to the point of causing thermal runaway, an avalanche phenomenon that leads to the complete destruction of the cell itself. For these reasons, it is necessary to implement a security system that can mitigate and intervene in abusive operating conditions on cells. In detail, considering a master-slave architecture as illustrated in Figure 1.6, such a security system is realized by the BMS, the module control unit and the switch box.

Other types of architectures will be discussed in the 2.1 section in more

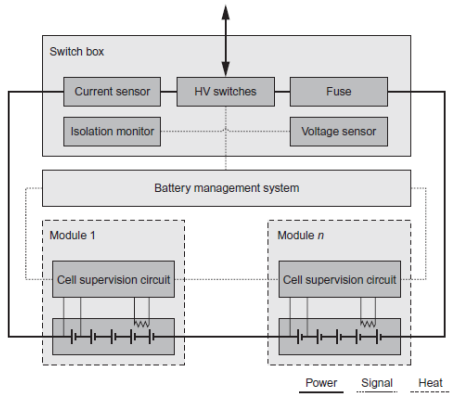

Figure 1.6: Schematic representation of Safety and control unit [6].

detail. However, the security system must necessarily include a monitoring and control subsystem and an implementation subsystem. The former collects data from measurements, processes it, and then sends commands to the actuation system, which must be sized to eventually disconnect the battery pack from the application, returning it to a new safe condition. The basic components of the switch box are two high-voltage relays, one for each terminal of the pack, and a fuse in order to protect the battery pack from a short circuit. In addition, the switch box integrates a pack current sensor and a sensor for measuring the insulation between the cell terminals and the ground.

1.4.3 Cooling and Heating System

Temperature has a strong impact on cell performance and, consequently, to the battery pack. It also play a key role in degradation mechanisms of the internal components of the cell, affecting cycle and calendar life of the pack. Therefore, it is possible to identify the optimal operating range for the temperature in which the cells achieve the best performance in terms of voltage-current response while preventing the acceleration of aging mechanisms and safety risks. Figure 1.7 summarize the temperature impact on life, safety and performance of lithium-ion batteries and suggests a range of 15-35°C as desired working temperature [7].

Within the battery pack, the heat is generated by several sources such as the internal resistances of lithium-ion cells and connectors due to the current flow as well as the electronic components related to the control boards. As discussed before, high temperature temporarily increases the capacity but accelerates the aging mechanisms affecting the lifetime of the

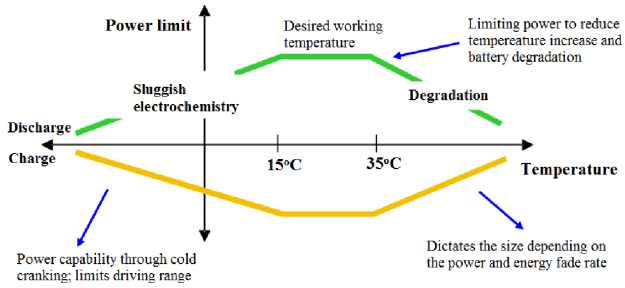

Figure 1.7: Temperature impact on life, safety and performance of lithium-ion batteries [7].

battery pack. Moreover,the heat generation is locally defined and creates a non-uniform temperature distribution within the battery pack described by the heat transmission laws. This leads to unbalances among the cells in terms of voltage and capacity, since the cell performance are strongly affect by the temperature. On the other hand, low temperatures in cold environments increase internal resistances of the cell limiting the performance of the battery pack. Therefore, an efficient thermal management system (TMS) that include cooling and heating systems must be implemented in battery pack in order to bring the battery pack to operate within the safe thermal operating range, increase lifetime and prevent safety risks. The cooling and heating system for a battery pack usually consist of either air-cooled, liquid-cooled or direct refrigerant-based systems. The main features and design aspects for TMS of electric vehicles are detailed described in [8].

1.4.4 Battery Housing

The battery housing consist in a mechanical architecture that houses all the components of the battery pack while meeting mechanical, safety, service and cost requirements. Since they depend on the specific application, the battery housing is a highly customized component. In particular, shape and size are determined by both the available space in the specific application and the components that have to fit inside it. Electric vehicles, more than other applications, impose strictly constraints for battery housing design. Considering automotive sector, mass and position of the battery pack have significant impact on the energy consumption of the vehicle and driving performance, respectively. The housing is typically made of an upper and lower housing separated by a sealing gasket. The seal prevents particles and liquid entering and it is tailored to a specific ingress protection (IP) class. Other components that are integrated into the battery housing are the pressure equalization element and a device cor condensate

handling. The former serves to balance the pressure of the air volume enclosed and sealed within the battery pack with respect to the outer pressure, the latter is implemented to avoid and remove condensate that may cause corrosion and dames to the electronic components. Lastly, battery housing provides mechanical, thermal and electrical interfaces to the vehicle or the specific application. These include the HV terminal header, the communication-data plug and a thermal interface for exchange heat with the cooling system.

1.5 Battery Modeling

Battery models are fundamental for research and development in the field of energy storage. They enable scientists and engineers to test new materials, technologies, and control strategies in a virtual environment before physical implementation. Battery models allow researchers and engineers to understand how a battery behaves under different conditions. This insight is crucial for optimizing the battery's performance, ensuring it delivers the desired power output. Tare used in the design and simulation of systems that incorporate batteries helping in sizing the battery pack in a correct way and predicting its behavior in real-world applications. Moreover, BMSs rely on accurate models to estimate and monitor information on variables that are not directly measurable such as state of charge and state of health as well as the state of power (SoP) in order to ensure the batteries to operate within the safety region. In the literature, several approaches to modeling batteries have been developed to capture the complex electrochemical and thermal processes involved in their operation. The choice of model approach depends on the specific application, the level of detail required, computational resources available, and the accuracy needed. In addition, different models can be adopted over the different steps which a battery pack follows during the entire lifetime, from the cell design to the cycle life. Among battery models, heuristic (or data-driven) and physic-based model (PBM) approaches aim to describe the dynamic response of the the terminal voltage of the cell with respect a given current profile. The first ones express the input-to-output behavior regardless the the physical processes within the cell whereas the second ones attempt to model each individual mechanisms that occur inside the cell. In turn, heuristic models can divide into lumped parameter models, such as equivalent electric circuit models, and black-box models, based on artificial intelligence and machine learning algorithms. On the other hand, the formulation of PBMs depends on the scale-stage where the phenomena occurs, as illustrated in figure 1.8.

Battery models include thermal models that focus on describing the

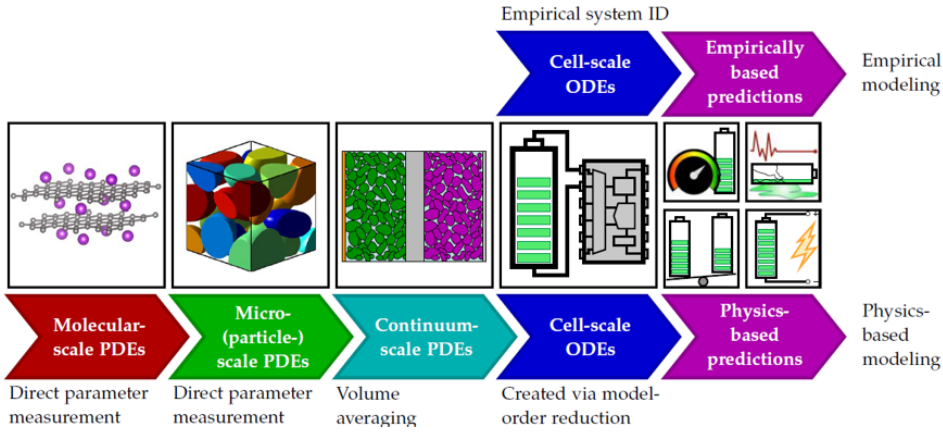

Figure 1.8: Comparison overview of different approaches to build cell models [9].

temperature distribution within the battery during operation. Beside these, aging models aim to predict the aging and degradation of batteries over time, which is critical for estimating the battery's remaining useful life (RUL) and optimizing maintenance. These models are often coupled and combined to leverage their strengths, for example thermal with electrochemical models to account for the thermal effects on battery performance and safety. The following discussion aim to give further details on electrochemical and heuristic model approaches.

1.5.1 Electrochemical models

Electrochemical models are physics-based and focus on representing the fundamental electrochemical processes within the battery, such as diffusion of ions, charge transfer reactions, and electrode kinetics. In details, physics-based models predict the voltage-to-current response by considering the following processes involved:

- *Thermodynamics* allow to define the equilibrium potentials of electrodes.
- *Kinetics*, to describe the polarization losses, the charge transfer and activation overpotential.
- *Mass transport*, to predict the variation of ion concentration in solid and liquid phases.

Referring to the micro-scale, theory of porous electrode is used to model the dynamics of intercalation-based electrode, developed by Doyle, Fuller

and Newman in 1993 [10]. In this model, the main assumption is to consider the cell divided in three regions, positive electrode, negative electrode and separator. The sctructure of the electrode is approximated as a superposition of active material, electrolyte and filler material, in which is possible do distinct two different phases, solid electrodes and liquid electrolyte. The active material is approximated as several spherical particles with uniform distribution and the electrochemical reactions are considered homogeneous, regardless the exact shape of the interface between electrode and alectrolyte. Hence, this model considers the lithium diffusion through the linear and spherical symmetry for the solid phase and only through linear symmetry in liquid phase. For these reasons, this model is called pseudo two-dimensional (P2D) reducing the geometry from a 3D (three-dimensional) problem. The model variables are the concentration of ions into the solid particles and into the electrolyte, the potential in the solid particles, the potential in the liquid electrolyte and the electrode current. The solution of the lithium diffusion is governed by the mass conservation laws for both homogeneous solid and liquid electrolyte, whereas the potential is given by the charge conservation in solid and liquid solution. The movement of the lithium ions between the two phases (solid-electrode and liquid-electrolyte) is governed by the Butler-Volmer equation, which define the reaction rate at the surface of the particles [9].

Beside the accuracy, this approach is generally applicable to all types of batteries, the actual form of the model equations and parameters will change depending on the cell chemistry. However, due to the mass transport occurs mostly through a diffusion process, the dynamic of ionic concentrations is described using coupled partial-differential equations (PDE). This mathematical description increase the model complexity and dedicated numerical methods are required in order to solve it. Therefore, a large computational effort is needed, then the complexity of the equations makes it difficult to apply to estimation and control problems, especially for run-time applications. Another issue is in the large number of physical constant and parameters to define, which make model tuning process very labor.

With the aim to reduce the complexity of multi-scale electrochemical models, single particle modelling (SPM) approach was developed. The central assumption of this model is to reduce each whole electrode into a single spherical particle, as the name suggests, that means the uniform utilization of the electrode with respect to the thickness. As a result, the intercalation current density is a function of time only and the surface concentration profile is obtained by solving a one-dimensional time dependent diffusion equation for a spherical particle. The Butler-Volmer equation is also sim-

plified because no spatial dependence is no longer present, resulting in a nonlinear algebraic equation. SPM approach leads to inaccuracies when the cell operates at high C-rates due to the dynamics of electrolyte concentration and potential are ignored. The extended single particle model (ESPM) has the aim to overcome this issue by including a representation of the lithium transport in the electrolyte, still considering the solide phase of each electrode as a single representative part [11]. ESPM results easier to implement and compute than the P2D, however remain inaccurate for low temperature, thick electrodes and high C-rates due to the approximation of uniform electrode thickness utilization.

1.5.2 Black-Box Models

Black-box models in battery applications are part of data-driven models that use artificial intelligence (AI) and machine learning (ML) algorithm to predict the voltage response from a given input current, without the need to understand the underlying electrochemical processes occurring in the cell. These models are arranged in a set of nonlinear equations in which the parameters have no physical meaning and are adjusted by a training process. The training of a neural network is usually conducted by minimizing a certain error function, usually related to the difference between the output of the black-box model and a target. A lot of data need to be involved into the training process in order to achieve good performance for all the possible operating conditions for a lithium-ion battery cell. Several AI approaches are reported in literature, such as artificial neural network (ANN), fuzzy logic (FL) and support vector machine (SVM). Although the black-box models have many advantages in terms of flexibility, high degree of non-linearity and self-learning characteristics, in the case of a small number of data samples the estimation accuracy is relatively general and the versatility is poor. Moreover, the implementation of the algorithm takes a long time, and the real-time performance of the application is difficult to guarantee.

1.5.3 Equivalent Circuit models

Equivalent circuit models (ECMs) are heuristic models that aim to describe the cell behavior, in terms of terminal voltage response to an input current, by using electrical circuit components properly connected. Thus, this type of models results very flexible, due to the possibility to change the topology for improving the accuracy of cell prediction, robustness and relatively simple to handle, because it is mathematically described by a set of ordinary differential equations (ODEs). Moreover, the same model

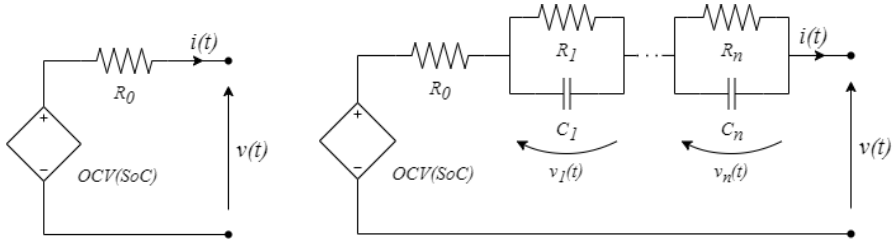

(a) (b)

Figure 1.9: ECMs: (a) zero-order and (b) generic n-order.

structure can be used for different chemistries by selectring the appropriate parameter evaluation. Currently, ECMs are implemented in the most of the BMS of large battery pack for ensuring the safety operating boundaries for the cells and for estimating the internal cell states. How to build equivalent circuit models for a lithium ion battery results very intuitive with respect the behavior exhibited by the cells. Indeed, it is possible to start from the concept that the cell represent a voltage source for the circuit in which it will be implemented and this voltage varies with the state of charge of the cell. Therefore, a voltage source is the first basic component with an equation that model how SoC varies with respect to the input. This voltage source represent the OCV of the cell. However, the open circuit voltage describe the equilibrium condition of the cell voltage, that is static. Indeed, if the cell is discharging the terminal voltage drops below the OCV and if the cell is charging it rises above the OCV. Hence, a equivalent series resistance can be added in series to the OCV to reproduce this voltage drop when the cell provide or receive energy. It also represents the power dissipated by the cell that can be integrated with a thermal model to predict the temperature behavior.

Then, this model is called, in literature, Thevenin model (Figure 1.9a)and can be described by the following set of equations:

$$\begin{aligned} \frac{dSoC(t)}{dt} &= -\frac{i(t)}{C} \\ v(t) &= OCV(SoC(t)) - R_0 i(t) \end{aligned} \tag{1.3}$$

where $i(t)$ is the input current at instant t, $v(t)$ represent the terminal voltage, $SoC(t)$ is the actual state of charge and R_0 represents the equivalent series resistance. It is important to point out that this resistance also depends on the state of charge, the temperature and the C-rate as well as it

varies with the aging of the cell. Coulombic efficiency should be taken into account in the equation of the state of charge as a multiplicative coefficient of the right side. Coulombic effiency refers to the actual capacity that a cell can discharge with respect to a full charge. However, this parameters is very close to 1 for lithium-ion battery cell, then it can be neglected. Moreover, this parameter varies with temperature, C-rate and aging condition, thus it is challenging to define thoroughly.

Series resistance models an instantaneous polarization of the cell. However, the voltage polarization is a dynamic phenomenon due to the diffusion effect occurring inside the cell and it varies over time, either a current is applied or in rest phase. This effect can be approximated by adding one or more parallel resistor-capacitor (RC) branch in series to the OCV voltage source and the resistance R_0. The number n of the RC branches added in parallel define the order of the ODE associated at that model (Figure 1.9b). For example, if two RC branches are considered the model integrate two state variables from the circuit perspective then the model will be called second-order ECM, and for the same reason, the Thevenin model is also called zero-order ECM. At this point the model equation can be written for generic n-order equivalent circuit model as follow:

$$\begin{aligned} \frac{dSoC(t)}{dt} &= -\frac{i(t)}{C} \\ v(t) &= OCV(z(t)) - R_0 i(t) - \sum_{k=1}^{n} v_k(t) \\ i(t) &= \frac{v_k(t)}{R_k} + C_k \frac{dv_k(t)}{dt}, \quad \forall k = 1, \cdots, n \end{aligned} \tag{1.4}$$

where $v_k(t)$ is the voltage across the k-th RC branch, which is modeled by R_k and C_k. The use of more RC elements in series, with different time constants, allows to account for multiple time-dependent dynamic reactions occurring in the cells, then improving the accuracy of the equivalent circuit. The more RC branches means the higher accuracy of the cell performance. On the other hand, the parameter identification process becomes more complicated due to over-fitting issues as well as it impact on the computational effort to solve the model. Since each model parameter is function of SoC, temperature, C-rate and also the sign of the current, several tests are needed to estimate them.

1.5.3.1 Parameters identifications

ECMs only approximate the behavior of the battery with an equivalent electric circuit, but no real resistor or capacitor exist in the cells. For this reason, the parameter estimation is derived by processing voltage and current data provided by several experimental tests, therefore an heuristic approach is needed to develop ECMs for lithium-ion batteries. In detail, the parameter identification process follows some generic steps which are resumed in figure 1.10.

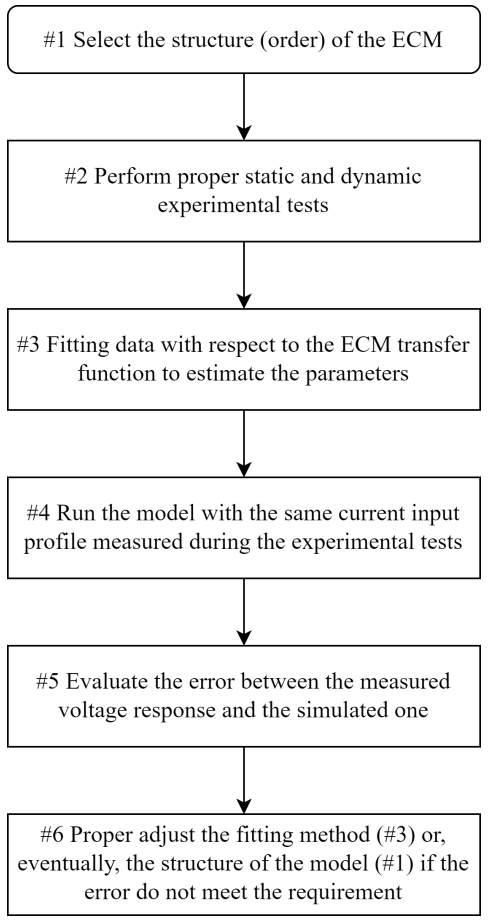

Figure 1.10: Parameter identification steps.

The first step consist of selecting the model architecture of ECM that allow to approximate the voltage response of the cell with respect to a current profile, thus the order of the equivalent circuit model. Therefore,

proper experimental tests need to be designed with the aim to characterize static and dynamic behavior of the battery cell. The static characterization regards the design of tests to assess the battery capacity and the OCV with respect to the state of charge. It is important to point out that both OCV and capacity depend on temperature while capacity is also related to the C-rate. To assess the discharging capacity of the battery, it need to be fully charged and then, after a rest phase, complete discharged in specific operating condition in terms of current and temperature. In order to fully charge a cell, it is necessary to brought the terminal voltage to the maximum operating one designated by the manufacturer at very low C-rate that strongly limit the ohmic and diffusion polarization effect keeping the cell in a quasi-equilibrium state at all times. Therefore, two different phases can be distinguished, namely: constant current (CC) and constant voltage (CV). With the CC charging phase the terminal voltage of the battery raises until the maximum voltage (v_{max}) at a specific constant-current rate and, subsequently, the cell is held to the maximum voltage and the current start to decrease. The fully charging process ends when the charging current drops below a specific threshold (typically C/30). However, the discharging process for capacity assessment involves only the CC phase and it ends when the terminal voltage hits the minimum operating cell voltage. Usually, lithium-ion battery increases capacity at low C-rates and higher temperature. For this reason, with lower C-rate it is possible to measure the fully usable capacity of the cell, even though the reference capacity adopted in the model can be different depending on the requirements of the specific application. Since the OCV represents the equilibrium points of the cell, very low constant C-rate can be used for good approximating the OCV characteristic with respect to the SoC. This strategy is a compromise between the desired true equilibrium condition and the practical realization of the test that already takes many hours. One more accurate test to determine OCV-SoC relationship is represented by the GITT (Galvanostatic Intermittent Titration Technique) test, which consist of discretizing the point of OCV characteristic. Indeed, starting from a fully charged cell, a low discharge rate is used to extract a small amount of capacity and a suitable rest follows. The last voltage point of the rest phase is considered as the OCV at that specific SoC. These steps are repeated until the terminal voltage reaches the minimum allowable. The GITT test results a very accurate experimental test for capturing both thermodynamic and kinetic parameters of the cell. Both low C-rate and GITT test can be used to extract the OCV characteristic in charging and discharging operations in order to capture the hysteresis phenomenon the cell exhibits. The presence of hysteresis makes the OCV-SoC relationship a "path function" and

not a state function. Several approaches have been reported in literature to take into account this voltage difference in ECMs, increasing the model complexity by adding non-linear equations. Therefore, the most used approach to implement it is to consider the average curve of OCV between the discharging and discharging OCV.

On the other hand, dynamic test are needed to calibrate the model parameters in such a way to better approximate the dynamic transient response of the cell, that related to the charge transfer resistance, accumulation of the charge carriers at the surface of the electrodes and the diffusion effect. The test reference for this purpose is represented by the Hybrid Pulse Power Characterization (HPPC), which consist of subjecting the cell to current pulses at different SoC. In detail, this test involves one discharging pulse and one charging pulse for each SoC step and a short rest period always follows each pulse. Then, a fixed amount of capacity is removed from the cell with a low constant C-rate and the pulse phase is repeated, after a long rest phase. High-power, short-duration pulses allow for the assumption of constant SoC and hence constant parameters, while also providing adequate dynamic behavior for predicting parameter values in charge or discharge. As it is possible to notice, HPPC enables to create a set of discrete value of each parameter with respect to the SoC. The same test can be performed ad different temperatures and different C-rates (regarding the pulses) with the aim to better cover all the possible operating condition a cell can experience during its entire lifetime. This test also allows to evaluate the capacity of the cell for a specific C-rate and merely approximate the OCV-SoC relationship. A further improvement of the HPPC is represented by the RC-Identification test (RCID). The latter follows the same approach of the HPPC but it involves multiple pulses at different C-rates for each SoC incremental step. This avoids to repeat the HPPC several times to capture the parameter dependency with respect to the current magnitude and sign. The calibration tests need specific testing equipment to be performed. They need to have the capability to control current and voltage in charging and discharging as well as the temperature of the cell, for safety and consistency of the experimental data. Battery cycler are programmable bidirectional systems (DC load and power supply) which allow to control voltage, current or power that need to be applied to the cell. These systems are specifically designed for battery cell with the aim to cover a large current range when a low voltage is applied, even ensuring high accuracy. Moreover, a proper set up for cell testing have to be design to guarantee that the experimental data are related only to the cell under testing and not to the external world. Thermal conditioning of the samples is ensured by using several solution such as thermal chamber,

thermo-electric coolers as the Peltier junctions or liquid cooling. These devices are controlled in such a way to control the heat exchanged between the cell and the external environment, then the cell surface temperature during the tests.

Once static and dynamic tests are concluded, the following step involves to gather all the data and to extrapolate the model parameters with the aim to minimize the error between the model output and the measured voltage of the cell under testing. Regarding static tests, nominal capacity is used to determine the SoC range, then OCV-SoC characteristic are directly determined itself. The evaluation of the series resistance (R_0 often differs between the order-model and higher-order models. Considering a single discharge pulse of the HPPC (which usually lasts 30 s), the zero-order model take into account the voltage drop between the data point at the beginning and at the end to the pulse to evaluate the resistance. This results more conservative with respect to consider only the instantaneous voltage drop of the voltage when the pulse is applied. On the other hand, for models that consider at least one RC parallel branch the series resistance is related only to the instantaneous voltage drop as soon as the current pulse is applied. Considering a first-order model, the resistance and the capacitance of the RC branch are evaluated by a fitting process which involve an optimization algorithm that aim to minimize the root mean square error between the exponential behavior of the RC branch and the experimental data. In particular, when a constant current ($i(t) = I$) is applied to the n-order model, the voltage response of every RC branch is expressed by:

$$v_k(t) = v_k(0)e^{-\frac{t}{\tau_k}} + R_k I(1 - e^{-\frac{t}{\tau_k}}) \tag{1.5}$$

where $\tau_k = R_k C_k$ is the time constant associated to the k-th RC branch. The main assumption of this voltage response is to consider each parameter constant that is true if SoC does not change. Hence, the fitting process is performed during short pulses or during the rest phase when the terminal voltage exhibits a relaxation after the instantaneous drop. Higher order ECMs aim to capture different voltage dynamic in terms of different time constant. Indeed, several electrochemical phenomena occur within the cell with different time response. However, increasing the order the identification process becomes complex leading to over-fitting issues.

The parameter identification procedure go ahead with the validation process. It consist of running the model with the obtained parameter under the same input current profile measured during the experimental test and compare the model output voltage with respect to the real one. The voltage error is evaluated under several conditions and compared to the requirements of the specific application. If the error does not meet the

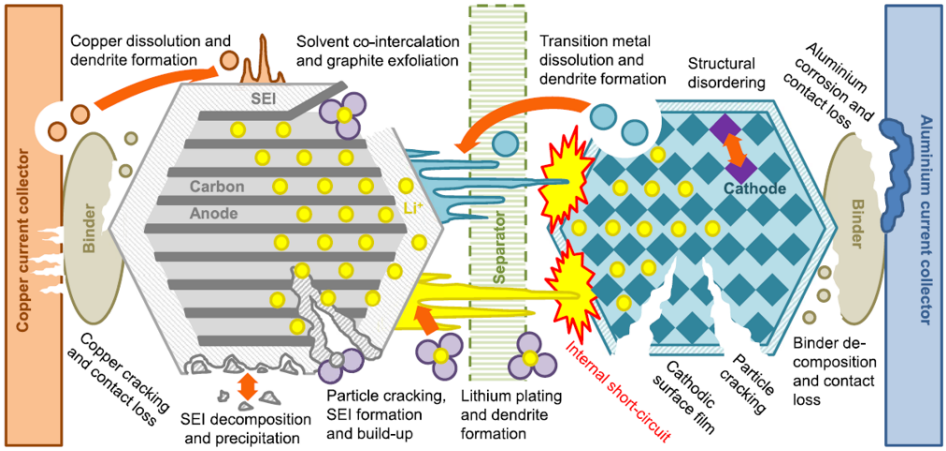

Figure 1.11: Degradation process within a lithium-ion battery [12].

requirements several strategies can be adopted to overcome this issue, such as either the order of the model can be increased, more dynamic tests need to be performed or the fitting process need to be improved.

ECMs need a lot of experimental tests to cover thoroughly big part of the possible operating range of the cell, in terms of SoC, current and temperature. The low computational cost and robustness of this modelling approach result very attractive for the implementation in real-real time applications. However, ECMs lose accuracy to predict voltage response of the cell is subjected to different input stimuli with respect to the calibrating tests as well as for some batteries and applications, even multiple RC elements may not be capable of accurately modeling the battery's response, and other modeling techniques are needed. Moreover, they lack to predict the cell behavior if the cell is aged and they are not able to predict faults.

1.6 Aging mechanisms

A better understanding of degradation mechanisms helps for finding strategies to improve the lifetime of the battery cells as well as to evaluate the performance reduction and to detect what mechanisms could lead to sudden failures that cause safety problems. Aging conditions are expressed in terms of loss of performance with respect to the performances exhibited at the beginning of life (BoL), thus when the cell directly comes from the manufacturer. In particular, battery aging is expressed as reduction of capacity as well as power fading due to internal resistance increases. Battery aging also gives an indication of the remaining useful life (RUL) of the cell

and the battery pack. This measure is usually defined as the number of complete charge-discharge cycles a battery can perform before its nominal capacity drops down the 80% of that at BoL. RUL is very challenging to evaluate since the battery life strongly depends on the usage, the temperature, prior history etc. It is important to remark that the most aged cell limits the performance of the whole battery pack in which it is integrated.

Aging phenomena are inevitable and they are driven by either chemical reaction or mechanical processes that involve the electrodes and the electrolyte. An overview of the aging mechanisms that occur inside the cell are schematically illustrated in figure 1.11

The aging mechanisms that naturally deteriorate cell performances can be mainly summarized by SEI growth, particle fracture and lithium plating. They are driven by chemical reaction or mechanical processed that cause, basically, loss of cyclable lithium or loss of active material.

- *SEI growth*

  Solid electrolyte interface (SEI) constitutes a passivation layer that forms at the electrode electrolyte interface when the solution comes in contact with the electron-conductive surface of the anode. SEI formation occurs because the negative electrode usually operates at voltages below the electrochemical stability range of the electrolyte. This process starts during the first cycle and SEI formation is necessary to stop surface reactions of the electrolyte at the anode, leading to loss about 10% of the usable lithium, though. Although this process is reduced after the first formation of this film, SEI continues to grow during cycle life resulting in a gradually reduction of the cell capacity over time.

- *Particle fracturing*

  This degradation process is mainly due to the volume change of both the electrodes during intercalation and deintercalation of lithium ions inside the chemical matrix of the anode and cathode, causing mechanical stresses. This stresses over time can cause fracture, delamination or similar phenomena that lead to the physical disconnection for part of active material from the conductive matrix. Therefore, it results in loss of active material and increase of the resistance due to reduction of the path for transferring lithium ions. Loss of active material bring a capacity reduction based on the amount of the lithium stored inside the active material disconnected. Particle fracturing phenomenon is induced by high DoD and high C-rate as well as low temperature promotes it.

- *Lithium plating*

  Lithium plating is a degradation process in which, during the charge operation, the lithium form a solid layer on the surface of the anode instead of intercalating within its matrix. The main consequences are loss of cyclable lithium, the raise of the internal resistance and dentrite formation that can also pierce the separator membrane creating a short circuit between anode and cathode, then causing critical safety issues. The plating reaction is favored when the anode potential becomes lower than the potential of Li/Li^+. This occurs at high concentration of lithium within the anode (high SoC of the cell) and high current that cause large overpotentials. Moreover, this phenomenon is promoted at low temperature. Lithium plating is a partially reversible process since part of the plated Li can be reversed to cyclable lithium by the process known as lithium stripping.

The degradation mechanisms just discussed occurs gradually even if the cells are used within the proper safety range. However, if a cell undergo to some uncontrolled operating conditions, called abuse conditions, they accelerate the aging process and causing failure with consequently safety concerns. Indeed, there are several abuse conditions that can induce hazard conditions, such as thermal runaway (TR) of one or more cells in a battery pack, which essentially consists in a series of exothermic reactions inside the cell that generate a large amount of heat, leading to destructive result as fire and explosion. Abuse conditions can be classified in electrical, mechanical and thermal.

- *Electrical abuse*

  Electrical abuse conditions include overcharging, overdischarging and overcurrent or external short circuit. The overcharging and overdischarging conditions consist of forcing the cell to go over the voltage limits. The worst condition is the overcharge abuse since excessive energy is filled into the cell. Overcharge can lead to thermal runaway, cell swelling, venting, and other serious events. On the other hand, the overdischarge involve the overdelithiation of the anode which leads to the decomposition of the SEI layer. The resulting reaction produce gases and cell swelling, compromising the structure of the cell and causing mechanical stresses. Moreover, it also causes loss of capacity and power fade due to change of the electrochemical characteristics of the negative electrode. Both overcharge and overdischarge conditions are related to a BMS failure. On the contrary, the external short circuit occurs when the two electrodes are directly connected together

by a conductor. Unlike overcharging and overdischarging, this abuse condition is not inherent to the cell chemistry but can be caused by an external event like deformation of the battery pack for a vehicle collision, water penetration or whatever that allow a direct external contact between the voltage terminals. External short circuit cause a very fast discharge of the cell that can also lead to overdischarging condition if the external short cannot be estinguished.

- *Mechanical abuse*

  These abuse conditions occurs when a massive force is applied to the cell that cause destructive deformation to the external and internal structure of the cell. Vehicle collision and nail penetration are the typical mechanical abuse conditions. Regarding the worst case scenario, mechanical abuses can cause internal or external short circuit leading to the thermal runaway. Moreover, mechanical damages to the cell can cause leakage of electrolyte which is flammable. In order to ensure robust safety against mechanical abuse, every step in development of the battery pack have to take into account the mechanical resistance of the battery pack, although this do not ensure that a severe impact will not create any irreversible damage to the cells.

- *Thermal abuse*

  Thermal abuse conditions involve the cell exposition to the temperature outside the safe operating region. High temperature increase the reaction rate at the electrode-electrolyte interface, therefore more heat is locally generated inside the cell. If this heat cannot be removed as faster as generated, a positive feedback phenomenon known as thermal runaway (TR) occurs, leading to the destroy the cell with severe safety issues. Hence, thermal abuse condition for battery pack are generally represented by a local overheat. This can be led by several causes, such as malfunction of electric component, resistance increases and manufacturing defects. Prolonged low temperature exposition also represent a thermal abuse condition, although it do not immediately lead to the thermal runaway. However, the performance of lithium-ion batteries are strongly limited with temperature decrease and lithium plating on the anode surface is promoting, with consequently irreversible loss of capacity.

1.7 Applications

Nowadays lithium-ion batteries are used in a wide range of application and also represent a promising technology for many others. Currently, they are largely adopted for portable electronic devices and road transportation, althought they have also found applicability in aerospace application, including in satellites and aviation due to their specific energy and lightweight. Portable electronic devices have represented the initial market for this battery technology and for long also the main market, but it is being overtaken by the Li-ion battery demand for road transport. For portable electronic application the main feature design is represented by the energy density, that leads lithium-ion technology to be the best choice as battery chemistry. Therefore, LCO chemistry is the most adopted because the presence of the cobalt increase the energy density. Moreover, consumers expect that the new generation of this applications exhibit less charging time and more capacity. Another challenging innovation is represented by the downsizing the battery cell for this application sector. This must keep high capacity and power as well as complying with safety standards.

Lithium-ion battery technology has enabled the possibility of electrification in road transportation allowing to develop vehicles which performance can be compared to the traditional vehicles equipped with ICE. Electric vehicle can be mainly classified in hybrid electric vehicles (HEV), plug-in hybrid electric vehicles (PHEV) and pure electric vehicles (EV), depending on the incremental level of electrification, defined by the ratio between the electric power and combustion power installed on board. The specific energy (both in gravimetric and volumetric) and power represent the main features that allow lithium-ion batteries to play this key role for vehicle electrification with respect to the other chemistries. Beside the amount of energy needed to meet long range requirement, in automotive application the size and the weight are two fundamental parameters to achieve good enough performance in vehicle driveability and comfort. Moreover, energy storage for electric vehicle have to exhibit good performance for large drive distance as well as a competitive cost in order to be a true alternative to the ICE vehicles. In addition, HEV, PHEV and EV have different requirement in terms of energy and power request. Indeed, HEVs install small battery pack, not chargeable by direct connection to the grid, which is mostly used to recover kinetic energy during deceleration and help during acceleration. Instead, PHEVs and EVs require to cover large driving range in pure electric mode beyond to ensuring adequate acceleration performance. Hence it is possible to define the power to energy ratio (P/E ratio) that allow to compare the requirement for the three different type of electric vehicles. As

it is possible to understand from the previous discussion, P/E ratio will decrease when the level of vehicle electrification increase. Typically, P/e ratio is in the range of 5-10 for PHEVs, and it is in the range of 2-5 for EVs [13]. Among the lithium-ion chemistries, the most used ones for vehicle application are NMC and NCA. Compared to the LCO, they improve the cycle life, safety and cost due to the presence reduction of the cobalt. LFP batteries also represent an attractive technology because it is inherently safer with the weakness of the specific energy. Comparing NMC and NCA, the majority of car manufacturers are opting for NMC cells. While the NCA cell is advantageous in terms of specific energy, the NMC cell presents higher lifetime and more flexibility in design, which promote the utilisation of the latter in PHEV. The current challenges for lithium ion battery remain the driving range, the charging time and lifetime. As discussed in this chapter, these three features are intrinsically related since large driving range needs high capacity which needs extreme high current to be charged in short time that strongly impact on battery lifetime. However, with current state of the art technology it is possible to reach a driving range above 500 km and fast charging technologies easily allow to charge 80% of the battery's nominal capacity in less than one hour. Moreover, most of manufacture assure the battery pack performance for 500-800 full cycles and a calendar life of approximately 8 years in warranty. The global conditions for an accelerated market growth are overall very favorable because the strong support in subsides and tax exemptions for EV and PHEV as they reduce GHG emissions, especially if harmonized with policy for emission reduction in power generation. Regarding lithium-ion batteries, the automotive industry is becoming the main market.

Lithium-ion technology represent an attractive solution also for energy storage systems which have to be integrated in the main grid as well as off-grid power generation. Large electrochemical storage can be used to carry out frequency and grid voltage regulation services as well as maximize the energy produced by renewable energy plants such as photovoltaic (PV) and wind. They also can be the response to the local high power request, for example in EV fast charging, without impact on the electricity grid. In addition there is an increasing degree of decentralization of small amount of energy production. However, for all of this range of application the main parameter design is represented by the cost with respect to the energy (€/kWh) and, although Li-ion presents several advantages in cell performance with respect to the other chemistries, this technology is not the most convenient for the first cost of investment. Lithium-ion technology is also characterized by the highest energy efficiency that means lower cost per charging-discharging cycle. For this reason long cycle life can invert

the scenario and enable the large adoption of lithium-ion battery as electrochemical storage systems for electric grid applications. More details of the lithium-ion battery applications and market trends can are illustrated in [13].

Chapter 2

Battery Management System

The increasing use of lithium-ion batteries has necessitated, in parallel, the development of efficient battery management systems (BMS) in order to ensure the proper operation of this battery technology. The BMS represents the control unit of a battery pack, and its design is highly dependent on the requirements of the specific application. Therefore, it needs to interface with both battery cells, additional components within the battery pack such as sensors and contactors, as well as the load network outside the battery pack. Looking at the battery management systems as a black-box, it have to measure the main parameters such as cell voltages, string current and cell temperatures, to process the data both to avoid unsafety condition and determine the battery state and then control the main contactors and communicate the battery status to the external world.

The inputs, outputs and the functions that have to be performed have a strong impact on the design and development for the BMS architecture. Hence, the main architecture of the BMS are detailed illustrated in the first paragraph of this chapter.

Subsequently, requirements and functionalities are explained, including criteria for evaluating possible solutions to realize these features. In particular, solution for sensing and measurement, estimation of the states, strategies for performance optimization, safety and protection circuits and control and communication are described in the second paragraph.

2.1 Architectures

The BMS design depends on specific requirements, the environment conditions and the cell technology adopted. The architecture design involve a relatively abstract description of the internal operation of the system and only a little distinction among hardware and software components or method of implementation is needed. Inputs are generally related to the measurement of the physical quantities of the cell and instruction from the outside external devices that exchange energy to the pack. On the other hand, outputs are represented by the state of the pack, such as SoC and SoH, power limits, the battery status and contactor controls. Accordingly, BMS have to implement the proper physical interfaces to interpret both the measurement information and the communication protocols. Best practice in system and software engineering is to develop an architecture that provides only the information needed to each device of the other subsystems connected to the battery pack, resulting in an effective system architecture. The design criteria to select the adequate architecture for the specific architecture also include the reliability, cost, easy of installation and maintenance and, last but not least measurement accuracy.

Once the behavior of the external subsystems has been defined, the design stage of the battery management system can begin. The BMS is realized on a printed circuit board (PCB) that integrates one ore more general-purpose microcontrollers with other electronic circuitry for measuring, power and control. For small systems, which involve low number of cells and resulting in low voltage battery pack and low capacity, it's possible to realize the BMS functionalities by selecting some defined-purpose integrated circuits (ICs), while for larger systems with high-battery voltage it becomes necessary to consider specific embedded systems. The differentiation between high-voltage and low voltage is related to the low voltage safety limit for human beings, that is 60 V in DC applications according to IEC standard. It is possible to distinguish two different boards, as embedded system for BMS, with respect to the proper task addressed: cell/module monitoring unit (CMU) and battery pack control unit (BCU). CMU usually implements an analog front-end (AFE) chip that is charged of cell voltages and temperatures measurement as well as communicate with the master unit of the BMS, that is the BCU. Analog front-end chips generally include high resolution analogic-to-digital converters (ADCs), high-precision voltage references, high-voltage multiplexers, and an SPI interface. Besides, the BCU integrates a microcontroller that is able to perform several calculations and integrate the interfaces needed to communicate with CMUs, such as SPI, and external world, such as CAN and Ethernet.

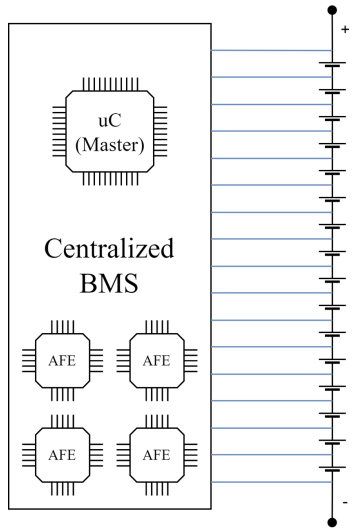

Figure 2.1: Centralized architecture for battery management system

The BMS architecture is classified on the basis of how CMU and BCU are integrated to realize the BMS. It is possible to distinguish two main architectures, namely centralized (or monolitic) and distributed.

2.1.1 Centralized

Centralized or monolithic architecture integrates all the required functionalities in a single system, hence CMUs are implemented together with the BCU on the same printed circuit board. Therefore, centralized architecture represent the simplest solution for battery management system considering the reduction in definition, design and cost of interfaces with respect to a scenario in which different boards are involved.

The centralized architecture is illustrated in figure 2.1 for a generic battery pack composed of n cells connected in series.

The scalability of monolithic battery management systems is inherently constrained. The ability to monitor cells is tied to the number of cell-monitoring circuits that are installed in the system. If there is a need to monitor a larger number of cells, additional circuits need to be added. Notably, this configuration may preclude the monitoring of arbitrary lower quantities of cells, thereby impeding adaptability. In contrast to the expectation, there are no cost savings for smaller batteries because the number of components in the battery management system cannot be easily reduced for smaller systems. In other words, the system may not efficiently scale

down in terms of cost when dealing with smaller batteries.

Monolithic systems require the single controller to support the entire pack voltage and all the cell measurement connections. The creepage and clearance distances must be larger due to higher voltages. Connector and component ratings must also be appropriate and the number of possible component choices for a given application may be restricted

Although a proper design of this architecture, the potential for much higher voltage and energy under fault condition remains. Furthermore, for a centralized BMS, the complexity of wiring and connections of measurement circuits and physical communication interfaces increases exponentially, especially for a large battery pack.

In the case of very large volumes, a battery management system offering only the required features will provide the lowest cost and complexity at the expense of flexibility and scalability.

2.1.2 Distributed

Distributed BMS architecture is based on the concept of modularity and hierarchy which allow to fractionate the whole battery management system in several board with different tasks. This results in a master-slave architecture, as illustrated in figure 2.2, in which the top level of hierarchy is represented by the BCU that oversees a certain number of similar or identical slave CMUs, each one directly connected to a group of cells of the whole battery pack. The number of the slave depends on the level of modularity required for the specific application.

Slave boards address specific low-level specific tasks such as measurement of cell voltages and temperature as well as activate or deactivate the balancing circuits. On the other hand, master board receive measures from slaves and perform several calculation for fault detection, state estimations, switch management, charge and discharge control and communicate with the external load network. The communication between master and slave devices can be facilitated through a variety of protocols. These may encompass proprietary protocols designed for specific applications or widely used, standardized protocols such as CAN (Controller Area Network), RS-232 (Recommended Standard 232), or Ethernet. The implemented communication have to ensure the synchronization of the measured data with delays as lower as possible.

The split of the calculation and monitoring tasks leads this architecture to present a better efficiency for each functionality. The intrinsic modularity of distributed BMS leaves the possibility to easy extend the battery pack and for a better distribution of module in such application with strong limits in available space.

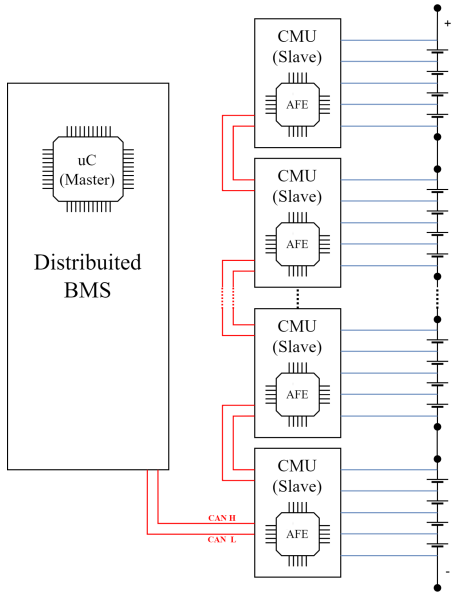

Figure 2.2: Distributed architecture for battery management system

The weaknesses of this architecture is the additional cost of physical interfaces for communication and support circuitry slave require with respect to the centralized architecture. Indeed, each slave present his own microprocessor that need to be supplied by a proper circuitry while assuring the isolation with the earth ground. Usually each module of the battery pack represent a low voltage system by itself. However, when they are integrated together, the upper module that compose a string on a battery pack is operating with a big voltage difference with respect to the earth ground of the system, and this it must be taken into account in slave board design to avoid hazardous condition for operators and peoples. These These extra circuitry also impact on cost and size of the BMS, thus, consequently on the entire battery pack design.

2.2 Functionalities

Regardless the architecture and the complexity, the battery management system is designed to address specific purposes. First, it has to protect the safety of the operator of the specific system in which the battery pack is integrated. Second, BMS is developed to protect the each cell of the battery pack from any abuse or failure condition. Hence, the primary goals of the battery management system are related to safety. Third, it should be

able to prolong the lifetime of the cells under normal operating conditions, coordinating the energy and power request with the external load network. Fourth, battery management system aims to keep the battery pack in a state in which it can fulfill its functional requirement as design condition. In order to address these specific purposes, it is possible to identify the functional requirements a BMS need to implement.

- *Monitoring*

  The BMS has to extract information of physical quantities from the cell by measurements. THey are represented by cell voltages, temperatures and string current. Furthermore, isolation measurement is usually implemented for detect any faults.

- *Safety and protection*

  As discussed before, the primary goal of the battery management system is to protect operators and the battery pack itself against hazardous conditions. This task is addressed to specialized electronic components that are able to operate both in normal and failure condition and allow to isolate the battery pack from the load.

- *State estimation*

  On the basis of the measurement within the pack, the BMS calculates the main cell/pack parameters related to the state of charge, aging condition and the limit in power to ensure the battery pack still operate within the safety operating area (SoA).

- *Performance optimization*

  The BMS implements software algorithms that aim to maximize the performance for every operating scenario. For example, several strategies to reduce the charging time of the battery pack while ensuring safety are implemented as well as balancing circuits that allow to maximize the overall usable capacity of the pack.

- *Interface and communication*

  The Battery Management System (BMS) is required to establish regular communication with the application powered by the battery pack. This communication involves reporting information on available energy and power, as well as relaying relevant details about the current status of the battery pack. An additional feature includes the capability to record uncommon errors or instances of abuse in permanent memory.

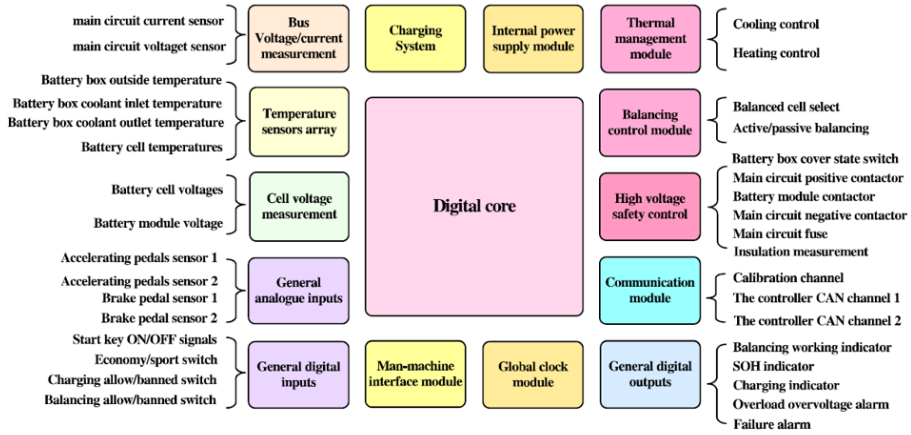

Figure 2.3: Basic framework of software and hardware BMS for EV [14].

Moreover, depending on the application, specific tasks can be required. As example, the main functional requirements for a BMS in an EV are summarized in figure 2.3.

2.2.1 Monitoring

2.2.1.1 Voltage Sensing

The cell voltage measurements are used to detect and avoid any overvoltage and undervoltage conditions, calculate SoC and SOH, calculate and enforce current and power limits, and detect battery failures. In a large-format battery system, the measurement of battery voltages can span various levels, encompassing individual cells, groups, or modules of cells, and extending up to the comprehensive assessment of the entire series-connected string. Since series-connected cells in the same battery pack are not necessarily of the same capacity or at the same state of charge, at least one voltage measurement of each series element is required.

In most cases, the battery cells are connected directly to the battery management system and the cell voltages are measured directly, hence the physical interfaces for the voltage signals are the cell voltages themselves. The battery management system design and implementation should aim to create a unity-gain transfer function such that the voltage measured at the battery management system is exactly that which is present at the terminals of the battery cells. Design concern of the voltage monitoring system is related to the parasitic power consumption. Indeed, the voltage measurement circuit need to exhibit a high DC impedance with respect to the

voltage terminals of the cell because it results as a load that draws current from the battery, discharging it. For this reason, cells with low capacity need much higher impedance to avoid that the measurement circuit of the BMS increases the apparent self-discharge of the cell. In addition, it is important ensuring each cell to experience the same power consumption with the aim to keep the states of every cell as uniform as possible, limiting imbalances and any reduction of the performance.

The characterization of the measurement circuit's impedance in both active and passive modes is crucial for designing an efficient and reliable battery management system. In the active mode, the BMS is actively taking measurements from the battery cells, whereas the passive mode, also known as standby mode, occurs when the BMS is not actively taking measurements, and the system is in a powered-down state. During this phase, the BMS still consumes a certain amount of current that need to be minimize in order to decrease the risk that the system goes towards undervoltage condition. The parameters that need to be considered for the optimal design of the measurement circuit's impedance are represented by the overall duty cycle of the battery system and battery management system, the capacity of the battery, the expected standby time and the minimum state of charge at which the battery may be operated.

Another requirement of the cell voltage measurement system is represented by the voltage range. Indeed, each individual voltage measurement channel have to cover the range of the cell voltage for the normal operating condition as well as it is desirable that the battery management system is able of handling cell voltages outside the normal operating area. This allows the BMS continue to behave if any abuse condition of overcharging or overdischarging occurs, preventing further abuse.

Measurement of the complete battery series string voltage, as well as module or substring voltages, is also commonplace. This additional layer of measurement provides a significant benefit in terms of failure detections by comparing the sum of the measured voltage of the single cell composing the string, and the measured voltage of the entire string itself. This comparison can be also used to detect calibration errors for measurements.

Since the string voltage is much higher than the cell voltage, the measurement unit for string is composed by a voltage divider, an impedance converter, a filter and the Analog to Digital Converter (ADC).

Measurement accuracy of cell voltage measurement system also represent an important decision parameter. Since cell voltages are used to compute the state of the battery pack, especially SoC, low accuracy in voltage measurements leads to high errors in state of charge estimation. Therefore, the specification for cell measurement accuracy is driven by the

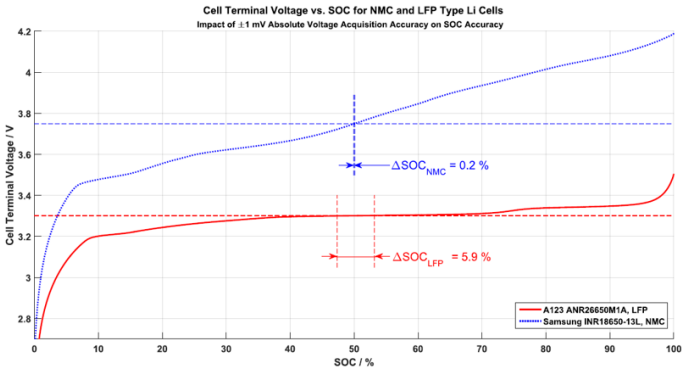

Figure 2.4: Comparison of SoC uncertainty between an NMC and LFP cells, depending on the voltage accuracy [15].

desired state of charge accuracy and the shape of the battery OCV(SoC) curve. Different cell chemistries exhibit different shape of the OCV characteristic and the low accuracy in voltage monitoring system leads a bigger errors for chemistries in which the static curve is flat. Figure 2.4 illustrates a comparison of the error generated in SoC estimation on the OCV-SoC curve between an NMC and LFP cells, considering the accuracy of 1 mV.

It results a large SoC estimation error for the LFP chemistry and the only voltage acquisition is not sufficient to thoroughly estimate the state of charge of the cell. Measurement system with higher voltage accuracy can also be implemented with higher cost.

The design and selection of the voltage monitoring system is crucial to prevent hazards asSoCiated to the overcharge and overdischarge conditions. In case of the measurement unit goes into a failure modes, the overall battery pack is not safe and a single cell can go towards the thermal runaway. For this reason, several BMSs implement a redundancy in voltage measurements or other solution to decrease the risk of possible unsafe states for the battery pack. However, a systematic analysis of functional safety aim to enumerate the risk asSoCiated with overcharge and overdischarge event connected to a failure mode of the measurement unit. Actually, the functional safety analysis takes into account the possible failure modes of the whole battery management system, in which several subsystems collaborates, for each task such.

2.2.1.2 Current Sensing

String current measurement is fundamental to compute SoC and SoH estimation tasks. As discussed above, the cell voltage in static characteristic can not be sufficient to determine the state of charge of the battery whereas the error in estimation increases if neglecting the internal resistance and dynamic phenomena during charging and discharging profiles. On the other hand, the accurate measurement of the total current allows for determining the extracted or filled capacity by integrating the current. This measurement is also important to detect any overcurrent conditions and thus provides safety. Since all cells connected in series experience the same current, a single current device for current measurement needs to be implemented for each string. Redundance measurements can be integrated for application in which the state of charge performance is a crucial factor or when the dealing with a significant range of currents that may exceed the battery limits (i.e., fuses).

Regardless the device for the measurement, some requirements need to be considered for design the current measurements. The first parameter is the range, which must be sufficiently large with the aim to cover the expected maximum and minimum current the battery can provide and receive, in discharge and charge, respectively. It is important to point out that the most battery cells/packs are asymmetric in power capability for charge and discharge.

The second important specification regards the accuracy which usually varies with respect to the current amplitude and results difficult to measure small and big current magnitude with the same degree of accuracy. The wide dynamic range of application currents in battery systems, especially in automotive applications, presents challenges in achieving accurate and consistent current measurements. The issues related to nonlinearity, discretization, and offset errors in current sensors can indeed impact the relative accuracy of measurements, particularly when attempting to measure both large and small currents with the same degree of precision. This can be particularly critical in applications where errors in small currents, over an extended period, significantly affect state-of-charge (SoC) determination through current integration.

To address the current measurement, there are two different sensors type: galvanically connected, such as shunt resistors, and isolated represente by the Hall-effect sensors. Shunt resistor current sensing is a cost-effective and widely used solution, while Hall-effect sensors provide electrical isolation, making them suitable for applications where isolation is a critical consideration.

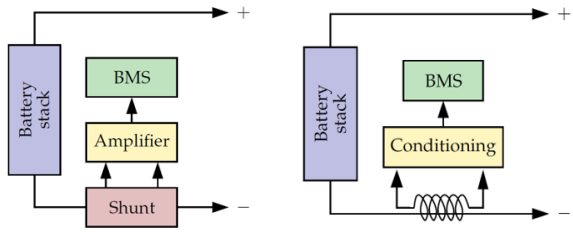

Figure 2.5: Sensing current with (a) shunt resistor and (b) Hall-effect sensor [16].

- *Shunt Resistor*

  Shunt current sensing is a low-value resistor with high-precision that is connected in series to the battery pack. The typical order of magnitude of the shunt resistor is fraction of milliohms, and the voltage drop across the shunt resistance is measured through an ADC. This voltage allows to evaluate the current through the Ohm's law. The resistance needs to be small for limiting the power losses associated with it, then the voltage drop is also small. Therefore, there is an amplifier stage between the voltage drop across the shunt and the BMS, as illustrated in figure 2.5a. Current shunts are characterized by four-wire (or Kelvin connection) with the aim to separate the current carrying terminals to the voltage sensing terminals. This type of current sensors has the advantage of zero offset in output voltage at zero current, regardless the temperature, resulting very important for the SoC estimation task. Nevertheless, the electronic circuit for the amplification stage can introduce an offset that needs to be calibrated. For these reasons, amplifier circuitry requires to present a high common-mode rejection ratio, low DC offset, high and accurate gain (typically 100 or more) and good stability with temperature.Moreover, they are relatively cheap, present an accuracy of 0.1% to 0.5% and they are characterized by an intrinsically large bandwidth.

  The biggest weakness is represented by the complexity of the circuit that is needed to both amplify the voltage drop across the shunt resistor for measurement and electrically isolate the high voltage circuit and the BMS circuitry. Indeed, the BMS is usually powered via a low-voltage supply (typically 12V for automotive applications) which is isolated with respect to the high voltage circuitry. Therefore, the isolation and amplification electronics add complexity to design the BMS boards. Furthermore, the resistance varies with the tempera-

ture and, for high-power applications, the size and the weight of the shunt current significantly increase.

- *Hall-effect sensors*

  The working principle of these sensor is related to the production of a voltage across a conductor, proportional to an electric field in the presence of a magnetic field. The presence of the magnetic field is generated by the main battery pack current-carrying wire and no direct electrical connection is made between the sensor and the high-voltage system. This represents the major advantage that distinct this current sensing solution because it avoids designing specific isolation circuitry to interface the output voltage to the BMS. Nevertheless, conditioning circuitry needs to be implemented to limit the hysteresis of the Hall-effect sensor. They also suffer of measurement offset at zero current, which tends to shift over time and vary with temperature changes and a meticulous calibration process must require to ensure accurate and reliable measurements. Since the Hall effect sensors is direction-dependent, the sensor will give negative values if it is installed incorrectly. Hall-effect sensors must be powered by an external source, which usually is the BMS electronics. This voltage source also defines the full range of the output voltage that prevents current measurement errors due to different voltage references. Hall effect sensors come with either unipolar or bipolar outputs. Unipolar Hall effect sensors translate the complete range of currents into a positive output voltage, while bipolar sensors generate positive voltages for positive currents and negative voltages for negative currents. Unlike many other types of control circuits, circuits for bipolar sensors necessitate a bipolar supply voltage.

2.2.1.3 Temperature

Unlike the cell voltage, temperature is a variable that varies with space indeed it is not possible to asses that a single cell is characterized by a single temperature, especially for large capacity cells in prismatic and pouch shapes. Since that, it results very challenging to define the optimal number and location of temperature sensing points within the battery pack. It is crucial to understand how the temperature distributes among the cells because its knowledge is important for estimating the states, predicting the performance of the pack and controlling the thermal management system (TMS) in order to maintain the cell temperatures within the safety operating range. Nevertheless, the cell temperature is not homogeneous among the volume of the cell, and it is often higher inside the cell where the reac-

tions occur. Thus, the ideal solution is to measure the temperature inside each cell of the pack but not all the cell commercially available are produced with an internal sensor, then external measurement for temperature needs to be implemented. In order to know the temperature distribution among the cell of the battery pack and minimize the total number of the sensor to be adopted, an accurate thermal model of the pack need to be calibrated. Reducing the total number of the temperature sensors means cost reduction, which is a specification for every task in designing a battery pack.

These sensors typically change in resistance or voltage in response to the temperature measured. The range of the signal must be appropriate in both the temperatures expected and the voltages produced by the sensors at these temperatures. Temperature measurements may be earth referenced, high-voltage stack referenced, or floating. Usually, the temperature sensors used for BMS applications are thermistors, which are characterized by a variation of the output resistance with the temperature. They represent the most adopted solution due to the low cost and the input-output characteristic that is approximated with a linear curve without loosing accuracy for a wide range of temperature. There are two commercially available types: positive temperature coefficient (PTC) thermistors, in which the resistance monotonically increases with respect to the temperature, and negative temperature coefficient (NTC) thermistors, in which the resistance varies inversely. Other possible solutions are represented by PT100, thermocouples or metal-based PTC. They offer higher lower uncertainties and a wider temperature range at the expense of higher complexity in terms of electronics and, then, higher cost.

2.2.1.4 Isolation

In many large-format systems, the DC battery voltage is not referenced to any earth or chassis ground. In the case of EV and HEV automotive battery systems, the high-voltage battery is isolated with respect to chassis ground, which is referred to the low-voltage ground system, typically 12 V. This provides an extra measure of safety in that a single point fault where the HV system is connected to earth ground does not create a large fault current. Isolation faults pose risks to individuals working on battery systems, and the presence of multiple distributed isolation faults at different potentials can create short-circuit hazards. Due to these safety concerns, many applications explicitly state that operation with compromised isolation resistance is either prohibited or, if allowed, must be accompanied by a warning to users. This is crucial to ensure the safety of those working on battery system and to prevent accidents or damage to the system due to

compromised isolation. These faults can result from moisture ingress, foreign objects bridging conductive parts, the formation of conductive bridges on circuit boards, internal faults within isolating components, insulation breakdown, and other potential hazards such as accident or vibration in a vehicle. Because the remainder of the system may not be energized if the battery is disconnected, it makes sense to place this functionality inside the battery system.

Electrical insulation can be modeled with the electrical resistance of the material that allows insulation. Actually, this resistance is distributed over the whole floating electric circuit, however it is possible to derive a concentrated model of isolation for the battery pack in which two equivalent resistances represent the isolation of the battery pack with respect to the earth ground, as illustrated in figure 2.6. In details, R_p and R_n represent the insulation resistances of positive and negative high-voltage terminals with respect to the reference ground, respectively, while C_p and C_n represent parasitic capacitances. On this basis, the insulation monitoring device (IMD) is installed at the high-voltage terminals of the battery pack and connected to the earth ground. This device is able to measure the equivalent insulating resistance between each high-voltage terminal and the ground reference (i.e., the chassis in electric vehicle) by means the connection of a known resistance with large value between one of terminal voltage and the earth ground of the system via a transistor switch. The measurement of the voltages between each terminal voltage and the earth ground are performed allowing to characterize the two isolating resistance of the concentrated model in figure 2.6.

Further details about the specific procedure for measuring the insulating resistance is reported in [15].

2.2.2 Safety and Protection

The first purpose of the battery management system is minimizing the risk and severity of possible hazard conditions can involve lithium-ion battery cells.These undesired conditions or events include excessive current during charging or discharging, short circuit, overvoltage or undervoltage, high ambient temperature or overheating, loss of isolation and other abuse. Hence, battery packs need to integrate some electronic devices which are able to prevent and avoid any fault condition occurs with a proper control performed by the battery management system. These electronic components are represented by the main contactors, precharge contactors, manual service disconnect (MSD), high voltage interlock loop (HVIL) and fuses. Moreover, bus bars, cell interconnect boards and wiring harness can be adopted for safety concerns as well.

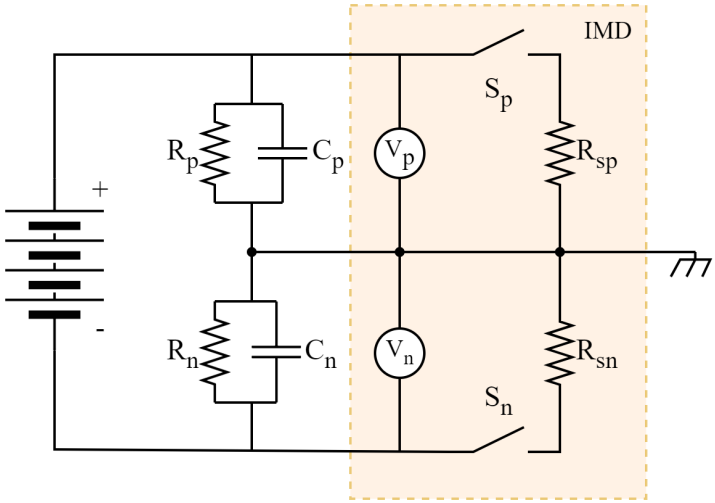

Figure 2.6: Insulation model considering concentrated parameters and insulation monitoring device connected.

2.2.2.1 High-voltage contactor control

High-voltage battery packs are designed to be electrically insulated with respect to the chassis ground with the aim of increasing safety if someone unintentionally contacts one of the battery terminals and the ground potential. However it is not a safety condition if there is another isolation or ground fault. For similar reasons, the battery pack is galvanically isolated to the external load network when the application is not in use. The connection and disconnection of the high-voltage terminals of the battery pack to the load is provided by two high current relays known as contactors. They are used in battery-powered system in normally-open configuration and the BMS implements and controls the electronic circuitry to connect the two contactor power terminals. Indeed, these devices present 4 clamps, 2 for the high-voltage system and the others for the command. Normally-open contactors allows the BMS to connect the battery pack to the load only after a positive check on both battery pack and external load as well as disconnect the battery pack when a severe fault condition is detected or in case the BMS loses power for any reason.

In addition, it needs to be consider that usually battery packs interface with a capacity load, as in EV application in which the fed electric drive (inverter plus motor) present large capacitor branch to filter transients generated by the inverter modulation, leading high rush current if a direct connection occurs from the high-voltage terminals of the battery

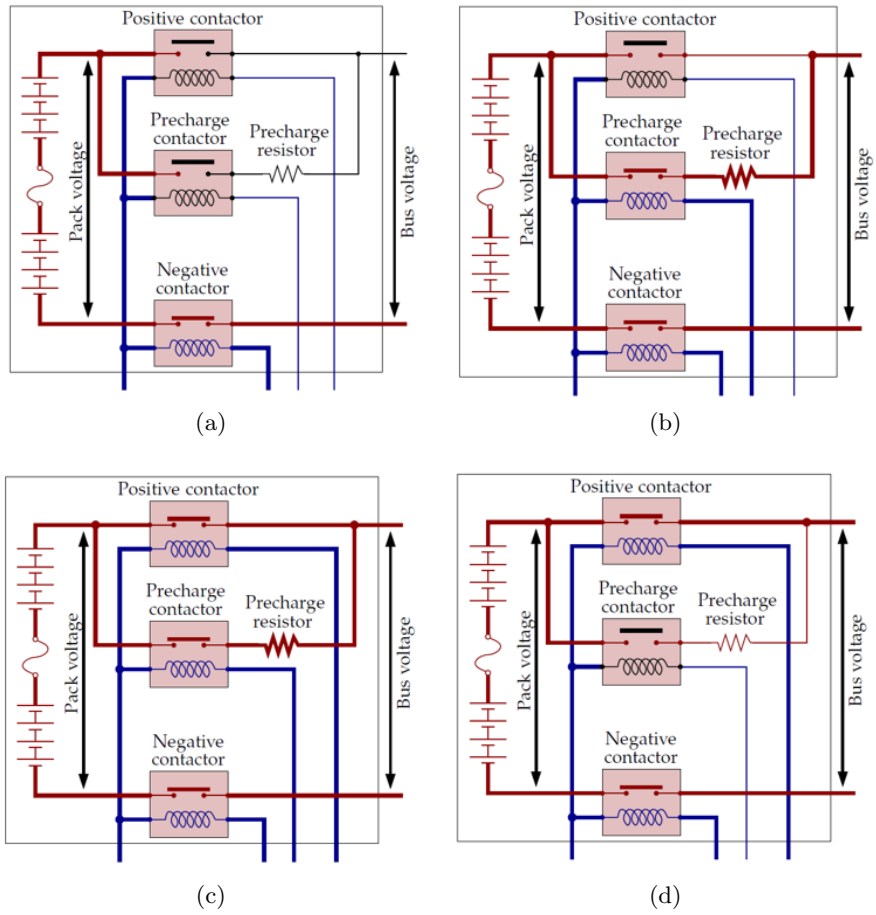

Figure 2.7: Precharge contactor procedure steps [16].

pack and a discharged capacitor. This represent an unsafety condition that can potentially weld the contactor or blowing a fuse. Therefore, a third contactor is always implemented with the aim of allowing to limit the in-rush current due to the high voltage difference between the capacitor and the voltage battery pack. In detail, this contactor, called precharge contactor, is connected in series with a resistance and together in parallel to the positive contactor offering an higher impedance to the current path. The complete precharge procedure is reported in figure 2.7 starting from a complete disconnection between the battery pack and the external world. The first contactor enabled is the negative one (figure 2.7a), then the precharge contactor is activated (figure 2.7b). The resulted equivalent

circuit is composed of the battery pack, the capacity load and the precharge resistance that limits the current magnitude, allowing to charge the filter capacitors slowly. Usually, during this phase the temperature of the resistance is monitored to eventually detect any short circuit condition in the external load. In case of fault the startup process is aborted and the battery pack is newly disconnected to the external circuit. If no fault is detected, the BMS proceed the battery pack connection to the load by closing the positive contactor (figure 2.7c) that is parallel to the precharge branch. In this phase, the voltage across the capacitive load is monitored and when it becomes greater than a specific threshold the positive contactor is closed and, subsequently, the BMS opens the precharge contactor (figure 2.7d).

On the other hand, no standard procedure exists for battery pack disconnection but it is necessary to know if the load present a large inductance for ensuring to drain the inductive energy before completing th disconnection of the battery. In this case, it is suggested to use the startup procedure in reverse.

2.2.2.2 High-voltage interlock loop

High Voltage Interlock loop(HVIL) is a safety feature that uses a low-voltage loop to monitor the integrity of a high-voltage circuit. This safety feature is designed with the aim of preventing people come in contact with components of the high-voltage system. Basically, HVIL creates a closed circuit when the battery pack is sealed. The role of the HVIL is to guarantee safety conditions in both service and maintainance operations. This feature is not realized by a single component integrated within the battery pack, but rather a number of components, software and control that involve not only the battery pack but all subsystem of the specific application. The interruption of the interlock loop causes the opening of the main contactors and, on the other hand, it disallows to open the battery pack if HVIL is not disengaged.

Interlock loop has to be designed in such a way that a conductive path between two elements of the loop signal is interrupted when a n insulating barrier becomes compromised. For example, additional low voltage terminals are included in high-voltage connectors which generally creates a short circuit (or a closed loop) only when the HV connector is mated. This status is reported to the BMS that command the main contactors. Another solution regards the possibility to connect the high-voltage wires through a Manual service disconnect device (MSD), which is a manual connector that also integrates a fuse. This device is usually placed at the middle of the pack in such a way to divide the energy stored in the battery pack in two when MSD is removed. Once removed, the HVIL results opened and the

BMS will command the opening of the main contactors. These solutions are useful to protect the battery pack from external short circuit as well.

2.2.2.3 Fuses

These devices are installed in a battery pack to prevent very high currents. They can be described as passive overcurrent protection devices since they do not require any input from the BMS to operate. However, battery management system needs to detect the state of the fuse to ensure the correct functionality of the battery pack. The BMS is able to know if the fuse is blown or not by measuring the high voltage on both terminal of the fuse with respect to the battery pack reference. Depending on the size of the battery pack, fuses can be installed along with the MSD device and/or in series of the high-voltage terminal of the battery pack. Several manufacturers also incorporate smaller-size fuses directly within the control boards interconnecting the cells. This way, safety enhancements can be accomplished in the event of a single cell failure, lowering the impact on the battery pack. Moreover, fuses can be also packaged together with the other safety components mentioned above, leading to a single physical unit named as battery disconnect unit (BDU), usually adopted for very large energy storage systems.

Reaction rate of fuses is usually very quickly, especially for semiconductor-based type designed to protect electronic devices, but it still depends on the current amplitude. Indeed, since they are characterized by the specific energy allowed to pass through, the lower the current the slower the fuse blow. It is important to take care of this in design protection fuses in order to avoid fuse oversizing which can lead in other battery components being exposed to the risk of overcurrent. Accordingly, battery management system have to integrate proper strategies to take action against moderate overcurrent that creates damages to the battery pack before clearing the fuse.

2.2.3 State Estimation

Battery management systems require to estimate some quantities that are not possible to directly measure but they result fundamental to describe the current condition of the battery pack. It is possible to distinguish between quantities that can experience a significant change even in a short period of time, and others that exhibit small changes over a long period of time. Considering lithium-ion batteries, the former quantities include SoC, diffusion current, hysteresis, whereas the latter are represented by the capacity and the internal resistance of the cell, for examples. Both of

quantities result fundamental for battery management requiring different strategies in order to perform a proper estimation. In this paragraph, the main aspect for the implementation of state of charge, state of health and state of power estimation algorithms are described.

2.2.3.1 State of charge (SoC)

State of charge (SoC) represents the ratio of the amount of electrical charge currently available for discharge from the battery with respect to the nominal capacity of the battery cell, considering the same standard conditions. It has the same function of a dashboard fuel gauge allowing to know the level of the available source. At electrochemical stage for a single cell, the information of the state of charge can be referred to the concentration of the usable lithium stored in the anode of the battery cell. As it is possible to comprehend, this quantity can not be directly measured, thus the BMS needs to integrate and implement a proper estimation algorithm in order to evaluate this quantity with an approximation consistent with respect to the requirements of the specific battery-powered application. Hence, in order to calculate a proper estimation of the SoC there is the need to somehow combine the measured variables of current voltage and temperature with the knowledge from the model of the cell. A generic overview of the main adopted SoC estimation algorithms with their pros and cons is reported in 3.1. Since the SoC ca not be directly measured, the true knowledge of the state of charge emerges as an issue, and it is important in order to evaluate and compare the different estimation methods. The main approach to overcome this problem result in the well definition of the fully charged and fully discharged conditions, which can be verified at equilibrium conditions at a specific temperature.

It is important to remark that there is not a uniform accepted definition of the state of charge. Defining the SoC becomes more complex by considering a battery module or the whole battery pack. Indeed, in any real battery pack, the different cells connected in series and in parallel have a capacity that is not perfectly equal, even if they are from the same production batch, as well as an imbalance of state of charge between the cells. Generally, for safety purposes, the BMS consider the SoC only of the most and the least charged cells for battery operations allowing to prevent any possible abuse condition of overcharging and overdischarging, even though the amount of charge stored in the battery pack with respect to its nominal capacity result as a different state of charge. The latter information becomes crucial when the BMS integrates an active balancing system to equalize and maximize the state of charge of the cells.

The information of the SoC is crucial in every process the BMS has

to control, thus its estimation represent the first process the BMS perform after the safety check of the cell voltages and temperatures. The state of charge also represents an information that is communicated to the connected external system resulting fundamental for optimize the energy management. It can be expressed both as a fraction between 0 and 1 and/or a percentage, and it is usually computed with a resolution that varies between 1% and 0.1%.

Another important thing to point out is that the SoC is not necessary an indicator of the useful energy content in the battery. The state of charge matches the indication of the energy only in case the terminal voltage is constant over every operating condition. However, the lithium-ion cells are characterized by a terminal voltage that varies with respect to the state of charge since either the internal resistance and OCV vary with the state of charge and because of the effect of the polarization and hysteresis. As discussed in chapter **??** several chemistries present a significant change of terminal voltage with the depth of discharge, thus the the first Ampére-hour delivered from the battery contains significantly more energy than the last one. In these cases, it is preferable to include methods for calculating the state of energy (SoE). This result another very challenging task since the amount of energy can be extracted from the battery is strictly depends on the discharging C-rate.

Depending on the application, the BMS could include algorithms for estimating both SoE and SoC. A lookup table can typically be used to determine SOE as a function of SOC.

2.2.3.2 State of health (SoH)

State of health (SoH) is a quantity that is used in battery applications to describe with a simplified metric the effects of the complex phenomena which combined produce degradation. Indeed, the SoH is an indicator of the present performance of a battery with respect those ones the same cell could offer at the beginning of life. When this parameters becomes lower than a certain threshold, defined proper for each specific application, the battery are considered at their end of life, since they are not able of providing the minimum power, energy and standby time the application needs, then the batteries have to be replaced. Degradation mechanisms described in section 1.6 produce externally observable effects such as capacity fade and the increase of both the internal impedance and the magnitude of self-discharge phenomenon. Usually, automotive and industrial applications consider the end of life of the battery pack when the battery pack is able to retain the 80% or less of its initial capacity, and/or internal resistance increases of 50-100%.

Capacity fade results in a reduction of the available charge capacity of the battery over time, whereas the impedance growth causes an increment of the internal resistance of the cell resulting in a significant reduction of the power capability of the cells. These effects are accelerated if the battery pack operates at very high C-rate, especially during charging processes, at high temperatures and at extreme state of charge. The understanding on how these parameters vary over time and under the different condition of current profile and temperature allows for modifying the battery management methods to account for aging. Therefore, the estimation of the state of health is integrated in the battery model to adjust the model parameter properly, allowing the model not to lose accuracy in prediction over time.

Since the SoH is a quantity that exhibits a small variation over a long period of time, a large amount of the data are necessary to achieve an accurate approximation of it. Usually, a very long experimental characterization is performed on the cells in order to calibrate aging models and predict how the capacity and internal resistance vary under certain circumstances.

The problem of the estimation of the SoH and remaining useful life forecast remain challenging because the models are non-exact, non-stationary and characterized by non-Gaussian noise, as well as batteries present strong non-linearities relationship between the different variables and parameters.

2.2.3.3 State of power (SoP)

The load device in most large-format systems is designed to accept information from the battery management system regarding the battery's capabilities for charging and discharging, as well as to respect the constraints set by the battery. Power limits change dynamically with the state of charge and temperature over the course of a single cycle, and also changes as the battery ages and becomes reduced in performance. As a result, the battery management system has to include algorithms to identify acceptable limitations based on battery state. These algorithms must be precise; if they are too conservative, the battery will perform badly and will need to be oversized; if they are overestimated, the battery may be mistreated by the load in operation.

The power limit algorithm is perhaps more essential than the state of charge computation in certain application. A hybrid electric vehicle is an excellent illustration of this. In a HEV, the battery serves as a power source/sink rather than a large energy storage device. Because there are various sources of energy, the vehicle management scheme will try to use electrical energy rather than combustion energy wherever possible, and to regenerate electrical energy rather than dissipate thermal energy through the friction brakes. Since the vehicle's performance should be independent

of the battery's state, the vehicle control system must know the real-time capabilities of the battery pack of providing and receiving power extremely precisely.

The first major goal the power limit estimate algorithms have to address is to maintain the terminal voltage of every cell composing the battery pack in the safety operating area during operation with the battery powered system connected. This statement means that any imbalances need to be taken into account and the most extreme cells, in charging and discharging, will limit the performance of the whole battery pack, even though the total power requested depends on the voltage sum of the series-connected cells.

Most battery cells have a maximum and minimum permitted terminal voltage. The limit method then computes the current or power at which the battery terminal voltage is projected to approach these limitations. However, it is also important to consider thermal limitations when estimating current and power capability of the pack, despite the temperature response is usually the slowest in battery operations.

Another important issue that needs to be considered for SoP estimation requirement is to determine in which form the limit needs to be communicated from the BMS to the load. In detail, charging and discharging power limits can be expressed either in terms of current or power. Despite for battery management system results more intuitive express the power limit in terms of current due to better control on voltage battery response, most of the applications prefer to receive the specification of the battery pack capability in terms of power. For example, in EV applications, the vehicle control unit (VCU) usually implements efficiency map for setting the torque request to the motor, thus the limit expressed in power is a specification in order to be easily converted in a limitation of torque for the powertrain by dividing that power limit to the motor measured motor speed.

2.2.4 Optimization of performance

Once the battery management system has ended the primary processes of acquiring the monitored variables among the cell, checking the safety operating condition and defining the state of the battery pack, it can perform some other tasks to allow for optimizing the performance of the battery pack in terms of power and energy exchanged as well as ensuring the durability of those performance over time. In detail, these requirements aim to ensure the cell are performing under the same operating conditions in terms of state of charge and temperature that allows for maximizing the usable capacity stored in the battery pack.

The BMS is able to perform these task by integrating some other additional circuits and component in which it acts as the brain. In particular,

the battery management system integrates a balancing circuit and a thermal system (generally cooling and heater).

2.2.4.1 Cell Balancing

Maintaining optimal battery performance over an extended service life in large-format battery systems necessitates the implementation of a carefully devised charge balancing strategy. This strategy is crucial for addressing variations in cell performance within the battery pack. An effective cell balancing system is essential to sustain the desired battery performance throughout its lifespan, ensuring a safety margin without introducing excessive cost, weight, or complexity. Designing an appropriate cell balancing approach requires a comprehensive understanding of the batteries themselves. Unlike some other types of batteries, lithium-ion batteries, owing to their high coulombic efficiency, do not naturally "self-balance." Without proper management, any initial imbalance among cells will not spontaneously correct over time.

Several critical system and battery cell parameters must be considered when conceptualizing a cell balancing strategy. Understanding the anticipated differences in cell capacity is paramount. In the absence of charge-transfer balancing, the overall series-connected string's capacity is limited by the lowest capacity cell. Charge-transfer capabilities can be employed to redistribute energy from high-capacity cells to low-capacity cells during discharge, effectively increasing the battery's usable capacity.

Additionally, real-time monitoring of the differences in state of charge between cells is indispensable for effective balancing. Balancing circuits must account for variations in self-discharge rates and discrepancies between cells. Battery self-discharge, generally undesirable, should be minimized by the cell supplier. Differences in self-discharge rates may arise from manufacturing variations or the presence of defects in individual cells. The sizing of the balancing circuit is influenced by these self-discharge rates, emphasizing the importance of a meticulous approach to cell balancing for ensuring the longevity and performance of large-format battery systems.

The design of a cell balancing system is driven by specific goals aimed at optimizing the performance and longevity of a battery pack. These objectives include:

1. *Minimize differences in charge between cells*: One of the primary goals is to reduce variations in charge levels among individual cells. Differences in charge directly impact the effective capacity of the entire battery pack. By minimizing these differences, the overall capacity of

the pack is maximized, ensuring that each cell contributes optimally to the pack's energy storage capability.

2. *Maximize available battery power*: Cells at different states of charge (SoC) exhibit varying power capabilities due to SoC's influence on cell impedance. Drifting cells to high or low SoC levels can limit both the battery's power output and energy capacity. The cell balancing system aims to prevent such drifts, thereby maximizing the available power from the battery pack.

3. *Maximize available battery energy*: In cases where cells within the pack have unequal capacities, a situation may arise where cells with higher capacity still hold useful energy when the lowest-capacity cells reach full discharge. However, extracting this energy is challenging without overdischarging the smaller cells. The cell balancing system addresses this by facilitating the transfer of charge from larger cells to smaller ones, enabling the recovery of stranded energy. This ensures that the entire capacity of the battery pack is effectively utilized, enhancing overall energy efficiency and utilization.

2.2.4.2 Thermal Management

Thermal management is a very important aspect of BMS design since the temperature strongly affects the performance of the cells, degradation mechanisms and safety. In general, lithium-ion batteries exhibit the longest durability if they are kept in a temperature range between 10°C and 35°C. Temperatures below 10°C leads to the reduction of the capacity and the increase of the internal resistances with an overall reduction of the performance, whereas temperatures above 35°C accelerate degradation processes and cen bring the cell to the thermal runaway.

During normal operating condition, a lithium-ion battery cell that delivers current generates heat which contributes to increase the cell temperature. Therefore, when the battery pack is sourcing or sinking a large amount of current per cell, heat generation is high. Moreover, other parasitic component integrated to the battery pack contribute to the heat generation. Local heat generations need to be prevented and mitigated by a proper thermal management system because they can create imbalance in performance among the cells.

The BMS is tasked with monitoring and regulating the temperature of individual cells to prevent overheating. This may involve implementing cooling systems, such as liquid or air cooling, to dissipate excess heat and maintain the battery within safe operating temperatures. In these cases,

more input can be added as measurement to the BMS such as the temperature for inlet and outlet air or coolant as well as feedback signals for pumps, valves or fans wit the aim of verifying the correct operation of them and allowing diagnosis of possible failures.

On the other hand, some battery-powered applications need to perform at very low ambient temperature such as an electric vehicle that need to charge in a place with ambient temperature below 0°C. In this case, it could be necessary to integrate an heating system for the cell to bring their temperature into the acceptable range, and the self-heating mechanism is not sufficient.

2.2.4.3 Charging Strategies

This requirements allows the BMS to properly select the instantaneous power request for the battery system from an external source. This information needs to be communicated to the charging system (charger) which is able to control its output power. In this paragraph, the charging strategies refers to the charging process in which the battery pack play continuously the role of the load until the end of this operating condition and a fine control of the power delivered to the battery pack is possible. However, a battery pack can experience a random charging phases where the power delivered cannot be predicted, such as for the regenerative breaking in electric vehicles. In this cases, the battery management system manage the maximum allowable regenerative power by means the charging power limit.

As every process regards the battery pack, the BMS has to ensure safety conditions in terms of operating cell voltages and temperatures. On the other hand, the goal during the charging process is to achieve the state of full charged battery pack as fast as possible, which result an important task for enabling large-scale adoption of EVs. Reducing the charging time is possible by delivering a very large amount of power to the battery pack that also increases the losses, the temperature and accelerates aging mechanisms. Thus, the elaboration of a charging strategy includes a trade-off between the charging time, the state of charge of the batteries and the safety conditions.

For a charging process it is possible to mainly distinguish two different charging phases, including a constant current (CC) phase and a constant voltage (CV) phase. The charging strategy consist of combining these phases in a proper way to achieve the desired state of charge, and defining the criteria to end each phases and the charging process itself. The most common charging technique for a lithium-ion battery cell consist of CCCV standard that includes only two phases. During the first phase, the cell is charged with a constant current as long as the cell voltage is less than the maximum one, usually providing the 60-80% of the nominal capacity,

depending on the cell chemistry and also to the value of the constant current. Indeed, since the OCV is the directly related to the SoC, the higher the charging current the higher voltage drop between the OCV and the terminal voltage of the battery cell which will hit the maximum allowable voltage when the SoC is far from the 100%. Then, a second phase is necessary in order to charge the entire capacity of the battery, where the voltage of the cell is kept constant (CV) to the maximum value and the current starts to decrease until reaching a specific threshold value defined in design process or when the charging time exceeds a predefined maximum value. Usually, the charging time is mainly influenced by the constant current value, especially for those cells which present low internal resistance.

However, the CCCV charging process can not easily scaled from a single cell to a battery pack composed by several cells connected in series and/or in parallel. In this case, it is important to consider any possible imbalances among the battery cells which do not allow to perform the CV charging phase at the theoretical maximum voltage of the battery pack, this defined as the product between the number of the cells in series and the maximum operating voltage of the single battery cell. For this reason, the CCCV charging strategy does not represent the optimal strategy when considering a large battery pack even from the safety perspective, since the possibility that at least one cell experiences the overcharge abuse condition becomes high. Reducing the risk of abuse condition of overvoltage in CCCV strategy is possible by performing the CV phase at voltage lower than the theoretical maximum one, even though this decrease the total capacity charged.

To overcome this safety issue with CV phase for a large battery pack and also keeping the charging time as short as possible several different charging strategies have been proposed in literature where a proper control algorithm is designed for maximizing the energy storable in the battery pack while minimizing the charging time **??**. Starting from the principle of the CCCV charging strategy, an effective alternative solution is represented by the multi-stage constant current (MSCC) charging, in which the CV phase is replaced by a series of different CC phase where the charging current is decreased step by step, as illustrated in figure 2.8.

In detail, a constant current is delivered from the charger to the battery pack until the most charged cell reaches the maximum cell voltage allowable, then the C-rate of the charging process is reduced to a lower value and another constant current phase is performed. This charging process is stopped when the terminal voltage of the most charged cell hits the upper cell voltage limit at the lower current stage. This strategy allow to perform very high C-rates for the first phases resulting in a significant reduction of the charging time. However, the maximum C-rate allowable depends on the

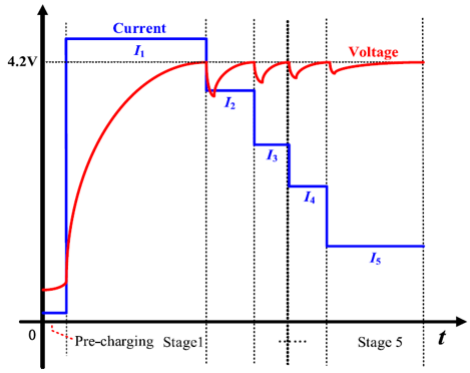

Figure 2.8: Example of the MSCC charging strategy [17].

cell chemistry and the cooling system installed in the battery pack, as well as the current magnitude of each stage needs to be optimized to achieve an effective charging process in terms of charged capacity and charging time.

Other charging techniques proposed in literature [18–20] involve the information related to the SoH to determine the charging rate of a battery pack in order to achieve any specific goal of durability of batteries.

2.2.5 Communication

Communication in battery management systems include transferring data between the battery system and the external load network as well as the communication among master and slave devices for distributed architectures. An effective communication architecture will provide only the information needed to each device. Indeed, many battery parameters do not usually need to be communicated to the external devices and are only required to be sent from slaves to master device, such as all cell voltages and temperatures. For large energy storage systems, cell voltages and temperatures represent a very significant amount of data and it would result a limitation to send these data also to the external bus. Cell balancing command also represent information regarding master an slave devices, instead of the battery charge and discharge limits, the pack status and load operation that regard the communication between the BMS and the load. The load device also need to communicate information about connection or disconnection of the battery pack. This can take form of a discrete signal, as handshake mechanism, or the state of a bit in the communication message.

Generally, serial communication is adopted in both communication directions due to the advantages in terms of number of wires required, high

data transfer rate over relatively cheap interconnections and robustness against message loss with respect of multiple discrete and/or analog signals. Accordingly, multiple communication ports and buses need to be implemented to facilitate an effective routing of information, even using different communication protocols. Moreover, it is recommended to provide an additional bus for transmitting large amount of data during development and testing procedure, allowing post-processing with the aim of debugging the whole system.

The design of the network communication systems depends on the specific communication method, the network layout and number of both internal and external nodes to the BMS, and other specification such as transmission rate and accuracy required by various bus types. These features will impact on both the hardware selection of components such as microcontroller that support the required communication ports, and the total system cost. In general, for the most applications, both internal and external transmission of battery data through BMS do not require large bandwidth, but they need to be reliable with respect to the corruption or loss of data, since the possible hazard condition and safety issue as a consequence. For this reason, redundancy for signals that communicates major faults status can be adopted as solution with the aim of reducing possible unsafety operating condition for battery pack. Another aspect that need to be consider regards latency in the communication network, that represents the delay time that data takes to transfer across the network. It increases the reaction rate of both the BMS to receive a command and actuators to execute an operation.

Several communication protocols can be taken into account to be integrated within the BMS with the respectively hardware. The following paragraph aim to give an overview of the most adopted solution which can be used for data communication both between master and slaves boards of BMS (internal) and between BMS and external load devices (external).

2.2.5.1 Interfaces

Communication methods can be characterized under two different aspects, including the physical interface and the communication protocol, harware and software implementation respectively. Physical interfaces are composed of one or more electrical circuits. In the case of communication buses, a single physical circuit may carry multiple logical signals. The electrical parameters of each physical interface should be clearly defined. A digital output will have a voltage range for both the logic 0 and logic 1 states, a maximum current which can be supplied and a transition time from on to off. Furthermore, it results important to identify the voltage

references for electric signals because the battery system architecture is composed by several galvanically isolated circuitry.

On the other hand, the communication protocol defines a number of rules to exchange information through a message sent or received on the specific network. These rules include the syntax, semantics, synchronization and method of addressing devices connected to the bus, and error detection method.

Most common communication standards developed for communication between ICs within a single printed circuit board (PCB) are I2C (Inter-Integrated Circuit) and SPI (serial peripheral interface). They are mainly used for short distances chip to chip communication, since they are not robust against disturbances on a longer line due to their non-differential physical interface.

RS-232 represent a point-to-point communication and it is not possible to build a bus or star architecture. The electrical interface is non-differential and requires dedicated wires for both transmit and receive communication direction. Single-ended transmission signals result unable to reject the common mode noise that produce a voltage offset to the ground reference, leading wrong communication messages. To overcome this issue the voltage level of signals is increased by means transceiver devices. Many microcontrollers include a UART port which is able to support RS-232 communication and it is usually used for debugging the behavior of the single subsystem.

RS-485, unlike RS-232, represent a differential serial communication protocol and is half-duplex, in which only one device to transmit at a time otherwise the data loss. The differential channel of communication allows communication for longer distances with respect to the RS-232 protocol even increasing the transmission rate of the data. The other difference that this protocol exhibits with respect to the RS-232 is the possibility to include more than two device within the communication bus, allowing to create a network of devices. However, for an effective network the number of devices included have to be limited. RS-485 standard defines the electrical characteristic of drivers and receivers for use in serial communication, which supports the implementation of Modbus communication protocol that is significantly used in industrial application. This can be useful for such battery systems that must interface with commercial and industrial components.

Currently, the most adopted technology for automotive application is the CAN (controller area network) bus. It has been developed for providing robust communication in operating environment that are characterized by high levels of electrical noise. CAN bus defines both physical interface

specification and message protocol. Electrically, it is composed by a differential two-wires serial bus which allow for robustness in data transfer. It has been developed to transmit data at very high speed (up to 1Mbps), even though CAN bus may result unsuitable for real-time application in which information need to be transmitted at fixed frequency. Flex ray bus can be adopted instead of CAN bus for application with those specific requirements. Every node on the CAN bus is identified by a specific ID that also specify the relative priority of each message, allowing to solve the issue related to interfering messages if bus loads are high. Generally it is not a master-slave architecture and each node on the network is capable of transmitting and receiving messages, although it is possible to implement the CANOpen protocol to change the communication in a sort of master-slave architecture. Moreover, messaging can operate at two different rate with the aim of discerning between high-priority messages (higher baud rate) and low-priority messages (lower baud rate). Automotive applications use the CAN bus almost exclusively for onboard vehicle messaging, even allowing the possibility to implement a wake-up-network strategy to prevent parasitic power consumption.

Local interconnect network (LIN) can be adopted as an alternative of CAN bus resulting simpler and cheaper at the expense of having lower transmission speed, less flexibility and non-differential. LIN communication is based on master-slave topology where slaves often do not require a microcontroller core or software implementation. Since LIN is characterized by good performance in latency time and other robustness features, it can be adopted both for BMS master-slave communications and low-bandwidth sensor integration.

A relatively new protocol developed specifically for automotive application is represented by FlexRay. It has been developed for increasing the communication speed and overcoming some limitation of CAN bus such as lack of deterministic time , redundancy, fault tolerance and time triggered behavior. Despite the improvement in terms of robustness related to the safety feature introduced, the use of FlexRay is not generally required in battery management system for enhance safety.

Ethernet communication can also be used in those cases in which battery management system needs to transmit a large amount of data to the battery-powered application with high communication speed.

2.2.5.2 Wireless BMS architecture

These represent a different approach about communication architecture in BMS including the wireless technology for transmitting data. Wireless communication on a BMS results suitable not only for transferring cell

voltages, current and temperature measurements between slaves and master in a distributed BMS architecture, but also enable the possibility to implement cloud-based BMS in which is possible to store a large amount of data and possibly overcome limitations of traditional embedded hardware terminals leading the use of very high computing power and memory.

Wireless communication among master and slave devices in a distributed BMS allows for reducing wiring complexity by eliminating the galvanic isolation and physical connectors. These result in improved system reliability, lower weight and cost, especially for large energy storage systems. Furthermore wireless solution impacts positively on system flexibility for both sensor placements within the BMS PCBs and the placement of the BMS modules inside the application, for example in a powertrain of EV. Furthermore, more flexibility is gained since wireless architectures enable the replacement of individual components without the need of involving the whole system. An attractive solution result the implementation of memory unit in each node of the wireless network which allows for recovering data once the wireless communication is restored after a temporary disconnection, improving the robustness and reliability of the communication network.

For these reason, wireless battery management systems are characterized by high fault tolerant capability and adequate system scalability with respect to the conventional wired BMSs.

On the other hand, the external communication channel can be realized between the master BMS and an external node that is an intelligent cloud that allows for massive data storage, big data analysis, historical data tracing and cloud computing. Cloud-based BMS allows for effectively integrate advanced functionalities of BMS, such as battery aging prognostics, real-time strategy optimization and others that are highly dependent on the longtime historical data, resulting unfeasible with low computational power. The cloud platform connected is used to develop a digital twin of the battery pack that allows to implement more complex but accurate algorithms for each BMS key function and requirement leading for a more effective battery management.

Despite the big advantages presented by this kind of communication architecture, there are some limitation to the large adoption of cloud-based BMS. First, in case of automotive application, it need a widespread and stable internet network for real-time data transfer between the BMS and the cloud platform. Second, extra components for cloud connection need to be included such as an IoT (internet-of-things) component, a cloud infrastructure, an application programming interface (API) and a user interface. These represent a significant addition to the current BMS design.

Chapter 3

SoX Estimation

Battery management system needs to estimate the two most important requirements during battery pack operation, that are the present total energy and power capability. Since there isn't a sensor that can measure either of these parameters directly, BMS has to compute their values using estimations of more basic parameters like resistance, total capacity, and cell SoCs.

This chapter aims to discuss about the state of the art of the estimation algorithms for evaluating the state of a battery pack present in literature and applied nowadays, in terms of state of charge, state of health with respect to aging condition and degradation mechanisms as well as the prediction of the power limits in charge and discharge operations. These fuctionalities results fundamental for managing the performance of the battery pack, prolonging its lifetime and ensuring safety.

3.1 SoC Estimation algorithms

At cell level, considering the electrochemistry, the state of charge is related to the concentration of the usable lithium ions in the anode electrode and it is impossible to directly measure in real time operation then there is the need to estimate this quantity by using the information that can be monitored in the battery pack.

SoC estimation represents one of the main requirement of the BMS because the knowledge of the state of charge of the cells is involved in other several functionalities of the BMS from which depends the successful operation of the battery pack. Unfortunately, this variable cannot be directly measured due to the nonlinear, time-varying characteristic and electrochemical reactions. In particular, the performance of the lithium-

ion batteries change with temperature, charge-discharge cycles and current rate. Moreover, the complexity of the estimation for the SoC is increased because the battery pack experience degradation and the capacity is the main parameter affected

SoC estimation task can be achieved by simple methods with a poor estimation or more complex methods that give very good approximation of this quantity. Usually, increasing complexity results in higher cost due to the higher engineering time for developing and validating the complex algorithm as well as it requires an hardware platform with better performance to be executed in such a way to achieve very high accuracy. It is always important to take into account that results difficult to compare different estimates between the different methodologies, since a reference value of the SoC can not be measured. However, it is possible to define some specific operating point where the state of charge is well defined and experimental tested where the performance of different estimation methods can be compared. An accurate estimation of the SoC provides several benefits for the battery pack in terms of lifespan, dynamic performance, reliability, density and investment cost. Indeed, a better accuracy in SoC estimates allows for avoiding any abuse condition of overcharge or overdischarge of the cell with consequently permanent damages to the cells, and conservative strategies in power limit estimation which leads the battery pack to be oversized also increasing the cost.

Several approaches are reported in literature from which have been derived different methods including conventional methods, adaptive filter algorithm, learning algorithm, nonlinear observer hybrid algorithm.

3.1.1 Open Circuit Voltage Method

This estimation method exploits the relationship between the OCV and the SoC for estimating the state of charge of the cell. The OCV-SoC characteristic is the only information that links the state of charge to a measurable variable, thus correlating the electrochemical description to the electrical description. Indeed, this relationship describe how the difference of potentials change with respect to the lithium concentration in equilibrium conditions, namely when the there are no exchange of charge between two electrodes and the current is zero. This method is implemented onto the BMS through lookup tables (LUTs) which consist of maps where the OCV is reported in different SoC conditions. In detail, the OCV is measured under several levels of SoC by means experimental tests in which a redefined amount of charge is exstracted to the cell and then it is rested for a long period of time for allowing the OCV becomes measurable. These experimental tests require a long period of time, especially when influence

of temperature, aging, and hysteresis phenomenon are taken into account for achieving better accuracy under different operating conditions.

The definition of the relationship between the SoC and OCV poses the first issue to use this characteristic as a methodology to estimate the present state of charge of the cell. Indeed, the battery management system needs to be able to determine the state of charge accurately during all operating condition of the cell. It is important to remember that the BMS can monitor the terminal voltage of each single cell but this becomes closely representative of the OCV only after a long period of time in which the cell is rested, that means zero current. Despite the dependence on the cell chemistry of the rest period to be wait before the cell terminal voltage becomes equal to the OCV, this period of time remain in the order of magnitude of hours. This represent the first issue that makes the OCV method for estimating SoC not suitable for real time application.

Another drawback this method present is related to the shape of the OCV-SoC characteristic and the measurement error that affect the terminal voltage of the cell in real applications. Indeed, as it has been showed in section 2.2.1.1, lithium-ion chemistries that present a very flat OCV-SoC relationship and/or significant hysteresis phenomenon can lead very large errors on state of charge interpolation. This result unsuitable for the most of the applications.

Lastly, although the OCV-SoC characteristic is relatively stable for lithium ion technology, this varies with temperature and aging of the cells. Therefore, a large campaign of experimental test is needed with the aim of avoiding to lose further accuracy over temperature condition and lifetime of this estimation algorithm.

For the drawbacks reported this estimation methodology find applicability only for those application in which the batteries have to deliver very low current and thus the terminal voltage can be assumed equal to the OCV.

3.1.2 Coulomb Counting Method

Another conventional approach used for SoC estimation is the current integration, which is called coulomb counting method. Starting form the first equation reported in (1.3), the formula for calculating the remaining percentage of charge of the battery with respect to the nominal capacity is as follows:

$$SoC(t) = SoC(0) - \frac{1}{C_n} \int_0^t \eta \; i(\tau), d\tau \tag{3.1}$$

where $SoC(0)$ represent the initial state of charge, C_n the nominal capacity, η the coulombic efficiency and $i(\tau)$ the instantaneous current involving the cell. It is important to point out that the (**??**) neglects the self discharge of the cell, which is very low for lithium-ion battery technology. The computational effort required to implement the coulomb counting method is very low and it can offer accurate results if the initial value of the SoC is correctly defined. The definition of the initial state of charge requires another estimation and represent a large weight on the performance accuracy of the coulomb counting method. It may be determined by means the OCV-SoC characteristic of the cell, taking the drawbacks of the previous method, or referring to a condition in which the SoC is well defined such as fully charged or fully discharged battery. However, these two conditions are not so common during the battery operation, especially for automotive applications.

Coulomb counting method relies on the measurement of the current of the battery pack and consequently the SoC estimation is affected by the measurement and bias errors which characterize the sensor installed and the measurement circuit. Indeed, a constant error, positive or negative, of the battery current integrated over time causes a drift effect on the estimated value of the coulomb counting, that leads the estimation further and further away to the real value of the SoC. A proper calibration of the current sensor can reduce the error, in which there is the need to consider that the operating conditions of the current acquisition could strongly affect the measurement. Moreover, the coulomb counting method needs to take into account also the aging effect in terms of the reduction of the nominal capacity for maintaining good performances over the lifetime of the battery pack.

Another factor that need to be considered is the overall value of the current a single cell experience. Indeed, assuming a battery pack composed of n cells in series, it is a poor approximation consider the current of the string equal to the current each cell experience. The cells also experience self-discharge, supply the electronic circuitry that realizes the BMS and experience equalization currents.

Summarizing, the coulomb counting methods for estimating SoC results very simple to implement in the BMS and offer good performance for short period of operation when initial state is well known. It is also suitable to integrate this algorithm in application in which there is the possibility to include some reset mechanisms when the battery frequently operates in condition where the SoC is well defined.

3.1.3 Filter-based Method

Filter-based methodology differs to the conventional methods described before because they do not only rely on voltage and current measurements, but they integrate the use of a battery model within the estimation process. The commonly adopted battery model to be integrated in filter-based methods include equivalent circuit models and electrochemical models. Indeed, they can also be classified as model-based estimation approach in which the actual behavior of the cell, monitored through the measurements, is compared to the response of the battery model. Moreover, the resulting methods is able to estimate SoC and the other internal states described in the battery model. Thus, this method follows two steps which consist of the prediction of the system state and output (cell voltage) based on our state estimate and the measured system input and update the system states based on the output error. If the prediction and the measured values are equal the model's state estimate is good, otherwise it is poor and the difference between the estimation and the measured value is integrated in a proper feedback loop to update the model's state estimate. However , it important to point out that the difference between the estimate and the measured value are affected by a number of factors, including state estimation error, measurement errors and modeling error. Filter-based methods are able to compute the state estimation also taking into account these different sources of errors separately. The most relevant aspect filter-based estimation method presents is the robustness with respect to the error measurement and to the model accuracy.

Generally they can be divided in two different categories: the Gaussian process-based filters, including linear Kalman filter (LKF), extended Kalman filter (EKF), unscended Kalman filter (UKF), adaptive Kalman filters (AKF), sigma-point Kalman filter (SPKF), central difference Kalman filter (CDKF) and cubature Kalman filter (CKD); and the probability-based filters which include Particle filters (PF), unscended paticle filter (UPF) and cubature particle filter (CPF).

Kalman filtering represent a mathematical technique that allow for estimating the state of an observable system considering a set of noisy input and output measurement. This technique is largely adopted in many engineering areas including aerospace and aviation applications, trajectory and position estimation for navigation systems and automotive applications. One significant advantage of the Kalman filter for SOC and battery state prediction is that it only requires the state variable values from the previous time step. An extensive history is not required, which reduces memory needs in real-time embedded systems. Consider a battery management system capable of monitoring current and voltage across several

battery cells. A state space model is developed, with the battery SOC and model elements' state variables as hidden state variables. In an equivalent circuit model, these may be the polarization voltages for specific RC elements, as well as the hysteresis voltage. Nevertheless, the parameter model representation offers only an approximation of the actual electrochemical phenomena and both input and output (current and voltage respectively) measurements are affected by an error. A smart way to combine all the information is based on the fact that SoC can be computed by integrating the measured current and providing a good approximation in short term period assuming a good approximation of the initial state of charge. The accuracy in short term of the coulom counting can be used to correct the state and output estimation of the model. However, at certain point the prediction of the model becomes more accurate of the current integration of the SoC and it could be used to update the state of charge. The Kalman filter addresses this problem optimally by calculating the ideal weight assigned to each of the two approaches.

The basic Kalman filter requires a linear time-invariant (LTI) description of the system, while the lithium-ion battery is not. Furthermore, in Kalman filters the equations are operated in state-space form considering the discrete-time version of the cell dynamics. Therefore, since the battery syste is a nonlinear system the Kalman filter technique can not be directly implemented. Firstly, the OCV-SoC curve is non linear and, in order to be consistent with Kalman filter theory, it is piece-wise linearized [21, 22]. The noise is categorized in two different contributes: the process noise and the observation noise. The former influences the evolution of the state of the system and is related to the input errors and the model errors, whereas the latter is responsible for the error in the output measurement. Thus, the state-space description in discrete form integrates the process noise in the state equations and the observation noise in the output equations. At each time interval the Kalman filter computes a gain that is used to adjust and optimize the weight of both the state estimated by the model and the system inputs, and the corrected state that rely on the measured outputs, with the aim of generating the optimal estimation of the state variables. The major assumption the Kalman filter makes is that both the noises modeled are Gaussian, with zero mean and a well defined variance and covariance. The determination of the covariance matrix values depends on the accuracy of both the model and the measurements. Regarding the voltage and current measurements, the variance value can be determined by testing the sensors while the covariance are usually assumed equal to zero, which means that there are no correlation between the noise of two different measurement. Moreover, this mathematical technique calculate a

state error covariance matrix updating it at each iteration, which reflects the degree of uncertainty of the state estimated. For this matrix, setting the initial value represent a crucial issue that need more consideration [23].

Despite the differences between actual battery systems and Kalman filter theory, this method has been shown to produce robust and reliable SOC estimation under a wide range of conditions, including immunity to errors in initial estimation, integration error, model inaccuracies, and measurement noise.

More suitable for battery application, and non linear systems in general, is an extension of the Kalman filer called extended Kalman filter (EKF), which differs to the LKF because nonlinear functions are considered instead of the state transition and observation matrix and the observation matrix in the discrete model description. In SoC battery estimation, EKF expands the nonlinear OCV-SoC characteristic with partial derivatives based on the local linearization of the non linear functions. However, the accuracy of the EKF in SoC estimation also depends on the model parameters that presents nonlinear characteristic with respect to the SoC, such as ohmic resistances, hysteresis, the Warburg impedance and other more advanced parameters.

The EKF results more complex than the LKF and it requires higher computational effort, especially due to the computation of the Jacobian, the matrix of the partial derivatives. The online implementation of EKF can be lightened by using lookup tables to represent the nonlinear function, and a large part of the partial derivative can be calculated offline and stored in the BMS as multi-dimensional matrices.

Another derivation of the Kalman filter is represented by the unscented Kalman Filter (UKF), which aims to approximate the distribution instead of the nonlinear functions, as occurs for EKF. Indeed, the principle is to perform the error propagation by selecting a number of points around the current state estimate, which maintain the same characteristic in terms of mean and covariance, and using the non linear function to obtain a more realistic estimation of the new distribution, in terms of mean and covariance. This methods presents several advantages with respect to the EKF, including a practical benefits of eliminating the computation of the Jacobian matrix, the nonlinear function are completely exploited providing advantages independent of any improvement in estimation quality. This mathematical technique includes the unscented transformation that results applicable even in cases where nonlinear functions are non differentiable. Unscented Kalman filter is a specific type of the sigma-point Kalman filters (SPKF) which tend to provide more accurate estimations of SoC with respect to the EKF, because considering nonlinear system the error propagation linearized from the statistic prospective performs generally better

than the error propagation through a linearized model by the first order Taylor expansion.

Another more complex extension of the Kalman filtering technique have been developed and proposed in literature with the aim to overcome those issue reported for the basic Kalman filter methods. The more complexity involve higher computational effort. In addition, the convergence rate and convergence time are major factors which need to be considered, since numerical, and not analytical, calculation is used to perform these algorithms. Adaptive Kalman filters are proposed in literature fot both EKF and UKF, where the covariance matrices are automatically updated every iteration step with a proper optimization algorithm. The adaptive covariance of process and observation noise can help the Kalman filter in avoiding the divergence or bias of the algorithm. These methods are also able to identify the model parameters with an online estimation and update the state space model in real time. This characteristic allow for achieving better performances over the lifetime and degradation of the batteries.

Other variants of the Kalman filter proposed in literature are represented by the CDKF and CKF. Central difference KF assumes that also the state variables are characterized by a Gaussian distribution, then this algorithm is able to estimates the mean and covariance of a random Gaussian variable after any nonlinear transformation, avoiding the computation of the Jacobian matrix. Lastly, cubature Kalman filter include the third-order spherical radial volume criteria to the KF theory.

As opposite to Kalman filter methods, particle filters (PF) have gained popularity to overcome those Kalman filter issues related to the assumption of Gaussian distribution of the process and measurement noises. The idea at the basis of PF it to generate a number of sampling points in the state space based upon the empirical distribution of the system state vector, then the position and state of particles are rearranged according to the particle sets.

Unscented PF and cubature PF are two variants proposed in literature for SOC estimation. The first one use the UKF to improve the sampling process of the PF, whereas the second type uses the same volume method reported for CKF for directly calculating the mean and variance of nonlinear random function and generating the suggested density function to get the weighted particles.

All of these variants result more accurate than the simple KF and PF. However, LKF and EKF apart, the estimation error among the other SoC estimation algorithm results comparable.

3.1.4 Observed-based Method

The estimation of state variables in a system is facilitated by a state observer, which relies on measured values of external variables. Initially introduced by Luenberg [24], the concept and construction method of a state observer have proven instrumental in achieving state feedback and addressing various control system requirements. The state observer not only enables the estimation of state variables but also opens up practical avenues for implementing state feedback technology, finding applications across diverse domains within control engineering.

Over the years, observer-based methods such as the Luenberger observer (LO), sliding mode observer (SMO), proportional-integral observer (PIO), and the H-infinity observer (HIO) have gained widespread adoption for battery state estimation. These methods offer sophisticated approaches to estimating the state of a system, providing valuable insights and enhancing the robustness of control strategies. As a result, the application of state observers has become integral to advancements in control engineering, contributing significantly to the development and optimization of state feedback technology.

Observer-based SoC estimation methods rely on the state space battery model, thus the can be integrated in the model-based estimation approach with the filter-based methods. Compared to the Kalman filter, the state observer method presents several benefits resulting simpler, more efficient, resilient, and accurate. The observer-based method estimates the SOC utilizing the properties of a switching function, limiting the impact of model uncertainty, measurement noise, and external interference.

Luenberger observer is largely used for state estimation in linear, nonlinear and time-varying systems and several examples have been reported in literature for SoC estimation task. An adaptive LO based algorithm is reported in [25] for performin an online estimation of the state of charge of a battery pack. An ECM has been used as the model description. A stochastic gradient technique is used to update the observer gain, reducing the mean square error between the estimated voltage and the measurement. The validation findings demonstrate that the absolute SoC estimation error may fast converge into an acceptable range within 2.5%, and the estimator is resilient to the inaccuracy of the initial condition and unknown disturbances at a reasonable computing cost. Another example is reported in [26], where a Luenberger observer have been developed for SoC estimation on a nonlinear fractional battery model. The global asymptotic stability has be proven by using Lyapunov's direct method.

The implementation of a sliding mode observers (SMO) allows for achieving robust tracking performances under the condition of model uncertainties

and external disturbances such as environmental interference. The fundamental principle behind the SMO lies in the creation of a sliding surface, a designated hypersurface in the state space, on which the estimation error is driven to zero. A specific characteristics of the SMO algorithm are including a switching gain, which is designed to ensure stability and convergence, and chattering phenomenon due to the state-feedback control law that not a continuous function of time. Sliding mode observer have been proposed in literature in different ways to address the task of SoC estimation. Indeed, a second-order discrete time SMO has been developed in [27] with the aim of reducing the chattering effect, whereas an adaptive gain SMO is proposed in [28, 29] where the adjustment helps for compensating model errors and reducing chattering. Moreover, this observed method has been combined with data-driven methods in [30, 31].

PI and H-infinity observers have been also adopted in order to develop a proper SoC estimation algorithm [32,33]. They are both suitable for battery application since PIO represent an efficient methodology that allows for estimating the state of systems where the input disturbance is unknown whereas the HIO can ensure robustness given the erroneous initial system state and unknown disturbance caused by the faulty or unknown statistical properties of modeling and measurement errors.

Using state observers for lithium-ion battery SOC estimation comes with certain drawbacks. Firstly, the accuracy of SOC estimation is highly dependent on the precision of the selected battery model. If the chosen model does not accurately represent the true behavior of the lithium-ion battery, the performance of the observer may be compromised. Secondly, state observers are sensitive to changes in system parameters. Variations in battery characteristics, such as aging or temperature fluctuations, can impact the precision of SOC estimation. Additionally, challenges may arise during the initialization phase of the observer, particularly when the initial state is uncertain. Inaccurate initialization may lead to errors in SOC estimation, especially in the early stages of operation. Lastly, real-time SOC estimation requires significant computational resources, depending on the complexity of the battery model and observer design. This can pose challenges in applications with limited processing power.

3.1.5 Data-driven based Method

The black box battery model treats the battery as an unknown system, utilizing online measurements of battery current, voltage and temperature as inputs to the model whereas the SoC is considered the output of this model. Through the application of intelligent algorithms, the black box battery model processes and learns from input and output data. By doing

so, it establishes a relationship or mapping between the input parameters and the corresponding output, allowing for a comprehensive understanding of the battery's behavior without explicit knowledge of its internal workings. The behavior of black box battery model can be usually achieved by ally uses neural networks (NN), support vector machines (SVM), fuzzy logic algorithms, genetic algorithms (GA), and deep learning methods. Unlike the model based approaches, it is important to notice that in this case only the SoC can be computed and updated as a state variable, sice it correspond to the output of these models.

Neural network models present very good adaptability to nonlinear systems, they are suitable multiple-inputs multiple-outputs systems, they present characteristics of fault tolerance, self-learning and wide range of use. Generally, the architecture of a neural network can be described with an input layer, an output layer and a certain number of the hidden layers, where each layer is composed of a specific number of nodes. Neural networks require a training process with a large amount of data, and only perform well if the inputs during operations are within the same data range used in the training process. Indeed, the battery SoC estimation error is affected by the training data and the training methodology used to build the neural network. This data-driven based method have been largely used in combination with other data clustering algorithms, such as fuzzy logic [34] and also Kalman filters [35, 36]. To implement alone the neural network for modeling and optimization, the particle swarm optimization have been used to define optimal number of nodes in the hidden layer. This strategy has several benefits, including the elimination of local solving problems, the reduction of the prediction error, and the improvement in generalization and applicability. Another approach involves the implementation of two different neural networks, one for the online battery parameter identification and the other one for battery SoC estimation, in order to solve the robustness issues related to the poor estimation of the initial state [37].

The Support Vector Machine (SVM) stands out as a widely adopted and well-established machine learning algorithm. Its primary objective is to minimize structured risk, thereby enhancing the generalization capability of the learning machine. This minimization extends to experience risk and confidence range, allowing for the derivation of robust statistical laws even when the number of statistical samples is limited. SVM is commonly categorized into Support Vector Classification (SVC) for addressing classification problems and Support Vector Regression (SVR) for fitting regression models.

In the context of battery modeling, SVM proves particularly effective in dealing with nonlinear and high-dimensional characteristics. It excels in

accurately estimating the SoC of batteries, although with an increase in computational complexity. To deal with the nonlinear nature of lithium-ion batteries, the SVM employs a kernel function to map input data into higher dimensions. The quadratic programming method is then applied to identify the optimal support vector, enhancing the model's predictive accuracy. When addressing the challenge of battery SoC estimation, both training and verification samples consist of data points including battery state parameters such as voltage, current, temperature, and SoC at specific moments. The selection of an appropriate kernel function plays a crucial role in training the SVM model. Subsequently, the model is fine-tuned to obtain the optimal hyperplane. The final assessment involves using a new set of samples to verify the model's accuracy and evaluate its real-time performance. This meticulous process ensures that the Support Vector Machine aligns with the precision and real-time requirements for battery SoC estimation.

Fuzzy algorithms replicate human reasoning using fuzzy sentences during decision-making. In battery SOC estimation, voltage, current, and temperature undergo the fuzzy process, converting precise values into fuzzy variables. Fuzzy rules, based on experience, guide the reasoning process. The final battery SOC value is obtained through decision and de-fuzzification processing, providing an output based on fuzzy reasoning applied to input parameters. Currently, fuzzy algorithms are frequently integrated with other intelligent algorithms to improve efficiency.

Deep learning is a more advanced type of neural network that uses numerous layers to extract detailed and expressive properties from data. This capability allows for the creation of complicated nonlinear mappings between input and output data. In deep learning, numerous neurons with simple processing capabilities are organized, empowering the creation of networks with strong generalization and parallel processing capacities. When used to battery state of charge estimation, measurements of voltage, current, and temperature are sent into the deep learning network's input layer. The network generates the final output, which represents the battery state of charge, using computations in the hidden layer nodes. Deep learning's training model is intricate, which results in improved estimation accuracy. However, it necessitates enormous computational resources and effort. Various algorithms implementing deep learning theories include the deep belief network (DBN), convolutional neural network (CNN), and recurrent neural network (RNN). An important variant of the RNN is represented by the long-short term memory (LSTM) network is becoming attractive for battery management system operation because it is suitable for predicting the state for a very long intervals and delays in time series.

The Genetic Algorithm (GA) is an intelligent optimization method that may be used for stochastic, nonlinear, constrained, and unconstrained problems. Its versatility in the dynamic field of optimization theory is demonstrated by its capacity to adapt. GA is known for its high level of computer parallelism, which allows it to efficiently produce progeny while simultaneously calculating individual fitness values. Self-organization, self-adaptation, self-learning, and collective development are some of its distinctive characteristics.

Currently, academic and industrial research has extensively explored various approaches such as neural networks, support vector machines, deep learning, and genetic algorithms to enhance the accuracy of SoC estimation methods and significant enhancement have been made in these methods. However, SoC estimation methods based on the black box battery model typically rely on a large offline database. The sample training process involves substantial computations, making it susceptible to issues like overfitting and the risk of converging to local optimal point. Consequently, the application of this method in engineering remains challenging due to these computational complexities and potential issues.

3.2 SoH Estimation

State of Health (SoH) estimation generally involves the estimation and tracking of internal parameters within a cell model as the cell undergoes aging. Due to the absence of a universally standard definition for SoH, it is common practice to estimate two indicators of aging: current cell capacity and series resistance. However, these two parameters are not measurable, then a algorithm need to be developed and implemented for estimating the variation over time of the capacity and cell internal resistance. The reduction in capacity is often referred to as capacity fade, while an increase in resistance results in power fade. These indicators serve as crucial metrics for assessing the health and performance degradation of a cell over time.

As with the methods of SoC estimation, SoH can be estimated through two different approaches, namely experimental and model-based. Methods that refer to the empirical experimental approach need a large amount of data obtained in different characterization tests in which batteries are subjected to different operating conditions. This makes it possible to create a baseline projection that allows direct determination of SoH. On the other hand, model-based methods define the SoH by estimating internal capacitance and resistance parameters. An overview of the different methods sued for SoH determination are summarized in figure 3.1, which are detailed described in [38, 39].

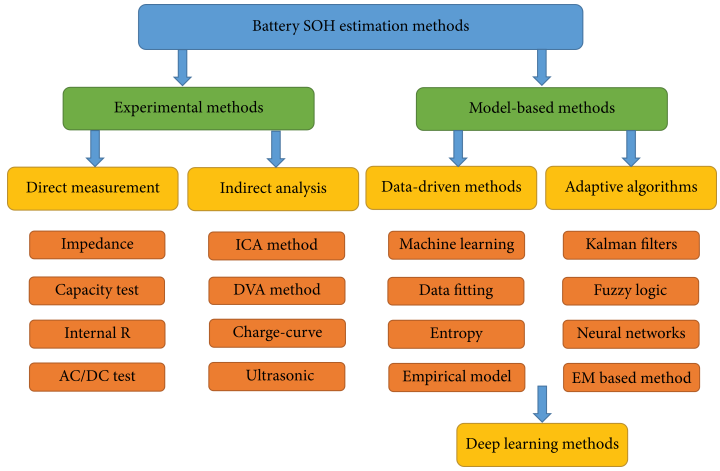

Figure 3.1: Overview of SoH estimation methods [38].

Typically, as far as experimental testing is concerned, most cell manufacturers provide data on the effects of cell aging in terms of capacity fade and power fade, either under resting conditions (calendar aging) or by subjecting the cells to consecutive charge and discharge cycles by varying temperature conditions. However, the operating conditions in real-world applications of cells differ greatly from those proposed by calendar aging and cycle aging. Thus, capacity fade and power fade data obtained from calendar aging and cycle aging processes give only a qualitative indication of the effect that cell degradation mechanisms have on cell performance, since cells are characterized by strongly nonlinear behavior. Hence, when characterizing cell degradation through experimental means, it is essential to conduct tests that account for the specific application's requisite current profiles. These methods should be fine-tuned to ensure they are easily implementable, repeatable, and can be carried out within a shorter time-frame than real-world scenarios, for practical efficiency.

3.2.1 Experimental methods

Experimental methods result fundamental to the assessment of state of health in batteries and necessitate a series of procedures for acquiring essential data. However, during experimentation, obtaining consistently reliable information can be challenging due to systematic errors and other various external factors. The application of experimental methods enables the measurement of internal resistance through both direct and indirect means. Direct measurements encompass battery capacity assessments, internal re-

sistance quantification, impedance measurements, and other related techniques. Indirect methods involve data optimization and processing to identify SoH parameters, incorporating approaches such as the charging curve method, the incremental capacity analysis (ICA) method, the differential voltage analysis (DVA) method, and ultrasonic inspection.

Typically conducted in laboratories due to the need for specialized equipment, these experimental methods are often time-consuming. They rely on a set of data and measurements that offer insights into comprehending and evaluating the aging behavior of batteries. This paragraph aims to report a generic overview into some significant experimental approaches, mentioning the benefits and drawbacks of this SoH estimation approach.

3.2.1.1 Direct measurement methods

The first methodology of direct measurement method for SoH estimation rely on the internal resistance measurement. In lithium-ion batteries the value of the internal resistance of a cell is influenced by battery materials and their structure, the state of charge, temperature, and discharge rate. It is possible to approximate the internal resistance with the sum of two different contributes: ohmic resistance and polarization resistance.

According to the literature the characterization of the internal resistance result consistent by using these several approaches: Current step methods, thermal loss methods, alternating current methods, and electrochemical impedance spectroscopy. Regarding the first approach, the resistance is calculated by the instantaneous voltage drop produced by a specific known current resulting in a theoretical straightforward formula for the calculation. The test need to be performed under different condition of temperatures and C-rate, while varying the level of the SoC. However, this method require very accurate measurement and high-quality instrumentation, limiting the applicability in online resistance calculation and then SoH estimation. The thermal loss method allows for calculating the internal resistance of the cell by using a calorimeter, which is able to detect loss for the duration of the charge/discharge current input profile, since a large amount of the heat generated when a cell experiences a current pass through is irreversible and then associate to the internal resistance. Therefore, the internal resistance is calculated by measuring the change in temperature in the cycle. This method can be performed only in laboratory environment due to the high-cost high performance instrument required. Moreover, considering brief period of time for charging or discharging profile these two methods produce the same results. The AC method is employed to measure the internal resistance of the batteries using small current ripples that induce voltage fluctuations at a constant frequency of 1 kHz. Key attributes

of the AC method include the capability to measure through the phase angle, making it suitable for complex measurements [40, 41]. this technique is also called electrochemical impedance spectroscopy (EIS) that is employed to estimate the SoH through the change of the impedance spectrum at a particular peak. A notable advantage of the AC method is its nondestructive nature when assessing internal resistance.

On the other hand, the battery capacity can be monitored only with coulomb counting if considering the direct measurement. However, this method is reliable only in laboratory environment, where the it is possible to use very accurate instrumentation for measuring the battery current, and performing test in which the fully charged or fully discharged condition are frequently reached. These operating conditions avoid any problem of uncertainties on the initial state of charge and current integration drift.

3.2.1.2 Indirect measurement methods

Indirect measurement methods for SoH estimation rely on differential analysis methods, which consist of differential calculations on voltage curves to get sensitive SOH-related features. Based on the differential analysis approach, two majoer methods are used in SoH battery estimation, including incremental capacity analysis (ICA) method and differential voltage analysis (DVA) method.

These methods observe the shape of characteristic curves of lithium-ion which are provided in specific operating conditions. One of the most common analysis is maded on the OCV-SoC characteristic, from which the incremental ratio of the capacity with respect to the voltage variation dQ/dV is derived. This curve exhibit some peak that are characterized in terms of amplitude and location with respect to the whole range of the battery capacity. It has been observed that the peak amplitude and position change with the battery capacity fading [42, 43].

One drawback of the ICA and DVA approaches is their time-intensive nature during experiments, as their curves are generated at low current levels. Moreover, these methods,related to the incremental capacity curves, are very sensitive with rtespect to the noise, which result in the presence of undesired peak value contained in the data.

To sum up, these differential analysis approaches do not assure accurate real-time state of health estimation across diverse operational conditions. Consequently, they are more likely to function as supplementary techniques for real-time SoH estimation.

Differential thermal voltammetry (DTV) analysis represent a good alternative to ICA and DVA. DVT considers the temperature change with respect to the voltage dT/dV providing an extra entropic feature with re-

spect to ICA and DVA. In detail, the entropy information that presents the variation of peak height and positions is used to observe the increase of battery impedance and deriving the SoH. Therefore, DVT analysis is capable for achieving good performance even in case of higher C-rates, results less complex, but exhibit high sensitivity to the environmental conditions may leading large diagnosis errors.

3.2.2 Model-based methods

These methodologies for SoH estimation encompass several different approaches which basically include bayesian-based estimation approach, empirical fitting approach and data-driven approach. They all rely on a battery model and they are commonly used for online SoH estimation. In detail, model based methods allow for estimating the capacity and/or resistance parameter changes over time, which can be used to reflect the battery state of health. However, any model adopted in case of battery applications must be calibrated on several experimental tests appropriately designed according to the current profile the battery pack has to account for that specific application. The model calibration also require a validation phase in order to avoid any safety issues. In case of the state of health, which is defined on the basis of the beginning of life and end of life conditions, it is easy to understand that the model calibration takes very long time.

Using a proper description of the model, Kalman filtering technique represents an attractive methodology for SoH estimation. Generally, the model description used in filtering methods for battery application is the ECM, where, aside the Kalman filter used for SoC estimation, another Kalman filter is developed for estimates the capacity fade or the power fade through the estimation ogf the actual capacity and resistances. As in SoC Kalman filter estimation, good performance can be achieved by considering any more complex variation of the linear Kalman filter, since degradation is a nonlinear phenonmenon.

Particle filters have been also proposed in literature for SoH estimation, which differs to the Kalman filters on the distribution properties. Particle filtering method offer a good performance where the battery pack is installed in uncontrolled environmental conditions. This method has been proposed in literature in combination with some other complex mathematical tools with the aim of achieving better performance in forecasting the remaining useful life of the batteries.

Another approach adopted for SoH estimation is the empirical fitting method which is usually based on battery models that relate to the degradation of one or more performance parameters. One of the weakness of this methodology is that the mathematical model developed does not describe

the electrochemical and physics phenomena occurring within the battery. The most general mathematical description these type of model take into account all the input factors that influence the degradation of a lithium-ion battery, including C-rate, the depth of discharge, temperature, storage time, number of cycles, and state of charge. All of these parameters are combined together in a nonlinear function for describing the change of the selected degradation parameter over time. Some coefficient parameters are also included and calibrated in such a way the mathematical model well fits experimental data of that parameter over time. Calendar and cycle aging represent the most common empirical fitting models of capacity fading.

The multi-variable nonlinear phenomena produced by the degradation mechanism makes the SoH estimation task of battery packs attractive for the adoption of artificial intelligence techniques and machine learning-based approaches. These methods are based on developing and calibrating a model through a training process by using a dataset of experimental data collected. In order to obtain good performance from machine learning-based methods, the dataset used for the training process must be large and need to cover all the operating condition the cell will experience during its entire lifetime. The collection of such large amount of data point would require very long time if considering specific experimental tests. To overcome this issue, OEMs of automotive applications monitor and collect data directly on their vehicles to transfer them into a proper cloud in which the data of all the vehicles are stored together [44]. This allows to collect very large amount of data for batteries which are experiencing several different operating condition in terms of ambient temperature, charging/discharging profile depth of discharge, degradation and so on. Moreover, the data collected onto the shared platform are used for update estimation algorithms.

3.3 SoP prediction

A power limit specifies the rate at which we may add or remove energy from the battery pack without breaching a set of design limitations, generally defined by safety operating conditions. Therefore, the charging and discharging power limits represent the power capability of a battery pack for a specific condition in terms of state of charge temperature and aging, and this is the reason why power limits define the state of power (SoP) of the pack.

Another essential reason for estimating the power limits of a battery pack is for optimizing performance of the battery pack while guaranteeing its expected lifetime. SoP is computed by taking into account the voltage limits of the cell in the attempt for preventing the acceleration of aging

mechanisms. Voltage limits are considered for this purpose because it is easy to compute, although they are not a direct and predictive indicator of how quickly the cell is aging.

The battery management system communicates power limits to the external load network, serving various purposes. In scenarios where the load relies exclusively on the battery pack for power, as seen in electric vehicles, the load controller's primary responsibility is to ensure strict adherence to the power limits defined by the battery management system. This commitment to limit compliance, even at the cost of potential performance loss, is essential for maintaining operational integrity. Conversely, in situations where the load has multiple power sources, such as in hybrid-electric vehicles, the load controller incorporates the maximum limits provided by the battery management system as a key element in its strategy. This strategic integration aims to intelligently blend the capabilities of both power sources, ensuring optimal satisfaction of load requirements while concurrently optimizing specific performance criteria.

In both cases, a slowly changing of real-time power limit values is preferable, since abrupt variations in load profile should be avoided, and a predictive estimation of power limits allows for better scheduling the power request over the next time horizon with respect to the estimation of the instantaneous power capability. Therefore, the SoP estimation consist of computing a constant power level the battery pack can provide or receive to the load over the next future time interval ΔT. It is straightforward to asses that estimating the power capability the battery pack can sustain for ΔT results a conservative approach with respect to estimate the instantaneous power capability.

It is important to highlight that the battery management system calculates and communicates the power limits more frequently then once every ΔT resulting in overlapping the power limit over time. This results a further conservative approach because the BMS does not let the external load to absorb the computed power limit for the whole time horizon, but rather regenerates power limits at the next calculation step moving forward the time horizon. Indeed, considering a time horizon of 30 s and a frequency estimation of power limits equal to 1 Hz (every 1 second). At the first step, the BMS calculates the power which, if it drew by the load, involves the battery pack to hit the voltage limit at $t = 30s$. However, at $t = 1s$ the BMS calculates again power limits allowing the pack to be in safe conditions until $t = 31s$, even if the battery had delivered power equal to the limit during the first second. This prediction steps are repeated continuously during the battery operations.

In summary, power limits represent the maximum amount of continuous

power, for both charging and discharging operation, the battery pack can safely deliver to the high-voltage system for the next fixed time horizon ΔT. In other words, if that power came applied it would bring the pack to hit one or both limits in voltage and temperature.

In the next paragraphs, the methodology for SoP estimation will be detailed described.

3.3.1 Voltage-based power limits

Voltage-based SoP estimation methods include all the methodologies in which the voltage response of the limiting cell for the battery pack is evaluated to determine which current leads the terminal voltage to approach either maximum or minimum limit at the end of the next time horizon considered. Therefore, this current results the maximum allowable.

A battery model needs to be involved to provide the estimation of the voltage evolution over time. This model needs to take into account, as accurate as possible, how the open circuit voltage varies with the state of charge as well as the maximum overpotential as a function of current and depending also to the SoC and temperature. Among them, the basic input for the SoP estimation results the SoC, since temperature can be generally ignored in most short-term prediction.

The most simple approach is to use a zero-th order equivalent circuit model (ECM) to compute the maximum current allowable for the battery cells. The model equations are described by (1.3) and they can be rewritten as follows:

$$\begin{aligned} \frac{dSoC(t)}{dt} &= -\frac{i(t)}{C} \\ i(t) &= \frac{OCV(SoC(t)) - v(t)}{R_0} \end{aligned} \tag{3.2}$$

Since the power limits are defined by means the constant current that force the terminal voltage to approach its limits after a specific time horizon, the second equation of (3.2) becomes:

$$\begin{aligned} I^d_{max} &= \frac{OCV(SoC)) - V_{min}}{R^d_0} \\ I^c_{max} &= \frac{V_{max} - OCV(SoC)}{R^c_0} \end{aligned} \tag{3.3}$$

where I_{max} represent the constant current limit for the next ΔT , V_{min} and V_{max} the upper and lower boundary voltage for the cell, and super-

scripts c and d refer to charging and discharging. However, these relationship describe an instantaneous voltage drop of the cell terminal voltage with respect to the OCV, then (3.4) allows to compute the instantaneous charging and discharging power capability.

To estimate power limits for a fixed future time interval, this method takes into account a different resistance, which value is greater in order to consider an higher change in voltage terminals due to the longer duration. Indeed, proper characterization tests are performed where a constant-current pulse is applied to the cell for a time equal to the prediction horizon ΔT and the difference between the cell terminal voltage at the beginning and the end is taken into account to evaluate the overall resistance. Since that, it is appropriate to update (3.4) with a proper notation for the overall resistance that carries inside the relation with the time interval:

$$\begin{aligned} I^d_{max} &= \frac{OCV(SoC) - V_{min}}{R^d_{0,\Delta T}} \\ I^c_{max} &= \frac{V_{max} - OCV(SoC)}{R^c_{0,\Delta T}} \end{aligned} \tag{3.4}$$

The most common experimental test to evaluate this resistance is the hybrid pulse power characterization (HPPC) test. This test consist of a current profile of a discharge pulse at constant current, followed by a relaxation phase at zero current and a constant-current charge pulse, as illustrated in figure 3.2. This current profile is performed after a long rest period in which the cell need to reach the electrochemical equilibrium, and it is performed at different SoC, usually with a 10& of step increment. Indeed, after this current profile, the cell is also discharged at low C-rate for a specific period of time that determine the next level of SoC to stimulate the cell with the discharge and charge pulses.

Figure 3.2 shows a discharge pulse that last 30 s while 10 s are considered for the charge pulse, however it is possible to change these times with the aim to evaluate the power limits for a different time horizon. Nevertheless, considering the HPPC pulses in figure 3.2 the resistance $R^d_{0,\Delta T}$ can be calculated by dividing the overall change in cell terminal voltage between t_0 and t_1 over the constant current used for the discharge pulse. Accordingly, $R^c_{0,\Delta T}$ is calculated by considering the charge (regen in figure 3.2) pulse.

$$\begin{aligned} R^d_{0,\Delta T} &= \frac{v(t_0) - v(t_1)}{I_{dis}} \\ R^c_{0,\Delta T} &= \frac{v(t_3) - v(t_2)}{I_{chr}} \end{aligned} \tag{3.5}$$

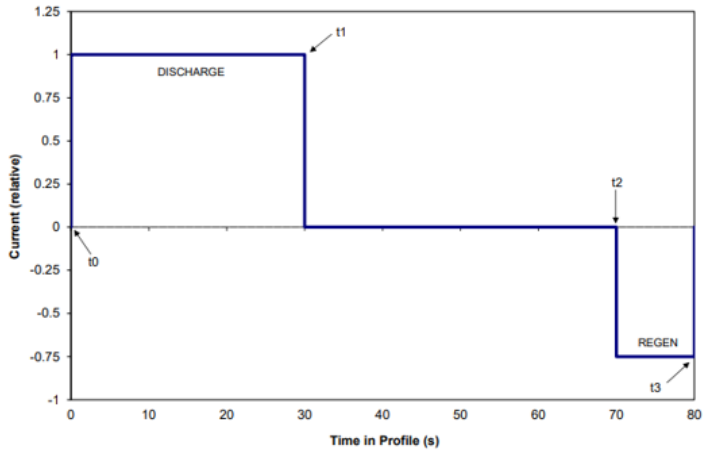

Figure 3.2: Discharge and charge pulses of the HPPC test [45]

where I_{dis} and I_{chr} are the constant current used in the discharge and charge pulses respectively, while the voltage differences have been rewritten to obtain a positive consistent value for the resistances. Each HPPC test is performed at a specific temperature, specific charge and discharge C-rate for the current pulses as well as for a specific time duration of each pulse, while the state of charge is the only parameter that varies. Therefore, there is the need to perform several test to include the resistance dependency with the other parameters and extend the map. Once the resistance is determined, it is possible to calculate the maximum current in charge and discharge by (3.4) as well as the power limits by multiplying those currents with the voltage limits, then V_{max} and V_{min} respectively, resulting:

$$\begin{aligned} P^d_{max} &= V_{min} I^d_{max} = V_{min} \frac{OCV(SoC) - V_{min}}{R^d_{0,\Delta T}} \\ P^d_{min} &= V_{max} I^c_{max} = V_{max} \frac{V_{max} - OCV(SoC)}{R^c_{0,\Delta T}} \end{aligned} \tag{3.6}$$

It is important to point out that the cell terminal voltage would not be constant during the next time horizon with a constant current applied, but rather it would change over time for reaching the voltage limit at the end of the ΔT, if the power limit prediction was correct. For this reason, it is possible to conclude that the charge power limit calculated in (3.6) is overestimated, instead the discharge power limit results underestimated, because they assume the voltage clamped to the limit during the whole future time horizon.

This method to determine power limits results relatively simple and cost effective regarding the implementation within the BMS, although several assumptions have been considered. Firstly, the state of charge is considered invariant during the time horizon for the prediction. It is important that the maximum current calculated by (3.4) usually results in a very high C-rate, since the lithium-ion batteries exhibit an internal resistance in the mΩ range. Therefore, even considering a short time for the prediction horizon the level of charge can vary significantly. For example, considering a power limit that correspond to 10C of current and a time horizon of 30 s, if that current was applied to the cell for the whole time horizon, then the SoC will drop of more than 8%. Since both OCV and resistance vary with the SoC, assuming them constant during the time horizon can lead a large error in power limit prediction, especially at very low and very high level of SoC, where both characteristic of OCV and resistance change a lot with state of charge. Moreover at those SoC levels result crucial the prediction of power limits because the probability to hit the voltage limits increases.

Second, considering a zero-th order ECM, the instantaneous state of the limiting cell used for SoP estimation is described only by its SoC (and temperature), thus the charge and discharge power capabilities are calculated assuming the cell starting from a rest condition, when its terminal voltage matches the OCV. However, SoP is performed, for the most of the time in system operation, when a generic current is just applied to the battery pack and the terminal voltage is at different level than the OCV due to the overpotential.

Third, this method relies on the overall resistance characterization but its value is affected by the magnitude of current that flows into the battery. For this reason, the estimation of the power limits results in an implicit prediction, since the current that is calculated also have an impact on the parameters needed to compute the maximum current itself. Moreover, performing HPPC tests at different C-rates does not help much to solve this issue.

These assumptions can lead a large error in power limit estimation, that means a big impact on designing the battery pack. Indeed, a too much conservative power limit estimation requires the battery pack to be oversized, whereas overestimating the power capability can lead abuse condition on the cell.

3.3.1.1 Map-based method

Map-based implementation represent those methods that calculate power limits by performing offline proper experimental tests on the cells and store the discharge enad charge power capability in lookup tables (LUT) in which

it is possible to include the variability of the power limits with respect to the SoC and temperature. In detail, LUT results a discrete map that came downloaded on the BMS, which computes the power limits by interpolating these maps with the measured temperature and estimated SoC.

The power limit calculated with a zero-th order ECM, experimentally calibrated by the HPPC test, is an example of a map-based implementation method. Other experimental test can be performed in order to capture the variability of the resistance with the C-rate such as the resistance capacity identification RCID test, that is similar to the HPPC but involves more charge and discharge pulses at different C-rates for each SoC step [46]. However, the current is not an input to the SoP estimation algorithm, then this information can be used offline to implement some effective adjustment on the SoP maps.

Map-based methods for the implementation of SoP algorithms present no flexibility in terms of time horizon to consider, which can result as a reduction of the performance the battery pack can provide. Indeed, the longer the time horizon considered the lower the power limit, and this can not correspond to the appropriate load performance at that time. Furthermore, power limit maps can present a vacancy of values, especially at high and low SoC and at low temperatures, because during the pulse test the voltage might hit its limit before the specified ΔT and resistance can not be evaluated. In this case, extrapolation can lead a large error in predicting limits and then a possible safety issue.

The variability of power limits with the aging condition can also be included in map-based methods, despite increasing the points that need to be stored and the number of experimental tests that need to be performed. This method of implementation results light in terms of computational effort for the battery management system, since only a few interpolations need to be performed.

3.3.1.2 SoC-based power limits

It is possible to evaluate power limits also by taking into account the SoC variation during the next time horizon and include this limits with the other calculated experimentally. First of all, it is important to determine the battery operating limits between the cell is designed to operate, SoC_{min} and SoC_{max}. Then, the second step is to evaluate the constant current that lead the instantaneous state of charge to approach one of its limit at the end of the future prediction window. Therefore, a constant current and a specific time horizon are considered in the recurrent SoC relationship, resulting:

$$SoC(t + \Delta T) = SoC(t) - \eta \frac{I}{C} \Delta T \tag{3.7}$$

where I is a generic constant current value and η is referred to the coulombic efficiency that model the coulombic losses during charging and discharging profiles, and it can be calculated considering the amount of energy extracted from the cell with respect to the charged one. Since the coulombic efficiency of the lithium-ion batteries is very high, in this analysis η is assumed equal to 1. Therefore, the maximum currents for the calculation of the power limits are obtained by simple algebra on (3.7):

$$\begin{aligned} I^d_{max} &= \frac{SoC(t) - SoC_{min}}{\Delta T} C \\ I^c_{max} &= \frac{SoC_{max} - SoC(t)}{\Delta T} C \end{aligned} \tag{3.8}$$

by replacing the SoC at $t + \Delta T$ with either SoC_{min} and SoC_{max}, as appropriate. After calculating all cell current limits by voltage and SoC methodologies, the pack discharge and charge currents that fulfill all design requirements are determined as the minimum in magnitude between those current limits and the one provided by the manufacturer, hence this method is called V-I-SOC. The overall power limit related to the battery pack is calculated by taking into account the series and parallel connections of the cells. VISOC method represent another map-based method that add more information than the sole HPPC but it is still limited.

3.3.1.3 Dynamic-model based method

The limitation described for the map-based methods in SoP estimation impose the need to consider an higher order of ECM that allows to take into account the dynamic phenomena that occurs within the cell and impact on the evolution of the terminal voltage over time. Too simplified model can give a result with low accuracy and high error, either posing safety and hazard issue in case of optimistic estimation, or limiting the performance of the pack if pessimistic estimation. Moreover, simplifying the voltage behavior of the cell wit a zero-th order ECM does not allow to consider the actual load condition of the cell, due to the assumption that the cell is in the rest condition.

Generally, the prediction of the power limits is performed for a time horizon that is not too long (typically 30 s), otherwise the performance of the batteries are significantly reduced regarding the instantaneous power requested from the load, whereas some electrochemical phenomena occurring

within lithium-ion batteries are characterized by time constant of hours. Therefore, it is sufficient to consider a first order EMC predict the voltage behavior and power limits for the future time horizon. Moreover, according to the assumption of a relatively short time horizon, the temperature is considered constant. Referring to the generic n-order ECM in (1.4), the model equations of the first order ECM with a constant current as input forcing can be written as follows:

$$\begin{aligned} SoC(t) &= SoC(t_0) - \frac{I}{C}(t - t_0) \\ v(t) &= OCV(SoC(t)) - R_0 I - v_1(t) \\ v_1(t) &= v_1(t_0) e^{\frac{t-t_0}{\tau_1}} + R_1 I (1 - e^{\frac{t-t_0}{\tau_1}}) \end{aligned} \tag{3.9}$$

where $\tau_1 = R_1 C_1$ is the time constant related to the RC branch considered for the first order ECM. This describes the evolution over time of the terminal voltage with respect to a constant current applied at $t = t_0$. In this case, the voltage $v_1(t_0)$ allows to take into account the actual load condition of the cell in terms of voltage.

Even in this case, power limits estimation follows the step of determining the maximum current, namely the current that causes the cell terminal voltage to reach its limit at the end of the time horizon considered. Hence, it is possible to calculate this current by substituting the third equation of (3.9) in the second one, inverting it and considering both $t = t_0 + \Delta T$ and the terminal voltage equal to its minimum or maximum allowable, for discharging or charging limit, respectively. It results in:

$$\begin{aligned} I^d_{max} &= \frac{OCV(SoC(t + \Delta T)) - V_{min} - v_1(t_0) e^{\frac{\Delta T}{\tau_1}}}{R_0 + R_1 (1 - e^{\frac{\Delta T}{\tau_1}})} \\ I^c_{max} &= \frac{V_{max} - OCV(SoC(t + \Delta T)) + v_1(t_0) e^{\frac{\Delta T}{\tau_1}}}{R_0 + R_1 (1 - e^{\frac{\Delta T}{\tau_1}})} \end{aligned} \tag{3.10}$$

Then, the limits in power are calculated by multiplying the maximum current in charge I^c_{max} to the maximum cell voltage V_{max} and the maximum current in discharge I^c_{max} to the minimum cell voltage V_{max}. However, $OCV(SoC(t + \Delta T))$ is not defined since the state of charge at the end of the time horizon needs the current to be calculated. The most simple method to solve this issue is assuming the OCV does not vary much within the time horizon and the OCV at the instant of the prediction is taken into account. A better approximation can be done by taking into account the

first order of the Taylor series expansion of the OCV-SoC characteristic, and neglecting the higher order terms:

$$\begin{aligned} OCV(SoC(t+\Delta T)) &= OCV(SoC(t_0) - \frac{I}{C}\Delta T) = \\ &= OCV(SoC(t_0)) - \frac{I}{C}\Delta T \frac{\partial OCV}{\partial SoC}\Big|_{SoC(t_0)} + h.o.t. \end{aligned} \tag{3.11}$$

This method is called VLEO (voltage-limited extrapolation in the OCV) [47, 48] in which the maximum current in charge and discharge for the calculation of the power limits becomes:

$$\begin{aligned} I^d_{max} &= \frac{OCV(SoC(t_0) - V_{min} - v_1(t_0)e^{\frac{\Delta T}{\tau_1}}}{R_0 + R_1(1 - e^{\frac{\Delta T}{\tau_1}}) + \frac{\Delta T}{C}\frac{\partial OCV}{\partial SoC}\big|_{SoC(t_0)}} \\ I^c_{max} &= \frac{V_{max} - OCV(SoC(t_0) + v_1(t_0)e^{\frac{\Delta T}{\tau_1}}}{R_0 + R_1(1 - e^{\frac{\Delta T}{\tau_1}}) + \frac{\Delta T}{C}\frac{\partial OCV}{\partial SoC}\big|_{SoC(t_0)}} \end{aligned} \tag{3.12}$$

It is straightforward to asses that this approximation results very accurate in a neighborhood of the starting point for which the OCV-SoC characteristic is linear. Typically, this is true within a large range of SoC, but at both extremes the OCV curve becomes exponential and the error with a linear interpolation can increase.

It important to highlight that the explicit solution of $v_1(t)$ reported in (3.9) assumes that the parameter R_1 and C_1 are constants over time, however the SoC change since a current different to zero is applied, then the parameters change their value as well. In general, ECM parameters change with SoC, temperature, current direction and current amplitude, and they exhibit nonlinear dependency with those variables, leading significant errors in forecasting the terminal voltage for a large time horizon in the future, even considering a constant current. It is possible to take into account also these nonlinearities with the same approach used for approximate the evolution of the open circuit voltage in VLEO method, but the ordinary differential equation that solve the voltage across to the RC branch will include non-constant coefficient, resulting in higher complexity to solve and invert in order to find the current limits. Another approach used to take into account the variation of OCV and parameters of ECM is to divide the whole time horizon in a finite number of sub-intervals and consider those parameters constant in each intervals but different between two sub-intervals, or rather piecewise linear parameters. An example of

this approach is represented by the multistep model predictive iterative (MMPI) method presented in [47], where the authors also highlight the necessity of an iterative process to calculate the power limits. This method results more accurate but requires much more computational effort to be implemented, and this can be a limitation for implementing MMPI method on a BMS.

However, among all the methods based on models which include a description of dynamic phenomena occurring within the cell, they result more flexible than the map-based methods allowing to change the time horizon for the prediction as well as to consider the actual condition of the cell. It is important to point out that SoP estimation methods, based on ECM to predict the behavior of the terminal voltage, also require an offline characterization phase performing several experimental tests with the aim to capture the parameter variability in terms of SoC, temperature, current magnitude and current direction. Hence, this does not constitute an advantage for SoP estimation method that consider ECMs with order higher than zero.

3.3.2 Comparison and validation

A better comprehension of the differences between the map-based methods and the model-based methods for SoP estimation can be possible by performing both of them on the same application and comparing the estimated values during the overall operating profile.

The difference in the two approaches lies in the fact that map-based methods neglect the current state of the cell in dynamic terms. In fact, map-based methods perform power limit estimation by calculating an equivalent resistance based on an impulsive experimental test, whereas model-based methods estimate the SoP of the battery pack by solving analytically or numerically. This makes it possible to include the estimation of various dynamic parameters such as voltage due to the effect of polarization.

The purpose of this comparison is to quantitatively evaluate the responses of the two approaches in estimating power limits in the application of an electric vehicle. In this regards, the estimation method considered have been integrated into the BMS controller of the battery pack. The SoP of each method is continuously updated at cell level and expanded to the battery pack by considering the total number of series and parallel connections of the cells. The EV model reference considered for this analysis is reported in [46] and is an energy-based vehicle model which is composed of four main subsystem, including the driver model, the vehicle controller unit, the powertrain model whereas the last subsystem models the vehicle dynamics. This model is able to integrate any possible driving

cycle standard, which represent the input of the driver subsystem. This is modeled through a PID controller and generates acceleration and brake reference to the vehicle control unit that transform this information in the torque request for the electric vehicle powertrain. This block consist of the model of the battery pack, the electric drive and the braking system. The electric drive is modeled through an efficiency map and a first-order filter for taking into account the machine inertia, whereas the high voltage battery pack is modeled through a first-order ECM combined with a lumped thermal model in such a way to also include the cooling system. The information about the power required to the electrical drive becomes the input of the battery model which update the output terminal voltage of the battery pack to the next step. The high voltage battery subsystem model also include the BMS controller which calculates the power limit at each time step of the operation considering a specific time horizon (30s). The friction braking system in also included in order to meet the braking request even in the case the regenerative braking results not sufficient. The output of the powertrain subsystem result the tractive force available at the wheel, which is used by the vehicle dynamic subsystem to calculate and update the vehicle speed that is sent to the driver subsystem with the feedback.

The battery pack considered for comparing the map-based SoP estimation methods and the model-based method presented in the previous paragraph is composed by 100 cells in series and 12 in parallel. The battery selected for this analysis is the 3-Ah Sony VTC6 cell, resulting a The resulting high-voltage battery pack with is characterized by a total energy of 12.9 kWh, resulting sufficient for the purposes of this analysis. The vehicle model has been tested with a modified Federal Highway Driving Schedule (FHDS), which is two times faster than the standard one. The initial condition of the battery is selected equal to 80% and the simulation has been continuously ran until the battery SoC becomes equal to 10%. This choice allows for evaluating the response of the SoP estimation methods over a wide operating range of the battery pack.

The result of the comparison of the power limit estimations of HPPC, VISOC and VLEO methods are illustrated in figure 3.3

It is important to point out that the power limits have not applied to the power request, in order to guarantee the same inputs to all the estimation methods and performing a consistent comparison. As expected, VISOC provide a more conservative power limit estimation than the HPPC method, since VISOC minimizes the HPPC power limit considering also the maximum current value provide by the cell manufacturer and the power limit estimated by the SoC based method. Moreover, it is possible to notice

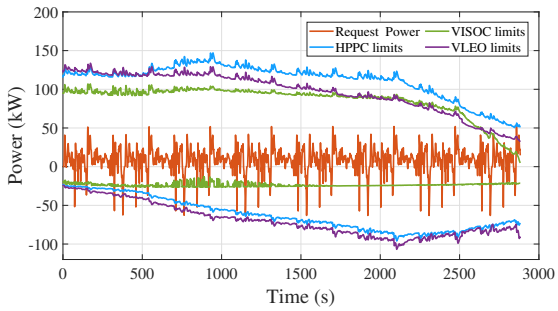

(a)

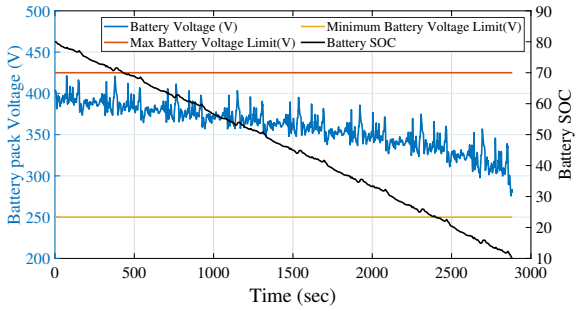

(b)

Figure 3.3: Simulation of power limit estimation applying different SoP estimation methods (HPPC, VISOC and VLEO). (a) Charge and discharge power limits, and power request to the battery; (b) Battery pack voltage and state of charge.

an offset between the HPPC and the VLEO power limit estimations because the VLEO model based method take into account the actual state of the batteries. Indeed, since the average current over the driving cycle results as a discharge current, VLEO discharge power limit result more conservative with respect to the HPPC estimation, and the situation reverses considering the charging power limits.

However, it is necessary to highlight that the comparison analysis reported does not assess the VLEO method is in general better with respect to the HPPC power limit estimation. Indeed, there is no true value of the power limit that can be taken as a reference and to be compared with. For this reason, the validation process of any estimation approach need to be execute though experimental tests, in which the power limit calculated in some specific condition in SoC and temperature is applied to the battery for the next time interval considered for the estimation, and evaluate the error between the actual terminal voltage at the end of the time interval

and the voltage limit.

Some experimental test have been conducted to the 3-Ah SONY VTC6 cell with the aim of better comprehending which are the factors that most influence the state of power of a lithium-ion battery cell. A static characterization was carried out initially in order to obtain the characteristic relationship between the SoC and OCV under different temperature conditions and how the capacity change by considering different temperatures and discharge C-rates. Then, the dynamic parameters of the cell were characterized through a series of RCID tests at different temperatures. In detail, the fixture has involved a Peltier cell system as a cooling system with the aim of dissipating the heat generated from the cell and keeping the temperature constant during the test. According to the SoP definition, power limits refers to the maximum power the battery can deliver or receive continuously for the next specific time horizon without crossing any voltage and/ or temperature limit. Therefore, power limits refer to an extreme C-rate (10C for SONY VTC6 18650) that leads very high heat generation. Fully discharge experimental tests performed on the SONY VTC6 cylindrical cell at the maximum rate provided by the manufacturer have shown a temperature increment of 30°C from a starting temperature of 23°C, including the Peltier system. However, performing the same test with the same fixture inside a thermal chamber, where the ambient temperature is controlled through a process of forced convection, the increment of the temperature of the cell becomes equal to 9°C. The comparison output data of these two experimental tests are illustrated in figure 3.4.

Consequently, the higher the temperature raise the more Ampére-hours can be discharged from the cell, but this quickly accelerates the degradation processes increases safety risks. Moreover, the highlighted phenomenon has a strong impact on the state of power estimation and the raise of the temperature can not be neglected, since it allows for extending the time interval in which the cell is capable to experience the predicted power limit without hitting the voltage limit.

Another experimental test have been demonstrated the impact of the actual dynamic condition and the previous state of the cell. In this case, a partial discharge test has been performed at the same extreme rate of the fully discharging test. A proper initialization process is needed to bring the cell at a specific state of charge, including at least a partial discharge and rest phases. The designed initial SoC is selected in such a way of comparing the time interval the cell needs to hit the voltage limit in both experimental tests. Since the usual time horizon selected for SoP estimation in electric vehicle application is equal to 30s, the initial state of charge of the partial discharge experimental test is selected as the SoC the cell exhibit 30s before

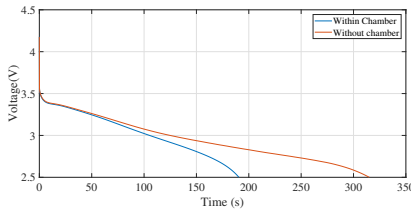

(a)

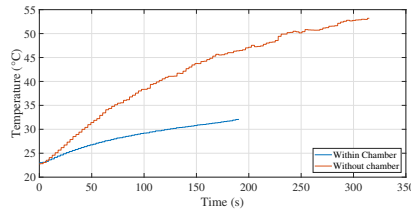

(b)

Figure 3.4: (a) Voltage and (b) temperature output data achieved in two different experimental fully discharge test with (blue) and without (red) the use of the thermal chamber.

hitting the limit in the fully discharging test.

The comparison of the experimental results are illustrated in figure 3.5, where the alignment of the data of the two different tests with respect to the x axis is made by referring to the OCV characteristic.

The time interval to hit the minimum voltage limit in the partial discharge test is equal to 64s. The purpose of this test is to show the impact of the previous current profile on the SoP estimation by considering the two extreme conditions: a fully rested cell and a cell which is delivering its maximum power for a long time. However, the results achieved for the SONY VTC6 cannot be generalized since they strongly depends on the cell technology under the test. Therefore, this experimental test give a quantitative indication of the impact of the previous dynamic state on the prediction of the power limits.

3.3.3 Discussion and final remarks

A power limit represent the maximum amount of power the battery pack can constantly hold (both in charge and discharge) for a specific future time interval while ensuring to behave within the safety operating area. Therefore, every cell voltage within the battery pack does not have to exceed operating limits in temperature and voltage. In other words, SoP

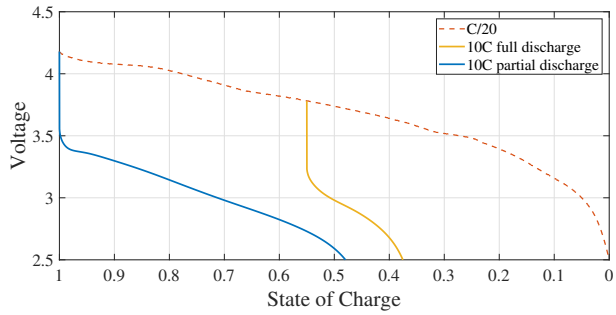

Figure 3.5: Fully and partial discharging test of SONY VTC6 18650 cylindrical cell.

represents the power that if constantly applied to the cell for the whole future time interval considered it leads the cell to reach the nearest limit. Some other limits can be added for the specific application such as current limits and SoC limits, with the aim of a better management of the battery pack over time.

The challenge in SoP estimation is the high-precision acquisition of the SoP reference value that allows for quantitative evaluating the SoP estimation algorithms. Indeed, there is no standard and uniform test methodology to validate the effectiveness of SoP estimation. Another way to compare two different SoP estimation algorithms consist of applying experimentally the power limit estimated by the algorithm to the cell and evaluate the error between the terminal voltage at the end of the time horizon and the voltage limit. However, it needs to be highlighted that the actual state of power of a battery pack does not depend only by the instantaneous measurement of the voltage, temperature and current, neither by the instantaneous SoC of a battery cell, but it is also related to the history of the current profile applied before the instant in which power limits are estimated. Indeed, in general, a rested cell exhibits a discharge power limit higher than a cell that has been experiencing a discharging current in the past, and vice versa considering a charging current. This represents the major obstacle to determine an SoP reference value that allows to quantitative compare different power limit algorithms. For example, considering a cell that is rested, the method that use the HPPC experimental test to estimate the power limit might perform better than the VLEO method to predict the SoP, but this results can be easily reversed if considering a cell that is undergoing a discharge profile for long time. Some experimental tests have been performed with the aim of pointing out the impact of the starting condition of the cell, which can be translated in a different terminal voltage at the same state of charge.

On the other hand, the second issue is determined by the methodology the power limit are defined. Indeed, SoP estimation algorithms address to calculate the maximum constant current in charge and discharge before calculating the maximum power, respectively. Nevertheless, if a constant current is applied to a lithium-ion battery the voltage response will not be constant and, consequently, the power will not be constant as well. As it is possible to notice, this lead to inconsistency between the definition of power limit and the calculation method. In order to validate and compare SoP estimation algorithms, validation can be performed on the estimated maximum current in charge and discharge, since those current would lead the voltage of the cell to reach its limit at the end of the time horizon considered, if applied.

Chapter 4

Balancing Circuits

Ensuring the cell balancing within the battery pack is a crucial requirement a battery management system needs to address, since imbalances lead to the reduction of the usable capacity. Imbalancing for lithium-ion battery pack is a phenomenon that usually occurs over long time that bring the cells at different state of charge with the consequence of inhomogeneous performance provided with respect to the same input current. Indeed, lithium-ion batteries exhibit distinct response in terms of cell terminal voltage if they are at different level of SoC. A battery pack can be defined balanced if at a reference condition, all the cells are at the same SoC. The choice of the reference balance point is important characteristic. For example, if the balance point is 100%, when cells are perfectly balanced, they all reach 100% SOC at the same time during charging, but they will diverge in SOC during discharge. Moreover, it is important to point out that the ideal condition for developing a battery pack represent the connection of cells that have the same capacity, since a string of series-connected cells experience the same load current instantaneously. Indeed, considering two cells connected in series with different capacity, the one with lower capacity will be fully discharged before the other one limiting the usable capacity of the cell with more capacity, which still stores some amount of charge that could be delivered.

In this chapter the causes and effect of the imbalance issue will be detailed discussed. Moreover, this chapter aims to report the state of the art of the main architectures presented in literature to bring the pack from an imbalance condition to the balanced one. Passive and active approaches will be described and the related solution to implement them in a BMS. For every balancing circuit presented the working principle, the components included, the main advantages and drawbacks are reported.

4.1 Imbalance issue

Starting from the scenario in which a battery pack, composed by n series connected cells, is perfectly balanced, after several charging and discharging cycles there will be a cell, or a group of cells, that will exhibit a different voltage, even in rest condition, that corresponds to a different state of charge. This phenomenon of divergence is not corrected and over time that imbalance grows. Whenever any SoC limit is hit by a cell, the respectively charge or discharge process is stopped and the imbalance start to accumulate as a positive average integral. Therefore, imbalances are caused by anything that can make the SoC of a single cell to diverge over time with respect to the other ones. In order to analyze the causes of the SoC deviation the general relationship between the state of charge and the current should be taken as a reference, and is reported here:

$$SoC_k(t) = SoC_k(t_0) - \frac{\eta_i}{C} \int_{t_0}^{t} i_k(\tau)\, d\tau$$

The first cause of imbalance between cells with the same capacity C can be identify in a different coulombic efficiency. Indeed, considering a string of series-connected cells starting from the same SoC, they experience the same current. Nevertheless, if they are characterized by a different coulombic efficiency (η_i, where the subscript k refers to $k-th$ cell) the increment or decrement of SoC over time results different, then their SoC diverge over time.

Imbalance occurs also when the series-connected cells experience different current among each others [16]. This can occur if the net current of the single cell takes into account the rate of the self-discharge and the current drawn by the electronic circuitry of the BMS. These two components can be different for each cell leading some cells to be affected by different net currents, resulting into imbalance over time.

Another important factor that have an impact on the SoC divergence is represented by the temperature. As reported in the first chapter, temperature strongly affect the performance of lithium-ion cells, in terms of capacity, cell parameters value, self discharge rate, coulombic efficiency and overpotential as well as high temperature accelerate degradation mechanisms. Actually, temperature is not a direct cause of the imbalance, but rather the presence of thermal gradient within the volume of the battery pack bring the cell working at different temperatures. Maintaining a uniform temperature across the battery pack will help to prolong the lifetime of the battery pack. Moreover, tolerance and defects in manufacturing process contribute to little differences in battery parameters and then imbalancing

over time.

Voltage and SoC imbalances in a battery pack not only limit the usable capacity stored within the pack, but the imbalance increase the risk of encountering in safety issues related to abuse condition of overcharging and overdischarging, then a balancing strategy has to be implemented in every battery pack. The implementation of an effective balancing strategy in BMS represent a crucial requirement to mitigate the imbalancing issues, for the purpose of increasing the useful capacity of the battery pack and reducing the risk of hazard safety conditions.

4.2 Balancing strategy

Designing a balancing system for a BMS can be divided in two different steps which consist in defining the balancing strategy and the balancing method. While the balancing method defines the interconnection structure to transfer energy between cells, the balancing strategy aim to determine the balancing criteria and the control strategy to be adopted. In detail, the balancing strategy include the selection of the balancing point, when perform the equalization of the cells and the control variable of the balancing algorithm.

The first thing that need to be determine is the balancing point, according to definition reported before. Indeed, it allows the BMS to evaluate the whether the battery pack is balanced or not as well as the quantitative imbalance of SoC if present. The definition of balancing point allows operating conditions in which the battery pack is not balanced, but it is sufficient that the SoC is the same only in one SoC level. The definitions of balanced pack and balancing point lead to take into account the unevenness of capacity among the cells. It is important to ensure that point is related a condition that the battery pack will experience over time in order to be easily verified from the BMS, even after several charging and discharging cycles. For example, the full charge of the cells (SoC = 100%) can be selected as the balancing point, but, in general, it depends on the specific application. Setting the balance point to the maximum allowable SoC optimizes the storage of energy in the battery pack, making the most of the available ampere-hours, since cells with higher SoC levels generate higher voltages compared to those with lower SoC. While this increased energy is advantageous for electric vehicles and similar applications, it's important to note that operating at high SoC can accelerate degradation mechanisms that contribute to cell aging. This drawback needs consideration as, during a discharge/charge cycle, all cells experience time at the maximum designated SOC. On the other hand, setting the balancing point to the lowest

allowable SoC might potentially limit discharge power when the pack is close to empty and it will tend to cause the battery pack aging much more quickly because the limiting cell experiences much more operating condition that accelerate aging with respect to all the other cells [16].

Once the balancing point is determined, some consideration needs to be done in order to determine when perform the balancing process, that is in which battery pack operating condition such as either charging, discharging, idle or both. In general, it is possible to consider to perform the cell equalization only during charging for the application that mainly receive charge from an external source, since any energy losses for the balancing procedure is compensated by the external source allowing to maximize the energy stored in the battery pack at the end of the charging process. Otherwise, it is possible to consider to turn on the balancing process continuously. Moreover, regardless the operating mode of the battery pack, two different approaches can be adopted to define when performing the balancing process. The first one consider only the present state of the cells whereas the second one consider the future state of the cell by means a prediction and programming the balancing process.

The last paramount criteria that defines the balancing strategy is the control variable the balancing process depends on. This allows to define the control strategy of the balancing circuit in terms of which cells need to be balanced and when stop the balancing process. So far, the discussion has been focused on the SoC level for each cell but it is possible to select other variables to control the balancing process, such as the terminal voltage or the OCV.

- *Voltage-based strategy*

  This strategy use the monitored cell terminal voltages to assess the imbalances among the cells. Therefore, this method is based on assuming that at the same terminal voltage correspond the same SoC. Since this method does no require any estimation algorithm and is influenced only on the measurement error, it result simple to implement. However, the assumption of this method is verified in rest condition, that is when the terminal voltage is equal to the OCV, since this method does not consider the effect of the internal resistance (that is SoC dependent) of the cell and overpotential. This can produce a counterproductive effect leading an higher imbalance among the cells.

- *OCV-based strategy*

  The enhancement of the previous strategy consist in basing the balancing control algorithm on the OCV. Indeed, it allows for compen-

sating the effect of the internal resistance with respect to the method based on the terminal voltage measurement. To do this, OCV-based method requires a battery model to estimate the OCV which allows a comparison with the OCV-SoC characteristic. Therefore, this method is influenced by the error on the estimation of the OCV and it does not result effective where the OCV-SoC curve is flat.

- *SoC-based strategy*

  This would be the preferred method, since the goal of the balancing system is to equalize the state of charge and coincides with the control variable of the balancing algorithm. Indeed, it allows for overtaking the issue related to the OCV-based method but it is still influenced by the estimation error of the SoC estimation method. Moreover, the computational effort for performing accurate SoC estimations is higher, especially for large battery pack where estimating the state of charge of each cell results very challenging.

4.3 Architectures

The implementation of the balancing process can be realized by different architectures. They are mainly classified based on the approach in passive and active, depending on the cells either dissipate or move the excess energy. Among them, the requirement of a cell balancing architecture are expressed in terms of efficiency, equalization time, voltage and current stresses on components, hardware and software complexity, size, weight and cost.

4.3.1 Passive

Passive equalization circuits aims to balancing the series-connected cells by dissipating the excessive energy stored in the most charged cell on a resistor placed in parallel to each cell. They represent the most simple and reliable approach to balancing the cell. Therefore, passive balancing circuits are the most common solution adopted in vehicular application, also due to the low cost [49]. However, there are various drawbacks associated with this architecture. In detail, they mainly include low equalization efficiency, unidirectional power flow, and thermal challenges arising from heat generation. The Joule's effect on the balancing resistors becomes significant, especially when aiming for high equalization speed, necessitating a specific circuit design [50,51] as well as a proper control strategy for thermal management [52]. In addition, the sizing of the balancing resistor strongly depends on the real operating conditions of the cells, including battery

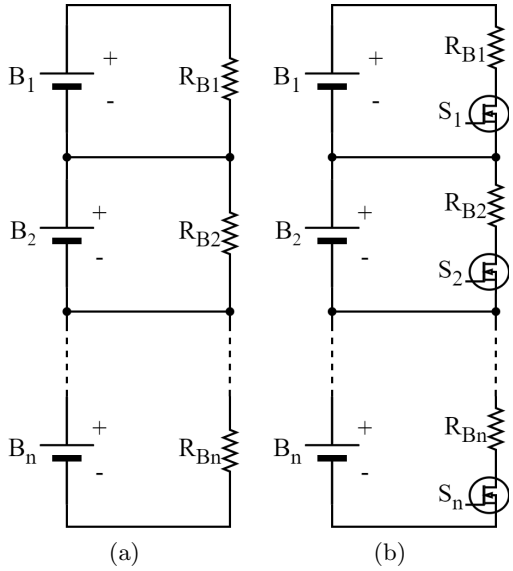

Figure 4.1: Passive balancing circuit architectures: (a) fixed shunting resistor and (b) switched shunting resistor.

technology, temperature, state of charge and voltage imbalance among the cells [53].

Passive equalization can be classified in two different categories: fixed shunting resistor 4.1a and switched shunting resistor 4.1b. The fixed shunt resistor architecture is realized by directly connecting a balancing resistor in parallel to each cell leading a continuous current leakage from the cell to that resistor. Since the cell voltage changes with respect to the state of charge, different balancing current are established if the series-connected cells result imbalanced. This solution result very simple and cheap, due to the small number of components needed and no control circuity is required. For this reasons, it is widely implemented for lead-acid, Ni-Cd and Ni-MH technologies in low power application to avoid overcharging conditions for the cells. The major drawbacks is the continuous energy dissipation that turns into heat causing an increment of the local temperature within the pack. This yields the fixed shunting resistor architecture unsuitable for high-performance applications such as EV.

Conversely, the switched shunting resistor solution allows to control the power dissipated by each cell including a power switch placed between the voltage terminal and the balancing resistor. The balancing process results optimized and more effective with respect to the other passive equalizer and

Family	Equalizer	AC2C	DC2C	P2C	C2P
Capacitor-based	Switched capacitor	✓			
	Single switched capacitor	✓	✓		
	Double-tiered switched capacitor	✓	✓		
Inductor-based	Single inductor	✓	✓	✓	✓
	Multi-inductor	✓			
Transformer-based	Single winding			✓	✓
	Multi-winding transformer			✓	✓
	Multiple transformers			✓	✓
Converter-based	Cúk converter	✓			
	Flyback converter			✓	✓
	Ramp converter	✓			
	Full-bridge converter	✓			
	Resonant converter	✓			

Table 4.1: Classification of the active equalization circuits with respect to the storage component adopted and the energy transfer technique.

only the most charged cell are involved in the balancing process. Therefore, an optimal control of the switches can be performed with respect to the cell operating conditions and depending on the performance required or desired allowing to increase the balancing current and reduce the balancing time if the same amount of heat generation is considered between the two passive architectures. Nevertheless, the heat dissipation issue still remain and proper balancing strategy needs to be implemented to reduce the equalization time while limiting the raise of the temperature.

4.3.2 Active

As opposed to the dissipative approach, active balancing circuits represent the alternatives to the passive equalizer allowing the energy transfer among the cells. Indeed, the balancing process is realized by transferring the excess of the energy in the most charged cells to the least charged ones leading high performance in terms of energy efficiency and equalization speed. These performance can be achieved because the heat generated from the balancing process is much lower than the passive solutions increasing the balancing current capability without encountering relevant thermal issues and, consequently, reducing the time needed to equalize the cells.

Different architectures for the active equalizers have been reported in literature, with detailed comparison in terms of efficiency, equalization speed, voltage and current stresses on components, hardware and software com-

plexity, size and cost [54–57]. They can be classified with respect to either the storage component adopted or the equalization energy flow. For what concerns the storage component, capacitors, inductors, transformers or converters can be adopted, whereas four categories can be identified regarding the specific energy transfer technique: direct cell-to-cell (DC2C), adjacent cell-to-cell (AC2C), pack-to-cell (P2C) and cell-to-pack (C2P). Table 4.1 reports all the main architectures of active equalizers presented in literature and the correlation with the transfer energy path. The first one allows directly transferring energy between the most and the least charged cells of the battery pack. It can be performed with both capacitor-based [58, 59] and inductor-based [60] architectures. In the second one, mainly realized by converter-based architectures, the cell with higher voltage is discharged on the adjacent one until the equalization is reached, resulting very slow and expensive for large battery packs.

Currently, transformed-based equalization circuits are mainly adopted for achieving C2P or P2C energy transfers since they can achieve high equalization speed and good control of the equalization dynamic. These architectures include single-winding transformer [61], multi-winding transformer [62], multiple transformer as well as several power conversion stages, which allow the energy transfer with a proper control operating mainly in flyback and forward modes. However, the losses of the power converter and the incorrect design of the transformer can strongly impact on the overall performances of these balancing circuits in terms of equalization efficiency and speed.

Active equalization circuits are now a potential alternative for enhancing battery pack performance due to the ability to transmit energy among cells and so prevent energy dissipation as do passive equalizers. Furthermore, active equalization procedures may be used during the charging and discharging processes, helping to maximize energy from and to the battery pack. However, the primary constraints preventing widespread use of active equalization circuits are the amount of components required for hardware implementation, which leads to size and cost issues. In addition, elaborate control algorithms must be developed for managing of active structures in comparison to the simplicity of passive equalization circuits.

4.3.2.1 Capacitor-based

These balancing circuits integrate capacitors as the passive storage components by means of which the energy is transferred among the cells. They can be classified in three main categories: switched capacitor, single switched capacitor and double-tired switched capacitor. They mainly differ for the number of the component included and the number of the cell

can be involved during the balancing process.

- *Switched Capacitor*

  For this architecture, a single capacitor is connected between two adjacent cells, as illustrated in figure 4.2a. The atomic unit of the switched capacitor architecture, defined as the circuitry with minimum number of components that still preserve the switched capacitor architecture, is composed of two series-connected cells, one capacitor and four power switches, 2 per each cell. In detail, each cell is connected in parallel to a leg of H-bridge while the capacitor is connected between the mid-points of the legs. This atomic architecture is repeated for each pair of series-connected cells within the battery pack. Thus, considering a battery pack with n-series connected cells the switched capacitor balancing circuit requires n-1 capacitors and $2n$ power switches. Regarding this architecture, the control strategy results very simple since the equalization process can be controlled by a common PWM signal with a fixed duty cycle equal to 50 % for every switch leg. The balancing current result self-limited since they are dependent to the voltage imbalance which decrease over time. Ideally, there is no energy transfer among the cell in case of the battery pack is balanced. This open loop control strategy also allows for avoiding the integration of sensing circuitry which is necessary in a feedback control loop an requires many electronic component in order to ensure the correct isolation. The major drawbacks is identified in the large number of components included, especially for a large battery pack. Moreover, since this architecture realize an adjacent cell-to-cell energy transfer, the equalization time can increase if the most and least charged cell are not close within the cell stack. In addition, regarding the open loop control strategy, all the cells participate to the equalization process, leading the overall efficiency of this active equalization circuit to decrease due to high losses.

- *Single Switched Capacitor*

  The single switched capacitor architecture, also known as flying capacitor, realize same working principle of the switched capacitor to transfer the excess energy between two cells but allows a DC2C energy exchange. This is possible even by using a reduced number of components with respect to the switched capacitor, since only 1 capacitor and n+5 power switches required. The electric circuit of the single switched capacitor is illustrated in figure 4.2b. However, a more complex control strategy needs to be adopted in this case since the most charged cells have to be identified enabling the corresponding

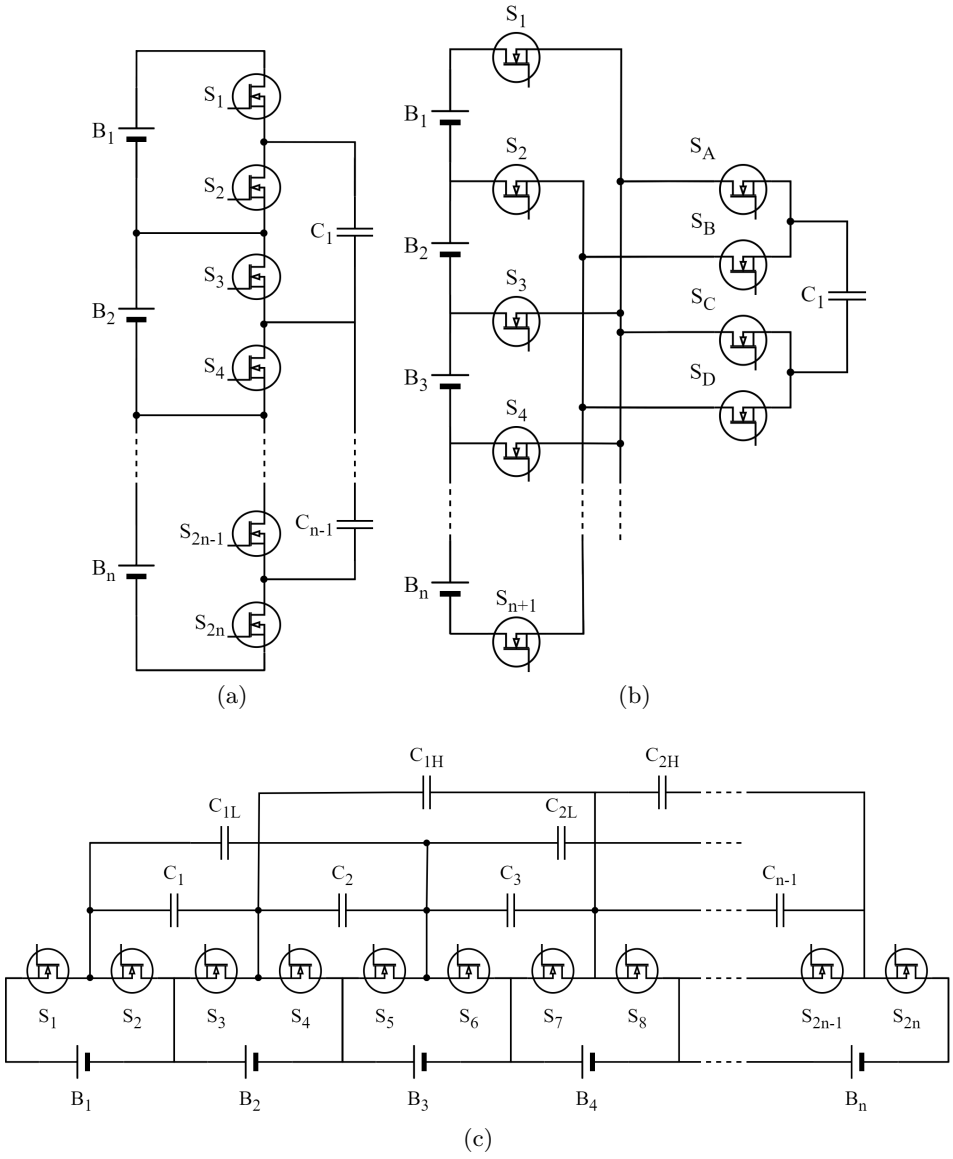

Figure 4.2: Capacitor-based equalizers: (a) switched capacitor, (b) single switched capacitor and (c) double tiered switched capacitor.

switches. This offer the possibility to implement advanced control algorithms with the aim of reducing the equalization time, especially for condition in which several cells are imbalanced with respect to each others. Furthermore, this architecture can exhibit higher efficiency with respect to the previous architecture because the energy path result shorter due to DC2C equalization. However, the major drawbacks can be represented by the parasitic inductances, especially for a large battery pack, because the distance between some cells and the capacitor increases, leading a big effort in design process of the BMS.

- *Double-Tiered Switched Capacitor*

  This architecture can be derived by the switched capacitor architecture by adding two additional capacitor tiers which provide other path for transferring energy among the cell of the battery pack, leading a reduction of the equalization time with respect to the switched capacitor architecture. Indeed, this balancing circuit allows to exchange energy between two non-adjacent cells in a single switching period leading to a DC2C equalization. However, unlike single switched capacitor, all the series-connected cells are involved in the balancing process to realize the energy exchange between two non-adjacent cells, as it is possible from the circuit architecture in figure 4.2c. For example, considering the energy transfer between the cell 1 and the cell 3, the energy path also include the cell 2 for the whole switching period, leading an average balancing current equal to zero for that cell. As reported, DC2C equalization can be achieved for Double-tiered switched capacitor architecture but with a larger number of components with respect to the flying capacitor one, since fo a $n$series-connected cells this architecture requires $2n$-3 capacitors and $2n$ power switches, resulting a more expensive balancing solution. Moreover, a proper control strategy needs to be implemented to take advantages from this architecture and reduce the equalization time. Indeed, the equalization time can be further reduced with respect to the flying capacitor because multiple DC2C equalization can be performed simultaneously.

4.3.2.2 Inductor-based

These type of balancing circuit use inductors as arrays to transfer the excess energy stored in the most charged cells to the least charged ones. The basic principle of this architecture consist of dividing the switching period in two sub-intervals, the first one serves to transfer energy from the

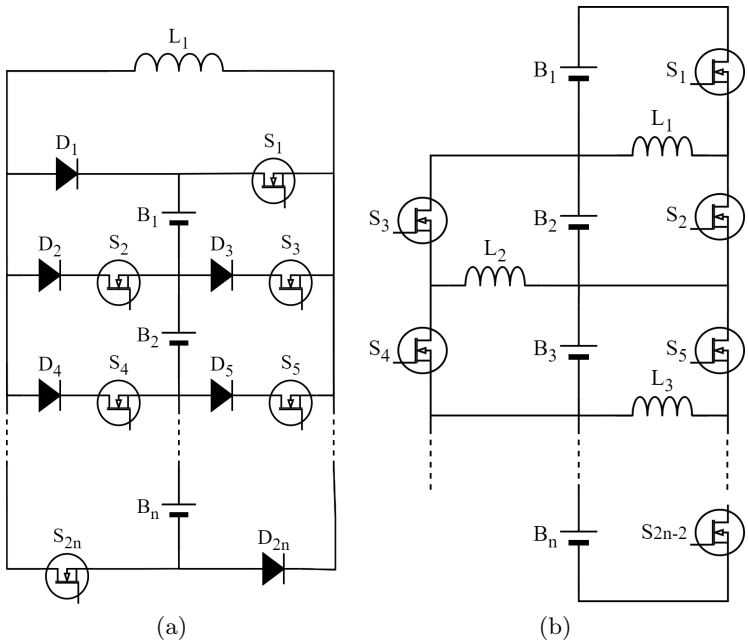

Figure 4.3: Inductor-based equalizers: (a) single inductor and (b) multi inductor architecture.

most charged cell to the inductor whereas the second sub-interval is used to discharge the inductor energy on the least charged cell. Two different categories can be identified as inductor balancing circuits, including single inductor and multi-inductor architecture. Unlike capacitor-based architectures, inductor-based ones do not have the characteristic of self limiting the current, since it is not related to the voltage imbalance between the cell involved. Furthermore, these architectures are characterized by a very high balancing current capability that means the possibility to significantly increase the equalization speed. However, a proper control strategy has to be implemented in order to limit and control the value of the balancing current. The main issue presented by the inductor-based equalizers regards the current stress on switches due to hard-switching operations.

- *Single inductor*

  This architecture integrates only 1 inductor for a generic battery pack composed by n series-connected cell, as made explicit in the name, while $2n$ of both switches and diodes require, as illustrated in figure 4.3a. This architecture results very flexible in terms of energy path

since it allows for achieving both AC2C, DC2C and C2P equalization transfer methods. For this reason, advanced control strategies can be adopted for achieving a very low equalization time. In addition, the control system senses the voltage of the cells and selects the two cells which will be used for energy transferring.

- *Multi-inductor*

  This architecture represents the dual version of the switched capacitor, mainly due to the AC2C energy transfer method. Moreover, it is possible to notice in figure 4.3b the similar approach to build this architecture with respect to the switched capacitor balancing circuit. Indeed, an atomic architecture composed of 2 cells, 1 inductor and 2 bidirectional power switches can be identify and it is repeated for each pair of the series-connected cells. Therefore, for a battery pack composed of n series connected cell this architecture includes $2n$-2 bidirectional switches and n-1 inductors. Furthermore, it is possible to recognize that the atomic architecture of a multi-inductor balancing circuit represents a buck-boost converter. However, as discussed before, the main difference to the switched capacitors results that the balancing current is not self-limited and not related to the voltage imbalance between two adjacent cells. This offer the advantage to achieve high balancing current even if the voltage imbalance is small, at the expense of developing a proper feedback-control strategy and including the electronic circuitry that ensure the isolation between the different sensing channels, increasing the cost.

4.3.2.3 Transformer-based

These architectures include transformers as the passive storage components that allow the energy flows among the series-connected cell of the battery pack. The main characteristics that can be individuated in a transformer include the possibility to adapt the voltage level at the primary side to the secondary side one and the galvanically-isolation between those two circuits. Hence, comparing to the inductor-based topologies, these architectures allow for transferring energy between two non-adjacent cells without the need of inserting other electric path to the circuit by using switches as well as easily perform either C2P or P2C equalization considering the whole cell stack as as another cell by means the appropriate turns ratio. Regarding the P2C the energy is moving from the whole pack to the least charged cell, whereas the most charged cell discharges to the pack in C2P operation. Two main categories can be distinguished: single-winding transformer and multi-winding transformer.

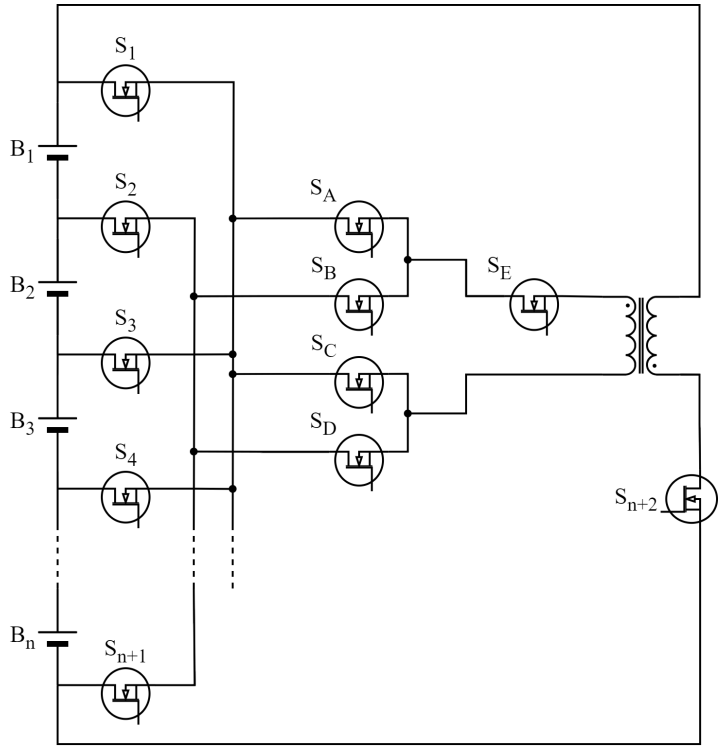

Figure 4.4: Active balancing circuit based on single-winding transformer (SWT).

- *Single-winding transformer (SWT)*

  The topology of this architecture is the same with respect to the single switched capacitor, but replace the capacitor with a transformer, as illustrated in figure 4.4. However, one more switch has to be included, which allows to connect the whole series of the cells. As result, this architecture counts n+6 power switches and 1 transformer if considering a battery pack of n series-connected cells. The primary winding of the transformer is connected to the overall module or battery-pack voltage, whereas the secondary can be switched to connect across any of the cells in the stack. Therefore, the transformer is characterized by a turn ratio equal to the number of series-connected cell of the stack considered. Faster balancing process can be achieved with this architecture with respect to the single switched capacitor architecture at the expense of higher costs for the transformers and electronics.

- *Multi-Winding Transformer (MWT)*

  Also called shared transformer architecture, it include a transformer

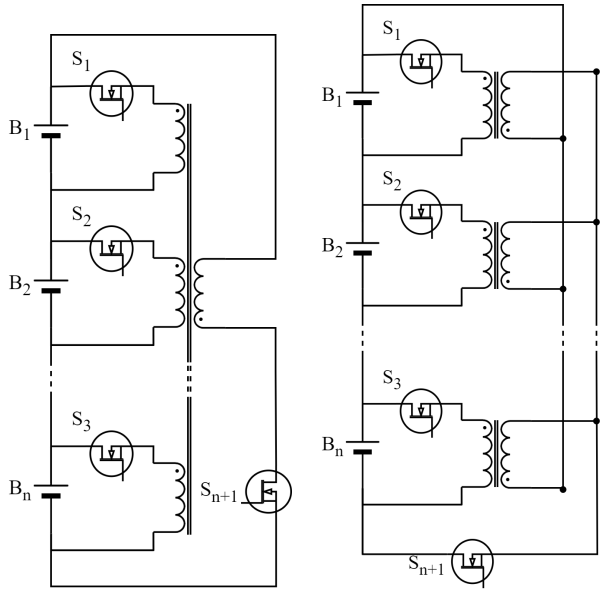

Figure 4.5: Balancing circuit architectures based on a multi-winding transformer (a) and multiple transformers (b).

composed by a number of winding equal to the number of the series-connected cell n plus one winding for the entire cell string. Usually the winding related to the battery pack is identified as the primary and all the others connected to the cell are identified as secondaries. Figure 4.5a illustrates the general configuration that include a power bidirectional switch (MOSFET in this case) for each cell and one more for the winding related to the whole battery pack. As for the single switched transformer architecture the turns ratio is equal to n by considering each cell winding and the pack winding, and then is unitary among each pair of winding associated to the cells. This architecture can work under two different operating principle, including flyback and forward mode. In flyback mode, the switch connected to the primary side is turned on and the energy is stored in the transformer. Then, when it is turned off, the stored energy is transferred to the cells by means of the internal body diodes of the MOSFETs. On the other hand, In forward mode, when a voltage difference among the cells is detected, the switch of the most charged cell is turned on and the energy is transferred to the battery pack flowing through the transformer and the internal body diode of the MOSFET at the

primary side. It is necessary to bear in mind that the secondary winding reactances are proportional to the appropriate cell voltages. The major drawbacks of this architectures are related to the design of the magnetic core of the transformer and the number of the windings that proportional increases with the number of the cells, limiting the flexibility of this architecture. Therefore, it result a better solution to consider this architecture for a modular design of the equalization circuit. For a large battery pack, an alternative can be represented by a multiple single transformer where a single-winding transformer magnetically connect the cell voltage to the pack voltage (figure 4.5b), allowing each cell to directly exchange the energy with the pack by C2P or P2C. This improve flexibility but also cost.

4.3.2.4 Converter-based

These architectures implement power converters for exchanging the energy among the cells. In detail, five main converters topologies are reported in literature for balancing circuits: Cúk, ramp, full-bridge, resonant and flyback converters. These equalization circuit usually include much more component for each cell with respect to the previous architectures as well as require complex control control strategy.

- *Cúk converter*

  A Cúk converter is implemented for each pair of series-connected cell, as showed in figure 4.6, allowing for performing a AC2C equalization. $2n$-2 switches, $2n$-2 inductors and n-1 capacitors are needed for implementing this balancing circuit in a generic n series-connected battery pack. The high number of the components needed does not represent a good trade off for a balancing circuit that allows only AC2C equalization, especially for a large battery pack, since the equalization time increases a lot.

- *Flyback converter*

  These converters find use in scenarios requiring isolation, and they can function either in a unidirectional or bidirectional manner, allowing for either P2C or C2P energy transfers. The equalization circuits with flyback converters are designed with either a single-winding transformer or a multi-winding transformer, allowing for centralized, modular, individual, or distributed control of the balancing process. This architecture shares the major drawbacks presented by the balancing circuit which include transformers such as complex design for the energy path, isolation issues, high cost and size.

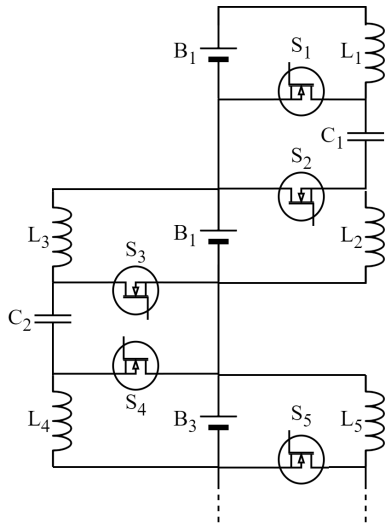

Figure 4.6: Cúk-converter based cell balancing circuit.

- *Ramp converter*

  This architecture derives from MWT-based balancing circuit but it allows for halving the number of the transformer winding, as illustrated in figure 4.7. Indeed, it is possible to notice that only one winding requires every two cells, while n power switches, n capacitors and n diodes are needed to complete the architecture. The working principle can be described by dividing the switching period in two halves. The first phase involve the odd numbered cells which provide energy to the associated capacitors, while the second phase permit the energy to be transferred to the even numbered cells. This operation can be inverted by changing the direction of the current in the primary transformer winding. This architecture results cheaper and more compact with respect to the MWT architecture at the expense of a more complex control algorithm.

- *Full-bridge converter*

  This architecture consist of an H-bridge and a capacitor in parallel with each cell of the battery pack, allowing to fully control the energy flow among the cells. Therefore, this architecture include $4n$ power switches and n capacitors for a n series connected cells. This configuration allows to implement intelligent control algorithms in order to optimize the performance of the equalization process. However, considering the large number of the components needed if consider-

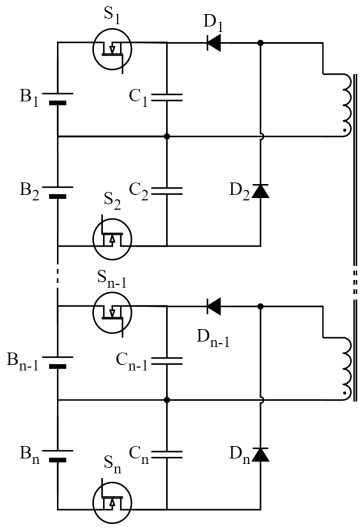

Figure 4.7: Cell equalization circuit with a ramp converter architecture.

ing this topology at cell level, full-bridge converter balancing circuit results more suitable if applied at module level.

- *Resonant converters*

  This balancing circuits use resonant converters for transferring energy among the series-connected cells. They can be further classified in two different categories, including zero current quasi-resonant (ZCQR) and zero voltage quasi-resonant (ZVQR). The aim of these architecture is reducing the switching losses by properly introducing a resonant branch into the circuit. An example of this architecture is illustrated in figure 4.8, in which is possible to notice the similarity with the multi-inductior architecture. Indeed, this introduce an L_rC_r parallel branch in series with the main inductor L that is still used for the energy transfer between the adjacent cells. In this case, 2(n-1) power switches, 2(n-1) inductors and n-1 capacitors have to be considered for a generic pack composed of n series connected-cells. Resonant converters equalizers allows for high equalization efficiency due to the high reduction of the switching losses at the expense of design cost and implementation complexity.

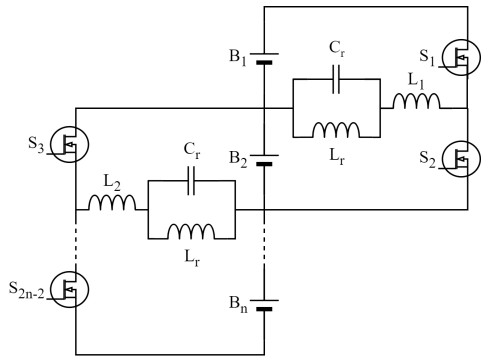

Figure 4.8: Cell equalization circuit based on quasi-resonant converter.

4.4 Final Remarks

Equalization circuits are critical in enhancing cell performance while also improving efficiency and durability. The major problems for high performance storage systems are the creation of new designs and the enhancement of existing balancing methods. Advanced power electronics research and development is taking place to create smart solutions for cell balancing circuits. Passive equalizers are now the most widely utilized option owing to their low cost and simplicity in design, installation, and control. Despite the fact that a high balancing current may be used, excessive heat dissipation restricts the equalization speed and necessitates careful thermal management. Active equalization circuits are known for their high efficiency and low power losses. Nonetheless, they struggle with time management and control issues.

Future trends can involve hybridization among different topologies present in literature and discussed in this chapter. One of the most promising approach result the integration of passive and active solution together at different modular levels, for example active balancing between modules and passive within each battery module. In general, the design and development of a cell balancing circuit need to take into account size, weight, cost, modularity, energy efficiency and equalization speed.

Chapter 5

Design methodology and performance analysis

5.1 General considerations

The development and installation of a battery equalization circuit requires a proper design methodology in order to maximize and improve the performance of lithium-ion battery packs. Furthermore, it allows for the precise selection and sizing of the equalization circuit architecture based on the needs of the specific application as well as considering the real components included for the specific architecture and the impact of parasitic parameters.

In this chapter, two different architectures have been explored by using the same systematic approach with the aim of proposing a proper design methodology based on the mathematical model. In detail, a novel architecture for a transformer-based active balancing circuit has been taken into account, which allows for equalizing simultaneously every cell while each balancing current results self-limited since is related to the voltage imbalance. Moreover, the multi-inductor architecture have been analyzed with the same approach. in particular, in both case studies, the mathematical model has been developed even considering parasitic parameters of the components involved, then a design methodology has been derived at the purpose of achieving the desired performance in terms of maximum balancing current. Accordingly, experimental prototypes have been developed with the aim of validate the design methodology and evaluate the performance of these active balancing circuits under different operating conditions.

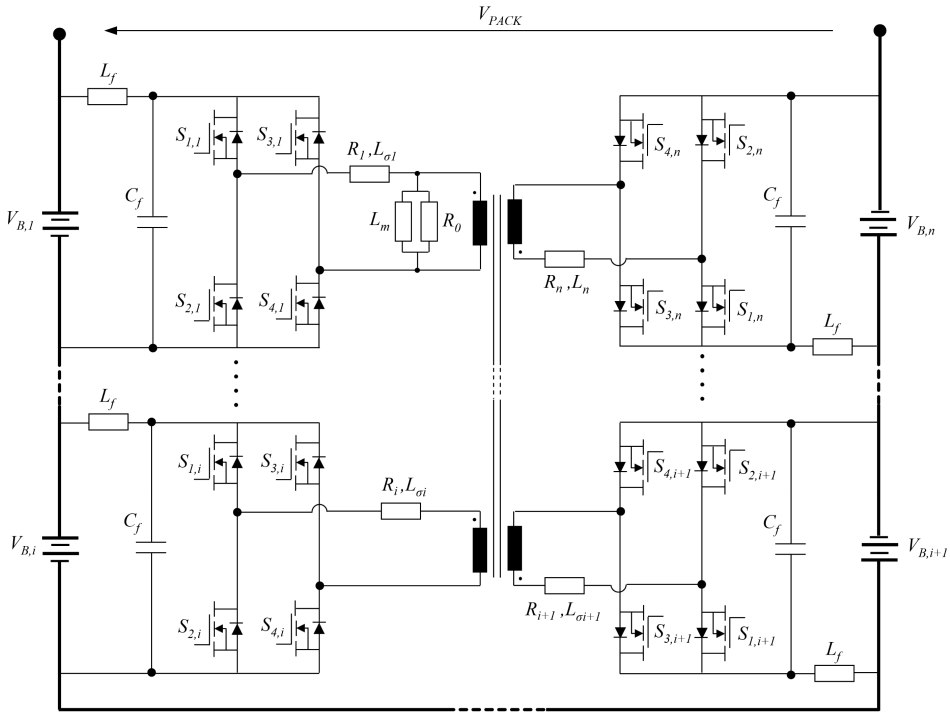

Figure 5.1: Electrical architecture of the MAB-based active equalization

5.2 Case study I: MAB-based architecture

The first active equalization circuit considered for model-based design is represented by a MAB converter, in which every cell is equipped with a H-bridge then connected to a medium-frequency multi-winding transformer (MWT), as reported in figure 5.1. This architecture has been firstly presented in [63] is based on a MAB converter [64].

Considering a battery pack composed of n cells connected in series, this balancing circuit requires n inductor filters (L_f), n H-bridges with snubber capacitors (C_f) and a transformer with n windings characterized by the same number of turns. Inductor filters (L_f) and snubber capacitors (C_f) are adopted in order to minimize the impact of the harmonic content introduced by the H-Bridge converters on the cells, whereas the MWT represents the passive component responsible for the energy transfer among the cells. Despite the hardware complexity due to the presence of a MWT and the H-bridges, this architecture presents several advantages, including short and bi-directional energy transfer path between cells, modularity, scalability and the capability of limiting the equalization currents by means

of both the transformer and the balancing circuit parameters.

High equalization speed can be achieved by simultaneously transferring energy among several cells of the battery pack. Indeed, a cells-to-cells balancing can be performed. The issue of managing a large number of switches is solved thanks to a proper control algorithm based on a single bipolar PWM signal for controlling the n power conversion units. Hence, The PWM signal is characterized by a duty cycle equal to 50% and a constant frequency. The control section requires the measurement of the cell voltages $\{V_{B1}, ..., V_{Bi}, \ldots, V_{Bn}\}$ to verify if the cells are within the desired voltage band ΔV (e.g. voltage difference between the highest and lowest cell voltages) or to apply the balancing action. In detail, if the V_{Bi} are unbalanced, the PWM signal S is provided to all the drivers of the n H-bridges. Thus, depending on the cell voltage levels, a current flow will be established from the cells with higher voltage to the cells with lower voltages. In principle, the control of the rectification stage could be disabled taking advantages of the free-wheeling diodes. However, to reduce the losses due to the diode forward voltages and to minimize the voltage drop, the rectification stage has been controlled as a synchronous rectifier through the same PWM signal S. The balancing action is stopped when the cells voltages are all contained in the desired band.

It is important to mention that this balancing architecture can operate even when the battery pack is in charge or discharge mode. This also allows for minimizing the equalization time required in idle state, when no load or charger is connected to the battery pack. Moreover, it does not require a very accurate estimation of the state of charge SoC, since the equalization of the cells is automatically and dynamically guaranteed by the voltage-controlled energy transfer across the transformer and by the unique control signal S. However, the selection and design of the electronic components and transformer have a great impact on the accuracy of the voltage balancing as well as on the equalization efficiency.

5.2.1 Model equations

The design of the MWT results fundamental for increasing the performances of the equalization process. Indeed, high balancing current can be achieved by properly sizing the transformer parameters, such as the magnetization inductance (L_m), the winding leakage inductances ($L_{\sigma k}$) and the winding resistances (R_k). According to figure 5.1, the generalized model of a n-winding transformer can be represented by the following system of

equations:

$$v_k(t) = e(t) + R_k i_k(t) + L_{\sigma k}\frac{di_k(t)}{dt} + \\ + \sum_{\substack{j=1 \\ j\neq k}}^{n} M_{k,j}\frac{di_j(t)}{dt} \quad \forall k = 1,\ldots,n \tag{5.1}$$

where $v_k(t)$ is the voltage of the k^{th} winding, $i_k(t)$ and $i_j(t)$ are the winding currents, $e(t)$ is the induced electromotive force (EMF) and $M_{k,j}$ are the mutual leakage inductances. In detail, three additional equations need to be added to the system in order to correctly described the overall model of the MWT:

$$e(t) = L_m\frac{di_m(t)}{dt} \tag{5.2}$$

$$i_m(t) + i_0(t) = \sum_{k=1}^{n}\frac{N_k}{N_1} i_k(t) \tag{5.3}$$

$$i_0(t) = \frac{e(t)}{R_0} \tag{5.4}$$

where $i_m(t)$ is the magnetization current, $i_0(t)$ is the current related to the iron losses, R_0 represents the iron losses of the transformer and N_k are the winding turns. Moreover, the following assumptions have been taken into account for adopting the model of the MWT in a design perspective:

1. the iron losses are neglected:

$$R_0 \to +\infty$$

2. the turn ratio is unitary in this specific application :

$$\frac{N_k}{N_1} \quad \forall k = 1,\ldots,n$$

3. a symmetrical structure of the MWT is considered:

$$R_k = R \quad \forall k = 1,\ldots,n$$
$$L_{\sigma k} = L_\sigma \quad \forall k = 1,\ldots,n$$
$$M_{k,j} \to 0 \quad \forall k,j = 1,\ldots,n,\ j \neq k$$

4. the model equations are evaluated in steady-state condition using a phasors representation $\mathbf{X}^{(h)}$, where $\mathbf{X}$ is a generic variable and h is the harmonic order. This allows for taking into account the harmonic contribution introduced by the voltages of the H-bridges.

In this way, a reduced system of equations is achieved for sizing the main parameters of the symmetric MWT (L_m, L_σ, R). Since the following analysis is performed in the harmonic domain, each output voltage of the H-bridges can be represented as follows due to the control strategy adopted for the equalization circuit:

$$v_k(t) = \sum_{h=1,3,5\ldots}^{\infty} \frac{4}{\pi} \frac{V_{B,k}}{h} \sin(h\omega t) \tag{5.5}$$

thus only the odd harmonics are involved.

Moreover, because of the control strategy adopted, all the n winding voltages are in phase. Therefore, according to the assumptions previously defined, the system of equations (5.1) can be yield in the harmonic domain as follows:

$$\begin{cases} \mathbf{V}_k^{(h)} = \mathbf{E}^{(h)} + (R + jh\omega L_\sigma)\mathbf{I}_k^{(h)} \quad \forall k = 1, \ldots, n \\ \mathbf{E}^{(h)} = jh\omega L_m \mathbf{I}_m^{(h)} \\ \mathbf{I}_m^{(h)} = \sum_{k=1}^{n} \mathbf{I}_k^{(h)} \end{cases} \tag{5.6}$$

where $\mathbf{V}_k^{(h)}$, $\mathbf{I}_k^{(h)}$, $\mathbf{E}^{(h)}$ and $\mathbf{I}_m^{(h)}$ represent the k^{th} winding voltage and current, the induced electro-motive force (EMF) and the magnetization current, respectively.

Moreover, the EMF can be directly correlated to the mean value of winding voltages ($\mathbf{V}_{avg}$), resulting:

$$\mathbf{E}^{(h)} = \mathbf{V}_{avg}^{(h)} \dot{\gamma} \tag{5.7}$$

with

$$\mathbf{V}_{avg}^{(h)} = \frac{1}{n} \sum_{k=1}^{n} \mathbf{V}_k^{(h)} \tag{5.8}$$

$$\dot{\gamma} = \frac{nh\omega L_m (h\omega(nL_m + L_\sigma) + jR)}{R^2 + h^2\omega^2(nL_m + L_\sigma)^2} \tag{5.9}$$

In detail, the EMF results proportional to $\mathbf{V}_{avg}^{(h)}$ and a complex factor ($\dot{\gamma}$), which depends on the MWT parameters (L_m, L_σ, R) and the switching frequency of the H-bridges.

5.2.2 Mean balancing current

In order to define a proper design methodology for the active equalization circuit, a relation between $\mathbf{I}_k^{(h)}$ and the balancing current for each battery cell ($I_{B,k}$) need to be identified. In particular, according to the control strategy adopted for the H-bridges, $I_{B,k}$ results equal to the mean value of the winding current evaluated in the half switching period. Therefore, it can be expressed as follows:

$$I_{B,k} = \frac{2\sqrt{2}}{\pi} \sum_{h=1}^{\infty} \frac{\mathrm{Re}(\mathbf{I}_k^{(h)})}{h} \tag{5.10}$$

where $\mathrm{Re}(\mathbf{I}_k^{(h)})$ represents the real component of the specific winding current. Then, according to the system of equations (5.6), it has been achieved the dependency of $\mathrm{Re}(\mathbf{I}_k^{(h)})$ with respect to the corresponding cell voltage ($V_{B,k}$), the mean value of the cell voltages (V_{avg}) and the design parameters of the MWT (L_m, L_σ, R), resulting:

$$\mathrm{Re}(\mathbf{I}_k^{(h)}) = \beta(V_{B,k} - V_{avg}\alpha) \tag{5.11}$$

with

$$\alpha = \frac{h^2\omega^2 n L_m (n L_m + 2L_\sigma)}{R^2 + h^2\omega^2 (n L_m + L_\sigma)^2} \tag{5.12}$$

$$\beta = \frac{R}{R^2 + h^2\omega^2 L_\sigma^2} \frac{2\sqrt{2}}{h\pi} \tag{5.13}$$

where α is a coefficient lower than 1. Hence, if $V_{B,k} > V_{avg}\alpha$, the k^{th} cell will experience a discharging current. On the contrary, if $V_{B,k} < V_{avg}\alpha$, a charging current will occur. It is important to highlight that the amplitude of the charging or discharging currents for each cell is proportional to the difference between the related voltage and the mean value of all the cell voltages. Consequently, the active equalizer allows for performing a self-balancing process of the cells since the equalization currents decrease as the voltage difference becomes lower.

5.2.3 Design methodology

In this section, the design methodology proposed for the active equalizer is illustrated, which aims to size the main parameters of the MWT for achieving the desired performances. Firstly, the worst condition in terms of equalization current for the cells has been investigated. In particular, according to eq. (5.11), the voltage imbalances among the cells that lead to the maximum balancing current for a single cell has been defined analytically. This has been carried out by considering the difference δV_k between the k^{th} cell voltage and the mean value of the remaining cell voltages:

$$\delta V_k = V_{B,k} - \sum_{\substack{j=1 \\ j \neq k}}^{n} \frac{V_{B,j}}{n-1} \tag{5.14}$$

Consequently, the mean value of all the cell voltages (V_{avg}) can be expressed as a function of δV_k:

$$V_{avg} = V_{B,k} - \delta V_k \frac{n-1}{n} \tag{5.15}$$

Therefore, combining eqs. (5.15) and (5.11), it can be yield:

$$\mathrm{Re}(\mathbf{I}_k^{(h)}) = \beta\Big(V_{B,k}(1-\alpha) + \delta V_k \frac{n-1}{n}\alpha\Big) \tag{5.16}$$

As result, $\mathrm{Re}(\mathbf{I}_k^{(h)})$ and thus the balancing current $I_{B,k}$ is directly proportional to δV_k. This allows for assessing the worst condition for the balancing current since the maximum value is achieved when δV_k is equal to the maximum allowable voltage imbalance among the cells (ΔV_{max}). It is important to highlight that ΔV_{max} can be positive or negative according to the cell voltage distribution. In particular, if $\delta V_k = \Delta V_{max} > 0$, the k^{th} cell voltage will be higher than the remaining cell voltages and conversely. However, since the proportionality between $\mathrm{Re}(\mathbf{I}_k^{(h)})$ and δV_k is characterized by a positive offset, the maximum balancing current ($I_{B,max}$) is obtained when $\delta V_k = \Delta V_{max} > 0$. Moreover, according to eq. (5.15), $I_{B,max}$ depends on the voltage of the most charged cell, thus the absolute maximum value is achieved by considering also the maximum cell voltage ($V_{B,k} = V_{B,max}$). Note that the maximum RMS winding current for each harmonic order ($I_{max}^{(h)}$) is obtained in the worst condition as well.

Consequently, the system of equations (5.6) in the worst condition can be yield as follows:

$$\begin{cases} \mathbf{V}_{max}^{(h)} = \mathbf{E}^{(h)} + (R + jh\omega L_\sigma)\mathbf{I}_{max}^{(h)} \\ \mathbf{V}_{min}^{(h)} = \mathbf{E}^{(h)} + (R + jh\omega L_\sigma)\mathbf{I}_{min}^{(h)} \\ \mathbf{E}^{(h)} = jh\omega L_m[\mathbf{I}_{max}^{(h)} + (n-1)\mathbf{I}_{min}^{(h)}] \end{cases} \tag{5.17}$$

where $\mathbf{I}_{max}^{(h)}$ and $\mathbf{I}_{min}^{(h)}$ represent the winding currents corresponding to the highest ($\mathbf{V}_{max}^{(h)}$) and the lowest ($\mathbf{V}_{min}^{(h)}$) cell voltages, respectively. This system results under-determined due to the higher number of unknown variables with respect to the number of equations. Therefore, several parameters need to be defined in order to correctly address the sizing procedure of the MWT. In detail, the proposed design methodology aims to identify the MWT parameters (L_σ, R) for achieving a desired $I_{B,max}^*$ and maximum value of the true RMS winding current (I_{max}^*) for specific operating conditions in terms of ΔV_{max} for the cells and switching frequency. In addition, L_m is also considered as a known parameter for properly solving the system of equations (5.17).

In order to take into account for the contribution of the overall harmonic contents on both $I_{B,max}$ and I_{max}, an iterative procedure has been developed, consisting in the following operations:

1. two coefficients k_1 and k_2, greater than zero and lower than 1, are defined for assessing the first harmonic contribution of $I_{B,max}$ and I_{max}, respectively.

2. The system of equations (5.17) is solved at the first harmonic, thus the related L_σ and R of the MWT are calculated.

3. On the basis of the MWT parameters previously designed, the system of equations (5.17) is solved for each harmonic order with aim of evaluating $\mathbf{I}_{max}^{(h)}$.

4. $I_{B,max}$ and I_{max} are calculated for verifying the respect of the desired performances. In detail, if $I_{B,max} = I_{B,max}^*$ and $I_{max} = I_{max}^*$, the MWT parameters result correctly designed. Otherwise, the two coefficients k_1 and k_2 will be modified until reaching the desired performances.

5.2.4 Experimental prototype

The proposed MAB-based equalization circuit has been prototyped for a battery pack composed of six cylindrical cells in order to evaluate its performances in terms of efficiency and equalization speed considering different imbalance conditions. In particular, the design of the experimental

prototype has been carried out with the aim of reducing the parasitic parameters of the circuit and ensuring structural symmetry among all the bidirectional power paths from the cells to the corresponding transformer windings. As shown in Figure5.2, dedicated holders for cylindrical cells have been adopted and properly distributed in a radial structure for improving their integration within the MAB architecture and further addressing the symmetry requirement.

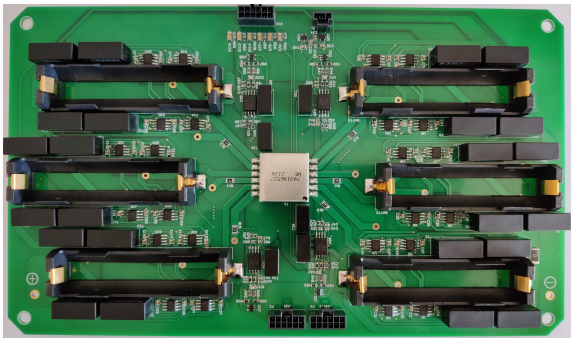

(a)

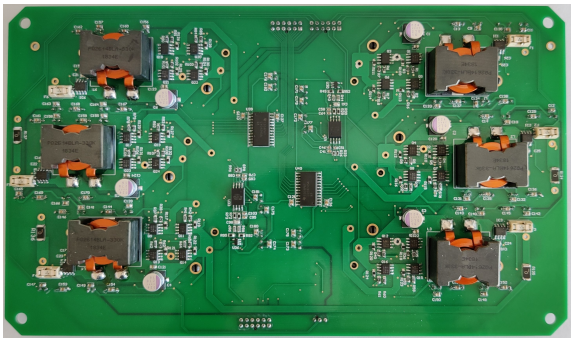

(b)

Figure 5.2: Picture of the experimental prototype designed for the proposed MAB-based equalization circuit: (a) top and (b) bottom sides.

The MWT has been placed in the center of this radial structure, resulting equally spaced with respect to the cells' holders displacement. Discrete MOSFETs by Vishay (model Si4186DY) devices have been adopted for the H-Bridge converters due to their small packages as well as low drain-source on-state resistances and low rise/fall times, which allow for achieving low conduction and switching losses, respectively. Note that all the power components selected for the experimental prototype are characterized by higher current ratings with respect to the desired maximum balancing current of

1A. This is mainly due to the need of minimizing the parasitic parameters of the circuit components, however it also allows for potentially extending the operability of the developed equalization circuit to higher balancing currents. Table 5.1 summarizes the parameters of the main components adopted for the proposed MAB-based cell equalizer.

Table 5.1: Parameters of the main components adopted for the proposed MAB equalization circuit.

Parameter	**Value**
MWT Wurth Elektronik 749196527	
Rated current base	2.3 A
Saturation current base	2.81 A
Inductance base	5.3 μH @100 kHz
Leakage inductance base	180 nH @100 kHz
DC resistance base	36 mΩ
Vishay MOSFET Si4186DY	
Drain-to-source on resistance	2.6 mΩ
Switching frequency	100 kHz
Rise time	21 ns
Fall time	41 ns
Filters	
Inductor filter	33 μH
Snubber capacitor	270 μF

5.2.5 Performance analysis

This section starts with the description of the experimental setup implemented for carrying out the performance analysis on the MAB-based cell equalizer developed. Experimental tests have been conducted by using the Hardware-In-the-Loop (HIL) validation with the aim of avoiding the impact of ununiform thermal gradients and aging conditions among the cells on the overall performances of the equalization circuit. In particular, the 3-Ah SONY VTC6 18650 cylindrical cell has been widely tested and the related second-order equivalent circuit model (ECM) has been experimentally calibrated considering different operating conditions in terms of charging/discharging current (C-rate).

Then, a multi-channel bidirectional power supply by Chroma (model 87001) has been adopted as cell emulator, which consists of 16 independent channels with maximum operating voltage and current ranges of 5V and $\pm$5A. Since the prototype of the MAB-based cell equalizer has been

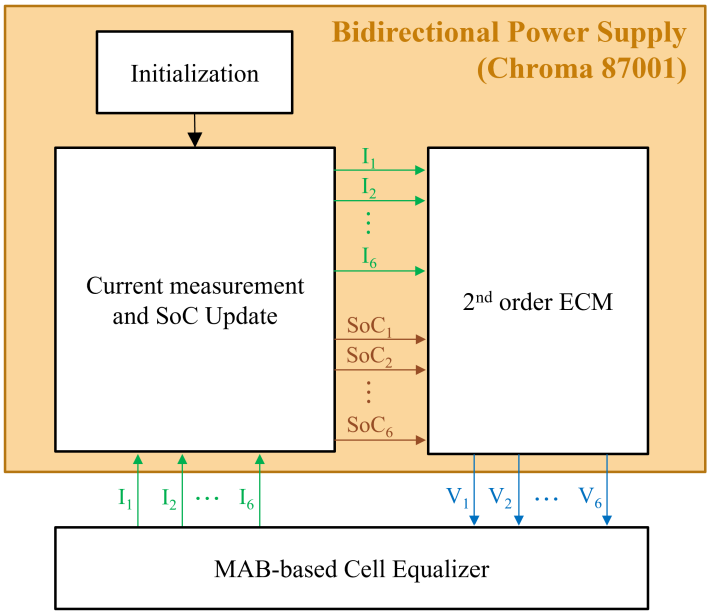

Figure 5.3: Block diagram of the HIL experimental setup implemented for carrying out the performance analysis of the MAB-based cell equalizer.

designed for a maximum of six cells, only a reduced number of independent channels from the Chroma unit has been taken into account, each one directly connected to the holder terminals of the corresponding cell. Therefore, a dedicated software has been developed for integrating the second-order ECM of the SONY VTC6 cells within the Chroma unit and properly managing the output voltages of the six channels requested in order to reproduce the electrical behavior of the cells during the experimental tests.

Figure5.3 shows a block diagram representation of the HIL experimental setup implemented, including details regarding the dedicated software developed for controlling the Chroma as a cell emulator. In detail, the following operational steps are performed for implementing the HIL testing.

1. An initialization phase is needed for enabling the six channels of the Chroma unit, uploading the cell parameters of the second-order ECM developed for the SONY VTC6 and defining the desired initial voltage imbalance condition among the cells by setting the related initial SoC of each cell.

2. According to the initial SoCs defined, the terminal voltages achieved from the second-order ECMs are imposed on the six channels of the

Chroma unit as output voltages, thus emulating the electrical behavior of the cells.

3. Once the terminal voltages are imposed on the MAB-based cell equalizer, it detects a voltage imbalance condition and starts to perform the equalization process by enabling the operability of the H-Bridge converters.

4. Depending on the operating conditions considered in terms of maximum voltage imbalance and initial SoC, a balancing current distribution is autonomously established among the cells.

5. Consequently, the Chroma unit is able to measure the current flowing through each channel and thus calculate/update continuously the SoC of each cell. As result, the cell terminal voltages achieved from the ECMs are adjusted in real time according to the C-rate and SoC that the specific cell is experiencing.

In this way, a correct evaluation of the performances of the equalization circuit has been carried out due to the possibility to set different initial conditions for the cells without encountering potential issues related to the replicability of the experimental tests. Moreover, it is important to highlight that the adoption of an experimentally-calibrated second-order ECM instead of real cells does not impact the validity of the results since it can reproduce accurately the real behavior of the cells.

5.2.5.1 Experimental results

Under the experimental setup described above, the experimental prototype of the MAB-based cell equalizer has been firstly tested considering the maximum initial voltage imbalance condition among the cells ($\Delta V_0 = 200mV$) in order to verify the correct functionalities of the experimental prototype developed according to the design methodology previously described. The worst operating condition for the MAB-based cell equalizer has been implemented, resulting in a single cell at the maximum voltage and the remaining five at the minimum voltage, as discussed in paragraph 5.2.3.

Figure 5.14 shows all the voltages, currents and powers of the cells during the equalization process in case of an initial SoC of the most charged cell ($SoC_{0,MC}$) of 100% and an initial voltage imbalance condition (ΔV_0) of $200mV$.

In particular, from the perspective of the equalization circuit, input and output powers (P_{IN}, P_{OUT}) have been defined as the sum of the instantaneous contributions of the cells that are experiencing a discharging and

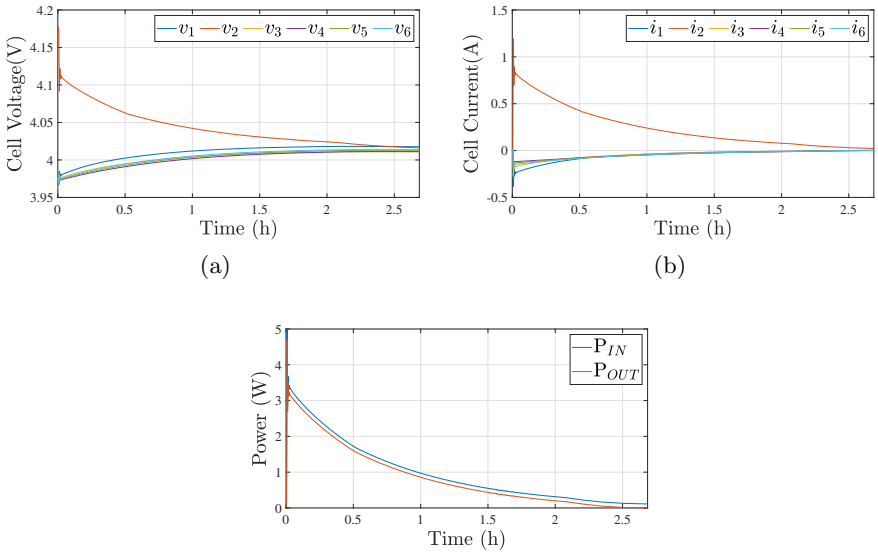

Figure 5.4: Experimental test with $SoC_{0,MC} = 100\%$ and $\Delta V_0 = 200mV$: (a) cell voltages, (b) cell currents and (c) cell powers (P_{IN}, P_{OUT}).

charging process, respectively. The difference between P_{IN} and P_{OUT} represents the power losses of the cell equalizer. Note that the equalization process is terminated once the zero output power condition ($P_{OUT} = 0$) is reached. As possible to notice in Figure5.14, the experimental results confirm the correct functionalities of the experimental prototype since the voltage imbalance condition is compensated at the end of the equalization process. The balancing current distribution among the cells has been autonomously achieved, resulting the most charged cell with a discharging current of about $1A$, as expected from the design methodology, and the least charged ones with a charging current of about $0.2A$ at the beginning of the experimental test. During the balancing process, the amplitude of the voltage imbalance decreases and consequently the cells' currents lower as well. Figure5.14 also highlights a slight difference among the behaviors of the least charged cells, which is only due to the minimal asymmetries introduced by the commercial MWT.

Besides the validation of its correct functionalities, the experimental prototype has been also tested considering different voltage imbalance conditions among the cells. In detail, ΔV_0 ranging from $50mV$ up to $200mV$ have been taken into account for the analysis. Furthermore, the variability

of the circuit performances with respect to $SoC_{0,MC}$ in the worst operating condition has been evaluated as well, ranging from 40% up to 100%. Note that all the experimental tests have been performed considering the worst operating condition for the MAB-based cell equalizer, thus the SoC of the least charged cells has been directly achieved by fixing the specific combination of $SoC_{0,MC}$ and ΔV_0.

Table 5.2 reports the value of the initial state of charge of the least charged cells, they computed by using the static OCV-SoC characteristic of the NMC SONY VTC6 cell and interpolating the initial imbalance conditions in terms of $SoC_{0,MC}$ and ΔV_0.

Table 5.2: Summary of the initial imbalance conditions considered for the performance analysis on the experimental prototype.

SoC Most Charged (%)	Voltage Imbalance (mV)	SoC Least Charged (%)
100	50	93.776
	100	86.619
	150	78.733
	200	74.58
80	50	75.621
	100	71.469
	150	66.121
	200	59.592
60	50	53.802
	100	47.802
	150	42.335
	200	37.343
40	50	35.571
	100	31.423
	150	27.167
	200	22.694

Different performance parameters have been considered for evaluating the functionalities of the experimental prototype in the different imbalance conditions defined, including the residual voltage imbalance at the end of the equalization process, the energy efficiency and the equalization speed. Figure 5.5a shows the variability of the residual voltage imbalance among the cells at the end of the equalization process with respect to the initial conditions in terms of $SoC_{0,MC}$ and ΔV_0. As possible to notice, both initial conditions do not impact the amplitude of the residual voltage imbalance, which remains lower than $7mV$ within a band of $1mV$ for all the experimental tests. Therefore, these results highlight the minimum volt-

age imbalance achievable among the cells when the proposed MAB-based cell equalizer prototype is adopted, representing a construction limitation mainly due to the parasitic parameters of both the MWT and the electronic components selected.

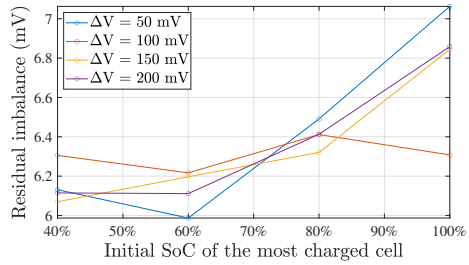

(a)

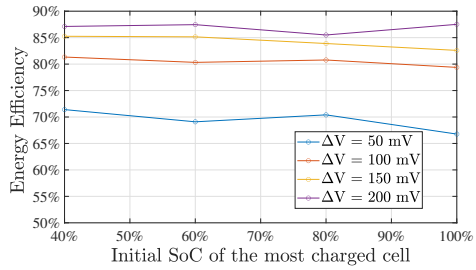

(b)

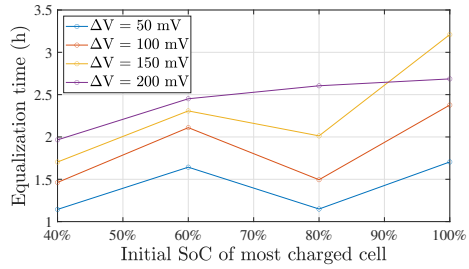

(c)

Figure 5.5: Experimental results for (a) residual voltage imbalance at the end of the balancing process, (b) energy efficiency and (c) equalization time.

Since the efficiency of the equalization process cannot be uniquely defined for each imbalance condition in terms of power, an indicator of the amount of energy exchanged among the cells has been provided within the performance analysis. In detail, an energy efficiency factor has been de-

fined as the ratio between the output and the input energies involved in the specific imbalance condition and calculated by integrating P_{OUT} and P_{IN} over the related equalization time. Figure 5.5b shows the energy efficiency results achieved for all the imbalance conditions considered for the performance analysis.

As result, a higher variability of the energy efficiency with respect to ΔV_0 is observed, with a minimum value of 66.77% and a maximum value of 87.51% achieved for $\Delta V_0 = 50mV$ and $\Delta V_0 = 200mV$, respectively. Therefore, higher energy efficiencies result for larger ΔV_0, highlighting the MAB-based cell equalizer to be potentially suitable for balancing processes also at module level. The lowering of the performances as ΔV_0 decreases mainly depends on the increasing impact of the parasitic parameters of the equalization circuit. On the other hand, figure 5.5b also shows a slight variability of the energy efficiency with respect to $SoC_{0,MC}$, with a major contribution for lower ΔV_0, where a maximum variation of 4.62% is noticed.

The performance analysis of the experimental prototype has also included the evaluation of the time interval needed for equalizing the SoCs of the cells starting from a specific initial imbalance condition. It is important to highlight that the HIL approach adopted for carrying out the experimental tests has allowed for avoiding the potential impact of temperature and aging conditions on the equalization time results.

Figure 5.5c shows the variability of the equalization times achieved for all the imbalance conditions considered for the performance analysis. s possible to notice, considering all the operating points characterized by the same $SoC_{0,MC}$, the equalization time increases as ΔV_0 rises. Only the equalization time achieved for $\Delta V_0 = 200mV$ and $SoC_{0,MC} = 100\%$ results to be unexpected since a lower value than the one obtained at $\Delta V_0 = 150mV$ is observed. This is mainly due to the intrinsic properties of the technology of the SONY VTC6 cell adopted for the performance analysis. Indeed, the equalization time results are strongly affected by the characteristic curve that correlates the SoC of the cell to its open circuit voltage, which presents exponential regions outside the SoC interval of 20%-80%. Moreover, an interesting variability of the equalization times with respect to $SoC_{0,MC}$ is observed, highlighting the possibility to perform the equalization process in specific operating conditions that minimize the time required by the balancing process.

5.3 Case study II: Inductor-based architecture

Inductor-based cell equalizers adopt inductors as storage components for transferring energy from the most charged cells to the least charged

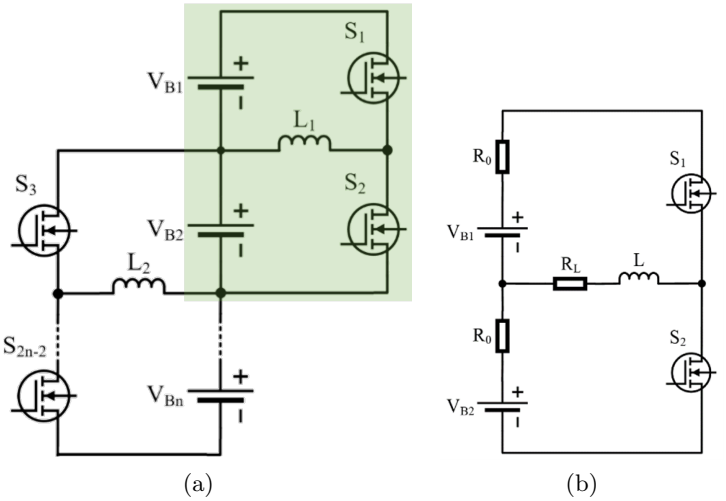

Figure 5.6: Multi-inductor equalization circuit (a) and its derived simplified architecture (b).

ones. Among the inductor-based equalization circuits presented in literature [57,65,66], this paper proposes a design methodology for the coupled or multi-inductor architecture (figure 5.6a), which also corresponds to a buck-boost converter configuration. Considering a generalized battery pack composed of n series-connected cells, the multi-inductor architecture requires $2n$-2 power switches and n-1 inductors. However, since this cell equalizer allows for performing an adjacent cell-to-cell energy transfer only, all the operating conditions of the equalization circuit involve just two cells and a single inductor. Therefore, as shown in figure 5.6b, a simplified architecture can be adopted for defining design strategies as well as evaluating the performances of the multi-inductor equalization circuit. Moreover, considering that all the inductor-based cell equalizers usually perform adjacent cell-to-cell energy transfers, the adoption of the simplified architecture also allows for extending the proposed design methodology to the other inductor-based architectures.

5.3.1 Model Equations

Analytical models have been developed for the simplified architecture considering the following operating conditions.

1. *Ideal operating condition*: includes the switches (S_1, S_2) and the inductor (L) as ideal components, whereas the cells to be modeled as constant voltage sources only.

2. *Real operating condition*: includes the internal resistance (R_0) of the zero-order equivalent circuit model for the cells, the series resistance of the inductor (R_L) as well as the static and dynamic parameters of the switches. In detail, considering MOSFETs as switches, the former are represented by the drain-source on-state resistance (R_{ds}) and the forward voltage of the internal body diode (V_d), whereas the latter are mainly related to the switching characteristics, such as rise and fall times, which are taken into account by implementing a suitable dead time (ρ) within the control strategy of the inductor-based equalization circuit.

The control algorithm is based on two pulse-width modulation (PWM) signals, one for each switch, with a fixed switching period (T_s) and a variable duty cycle (D). In particular, assuming the voltage of the top cell (V_{B1}) to be greater than the voltage of the bottom one (V_{B2}), the switches S_1 and S_2 are respectively turned on and off during the t_{on} period, thus the energy is transferred from the most charged cell to the inductor. Then, the opposite configuration for the switches is operated during the t_{off} period, and the energy previously stored in the inductor is transferred to the least charged cell. In real conditions, a dead time (ρ) is also included within the control strategy for taking into account the dynamic characteristics of the switches during the related opening and closing operations. This delay time between the PWM signals for the switches S_1 and S_2 represents a crucial parameter to be considered in order to avoid undesired short-circuit conditions for the cells.

With reference to the control algorithm, it is important to highlight that the duty cycle of the PWM signals needs to be controlled in both ideal and real conditions depending on the voltage difference between the two cells (ΔV) for ensuring the correct behavior of the inductor-based cell equalizer. In detail, it is always preferable to operate at the limit of the continuous conduction mode (LCCM) for cell equalization purposes. Indeed, in ideal conditions, the inductor current does not reach the steady-state condition if a duty cycle different from the one evaluated for the limit of continuous conduction mode (D_L) is considered. On the other hand, in real conditions, ρ introduces two additional time intervals with respect to the ideal condition, in which the equalization circuit performs differently depending on the value of the duty cycle. In particular, when $D > D_L$, the mean value of the inductor current rises during the transient until reaching a positive value in steady-state, potentially resulting in higher balancing currents than the ones achievable by imposing D_L.

Moreover, the freewheeling current that flows during the additional time intervals introduced by ρ contributes to further recharging the least charged

cell. Nevertheless, despite these advantages, it is still preferable to perform the balancing process at $LCCM$ due to the possibility of better managing the energy flows among the cells and easily interrupting the equalization process without encountering undesired and uncontrolled freewheeling currents. On the other hand, when $D < D_L$, a negative mean value for the inductor current is reached at steady-state, resulting in incorrect operability of the cell equalizer since the energy is transferred from the least charged cell to the most charged one. This issue can be solved by controlling the switches S_1 and S_2 in order to operate in discontinuous conduction mode (DCM) when $D < D_L$, however the DCM strongly limits the energy transfer capability of the equalization circuit with respect to the $LCCM$ operation.

Considering the circuit to operate at the L ($D = D_L$), the model equations of the simplified architecture for the inductor-based cell equalizer in both ideal and real conditions can be carried out according to the KVL and KCL by describing the current that flows through the inductor (i_L).

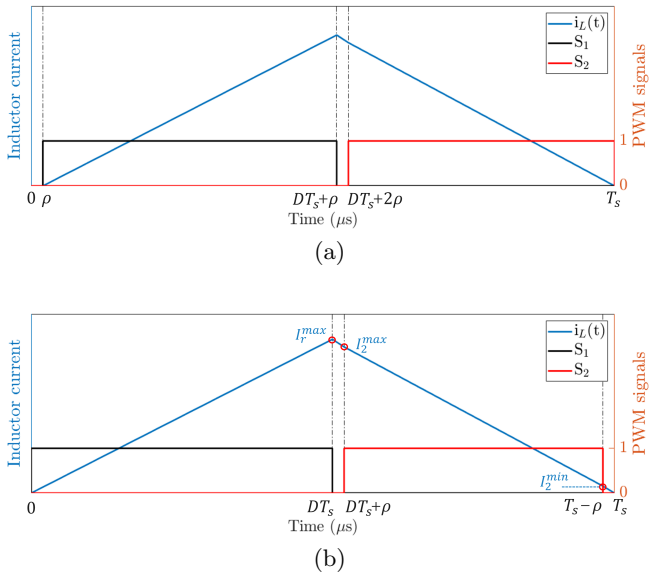

Figure 5.7: Switching signals and current of inductor-based cell equalizer at LCCM in real operating conditions: (a) traditional and (b) proposed approach.

1. *Ideal operating conditions*

The model equations that describe the behavior of the inductor cell

equalizer in ideal conditions are reported as follows:

$$i_L(t) = \begin{cases} \dfrac{V_{B1}}{L}t & 0 \leq t \leq DT_s \\ I_{id}^{max} - \dfrac{V_{B2}}{L}(t - DT_s) & DT_s \leq t \leq T_s \end{cases} \tag{5.18}$$

where I_{id}^{max} represents the peak value of the inductor current that occurs at $t = DT_s$.

2. *Real operating conditions*

In order to define the LCCM in real conditions with the hypothesis of $i_L(t = T_s) = 0$, the behavior of the circuit during the dead time has to be considered. As for the state of the art, the control strategy used for LCCM operations under real conditions includes the dead time intervals at the beginning of T_s, within which the inductor current is considered zero, and after t_{on} (figure 5.7a). In this paper, a different approach has been considered in order to maximize the mean balancing current for each T_s, still guaranteeing the LCCM. A compensation technique similar to the one proposed in [67, 68] is implemented. The first dead time interval has been introduced after t_{on} while the second one is located at the end of T_s (figure 5.7b). In this way, there are no control intervals with zero current, resulting in improvements in terms of efficiency and maximum balancing current in LCCM. As result, the model equations in real conditions are:

$$i_L(t) = \begin{cases} \dfrac{V_{B1}}{R_{tot}}\left[1 - e^{(-\frac{t}{\tau_{tot}})}\right] \\ 0 \leq t \leq D_L T_s \\ \\ \dfrac{V_{B2} + V_d}{R_r}\left[e^{(-\frac{t - D_L T_s}{\tau_r})} - 1\right] + I_r^{max} e^{(-\frac{t - D_L T_s}{\tau_r})} \\ D_L T_s \leq t \leq D_L T_s + \rho \\ \\ \dfrac{V_{B2}}{R_{tot}}\left[e^{(-\frac{t - D_L T_s - \rho}{\tau_{tot}})} - 1\right] + I_2^{max} e^{(-\frac{t - D_L T_s - \rho}{\tau_{tot}})} \\ D_L T_s + \rho \leq t \leq T_s - \rho \\ \\ \dfrac{V_{B2} + V_d}{R_r}\left[e^{(-\frac{t - (T_s - \rho)}{\tau_r})} - 1\right] + I_2^{min} e^{(-\frac{t - (T_s - \rho)}{\tau_r})} \\ T_s - \rho \leq t \leq T_s \end{cases} \tag{5.19}$$

where τ_{tot} and τ_r are respectively the time constants of the current transient due to the overall circuit resistance ($R_{tot} = R_0 + R_{ds} + R_L$)

and a partial resistance contribution that does not include the drain-source on-state resistance of the switch ($R_r = R_0 + R_L$); I_r^{max} represents the peak value of the inductor current calculated at $t = DT_s$, whereas I_2^{max} and I_2^{min} correspond to the current values calculated at $t = DT_s + \rho$ and $t = T_s - \rho$, respectively.

5.3.2 Mean balancing current

In both ideal and real conditions, the duty cycle that allows the inductor-based cell equalizer to operate at the $LCCM$ can be analytically determined by imposing $i_L(t = T_s) = 0$. In particular, according to (5.18), it results in ideal conditions:

$$D = D_{L,id} = \frac{V_{B2}}{V_{B1} + V_{B2}} \tag{5.20}$$

Therefore, the duty cycle can be directly calculated on the basis of the cell voltages. On the other hand, according to (5.19), it results in real conditions:

$$D = D_{L,r} = 1 - \frac{2\rho}{T_s} - \frac{\tau_{tot}}{T_s}\left(\ln K_1 - \ln K_2 - \frac{\rho}{\tau_r}\right) \tag{5.21}$$

where the constant values K_1 and K_2 are expressed as:

$$K_1 = \frac{V_{B2}}{R_{tot}} - \frac{V_{B2} + V_d}{R_r}\left[1 - e^{(-\frac{\rho}{\tau_r})}\right] + \frac{V_{B1}}{R_{tot}} e^{(-\frac{\rho}{\tau_r})} \tag{5.22}$$

$$K_2 = \frac{V_{B2} + V_d}{R_r}\left[1 - e^{(-\frac{\rho}{\tau_r})}\right] + \frac{V_{B2}}{R_{tot}} e^{(-\frac{\rho}{\tau_r})} + \frac{V_{B1}}{R_{tot}} e^{\left[-\frac{2\rho(\tau_{tot} - \tau_r) + T_s\tau_r}{\tau_{tot}\tau_r}\right]} \tag{5.23}$$

With reference to (5.20) and (5.21), considering the same operating conditions in terms of cell voltages, inductance and switching frequency, it is possible to demonstrate that a higher duty cycle has to be imposed in real conditions, resulting always $D_{L,r} > D_{L,id}$.

The mean values of the currents related to the most charged cell ($\bar{I}_{1,id}$) and the least charged one ($\bar{I}_{2,id}$) are different due to the specific architecture of the inductor-based equalization circuit. In detail, according to (5.18) and considering $D = D_{L,id}$, the following equations can be yielded in ideal conditions by calculating the two contributions during the t_{on} and t_{off}, respectively:

$$\bar{I}_{1,id} = \frac{V_{B1}}{2L} D_{L,id}^2 T_s \tag{5.24}$$

$$\bar{I}_{2,id} = -\frac{V_{B2}}{2L}(1 - D_{L,id})^2 T_s \tag{5.25}$$

where the sign of the currents is consistent with the direction of the cell current, positive in discharge and negative in charge. It is possible to notice that both mean balancing currents, $\bar{I}_{1,id}$ and $\bar{I}_{2,id}$, depends on the actual cell voltages, the inductor size L and the switching frequency $f_s = 1/T_s$. In particular, the voltage operating conditions determine $D_{L,id}$ (5.20), whereas the inductor size and switching frequency are inversely proportional to the amplitude of the currents. Likewise, according to (5.19) and considering $D = D_{L,r}$, the mean values of the currents related to the most charged cell ($\bar{I}_{1,r}$) and the least charged one ($\bar{I}_{2,r}$) in real conditions can be achieved as follows:

$$\bar{I}_{1,r} = \frac{D_{L,r} V_{B1}}{R_{tot}} - \frac{\tau_{tot}}{T_s} I_r^{max} \tag{5.26}$$

$$\begin{aligned} \bar{I}_{2,r} = & \frac{D' V_{B2}}{R_{tot}} + \frac{2\rho\,(V_{B2} + V_d)}{R_r T_s} + \\ & - \frac{\tau_{tot} - \tau_L}{T_s}\left(I_2^{max} - I_2^{min}\right) - \frac{\tau_L}{T_s} I_r^{max} \end{aligned} \tag{5.27}$$

where the sign of the currents is consistent with the direction of the cell current and D' is expressed as:

$$D' = 1 - D_{L,r} - \frac{2\rho}{T_s} \tag{5.28}$$

Note that the amplitudes of the mean values for the cells' currents can be accurately calculated through these equations since they include all the main static and dynamic parameters of the circuit components. For the control perspective, even under real-world conditions, the variables which have an impact on average currents are the voltage operating condition, thus the duty cycle, and the switching frequency. In particular, it is possible to prove that if $D_{L,r}$ increases, the amplitude of $\bar{I}_{1,r}$ increases and $\bar{I}_{2,r}$ decreases, whereas when the switching frequency becomes higher the amplitude of $\bar{I}_{1,r}$ and $\bar{I}_{2,r}$ decrease.

5.3.3 Efficiency

An efficiency model that includes both conduction and switching losses for the switches has been developed for the inductor-based cell equalizer in real conditions. In detail, it has been defined on the basis of the mean

values of the input and output powers, resulting $\bar{P}_{in}$ the power provided by the most charged cell and $\bar{P}_{out}$ the power received by the least charged cell. The following relations can be achieved:

$$\eta = \frac{\bar{P}_{out}}{\bar{P}_{in}} = \frac{V_{B2} \cdot \bar{I}_{2,r} - P_{sw}}{V_{B1} \cdot \bar{I}_{1,r}} \tag{5.29}$$

where P_{sw} represents the switching losses, whereas the conduction losses are already carried by the model in the term $V_{B2} \cdot \bar{I}_{2,r}$. Regarding P_{sw}, the contribution of each switch for turning on and off operations has been modeled. However, considering the operation of the circuit at LCCM, only the switching losses during the turn-off of S_1 ($P_{S1,off}$) and the turn-on of S_2 ($P_{S2,on}$) have been considered since the turning on of the switch S_1 and the turning off of the switch S_2 occur at zero current, resulting:

$$\begin{aligned} P_{sw} &= P_{S1,off} + P_{S2,on} = \\ &= \frac{1}{2}\left[V_{B1} + V_{B2} + R_0 I_2^{max} + V_D\right] I_r^{max} t_{fall} f_s + \\ &+ \frac{1}{2}\left[V_{B1} + V_{B2} - \left(R_0 + R_{ds}\right) I_2^{max}\right] I_2^{max} t_{fall} f_s \end{aligned} \tag{5.30}$$

where f_s is the switching frequency, t_{rise} and t_{fall} are the rise and fall times of the switches, respectively.

5.3.4 Design methodology

On the basis of the model equations in real conditions, a design methodology has been defined for the multi-inductor cell equalizer, which can be adopted for all the inductor-based equalization circuits. According to (5.21) and (5.27), the objective of the design methodology is to define the inductor size L that allows to meet the balancing current specification when specific cell voltages (V_{B1}, V_{B2}) and imbalance conditions (ΔV) occur, operating at the limit of continuous conduction mode for a specific designed switching frequency.

First of all, it needs to be defined which is the balancing current the proposed design methodology addresses because generally the mean balancing current of cell 1 is not equal to the one of cell 2, as described in section 5.3.2. Considering the ideal conditions, from the following equation:

$$\frac{V_{B1}}{V_{B2}} = \frac{\bar{I}_{2,id}}{\bar{I}_{1,id}} \tag{5.31}$$

It can be assessed that the mean balancing current of the least charged cell ($\bar{I}_{2,id}$) is greater than the most charged one ($\bar{I}_{1,id}$), assuming V_{B1} greater

than V_{B2} Thus $\bar{I}_{2,id}$ is considered account for design purpose. However, in real conditions, it is not always true that $\bar{I}_{2,id} > \bar{I}_{1,id}$ because it depends on both the efficiency and the parasitic parameters. With the aim of correctly comparing the design strategy in ideal and real conditions, the charging current $\bar{I}_{2,r}$ in (5.27) has been taken into account for the proposed design methodology. For what concern the cell voltages, it can be demonstrated that the highest charging balancing current occurs when the voltage of the most charged cell is equal to the maximum allowed one for the specific chemistry and the least charged cell is characterized by the maximum voltage imbalance with respect to the most charged cell. It is important to point out that a transcendental equation is obtained by combining (5.21) and (5.27) that cannot be expressed in closed form in a finite algebraic step. Thus, an iterative process based on the following steps is used to solve this issue:

1. On the basis of the data available from components' manufacturers, a set of system parameters is considered: R_0, R_{ds}, R_L, t_{rise}, t_{fall}, ρ and V_d.

2. A desired mean balancing current $\bar{I}_{2,r}$ is defined for a maximum voltage imbalance among the cells ($\Delta V = V_{B1} - V_{B2}$) and a specific switching frequency (f_s).

3. Considering different sizes of the inductor, the related duty cycles are calculated by (5.21) with the aim of adopting the pairs $(L, D_{L,r}(L))$ for evaluating the mean balancing current in (5.27). In this way, it is possible to generate the function graph of the mean balancing current depending on the inductor size.

4. Based on an interpolation tool, the value of the inductor size can be determined to obtain the desired mean balancing current $\bar{I}_{2,r}$.

As result, in case of maximum voltage imbalance among the cells, the proposed design methodology allows for sizing the inductor of the cell equalizer with the aim of achieving a desired mean balancing current $\bar{I}_{2,r}$ by taking considering realistic parameters of the circuit and varying the control parameters, such as switching frequency. Then, multiple combinations of L and f_s can be adopted for achieving the desired performances, thus other parameters, such as the efficiency of the equalization circuit, have to be considered for defining the optimal design conditions.

5.3.5 Validation

Numerical and experimental analyses are here reported with the aim of verifying the goodness of the proposed design methodology. The experimental prototype represents the simplified architecture of the multi-inductor balancing circuit. The main parasitic parameters are derived from the datasheets of the circuit components selected and considered as input values for performing the design methodology. Then, according to the results achieved, experimental tests are out considering three sizing case scenarios and the difference between the numerical and experimental results are evaluated in terms of balacing current and efficiency of the inductor-based prototype.

An experimental prototype for the simplified architecture of the multi-inductor equalization circuit, based on two cells and a single inductor, has been designed and implemented specifically for cylindrical cells, as shown in figure5.8. The overall architecture is composed of a power board and a driving board, properly integrated to fully decouple power and control sections. The former includes the holders for displacing 18650 cylindrical cells, the inductor and the power switches, whereas the latter includes the related gate drivers as well as isolated voltage and current measurement circuits. The power board has been also designed to limit stray inductance, thus the switches' voltage stress is reduced and the switching operations are improved. In addition, accessible measurement points have been considered on the developed prototype in order to measure the inductor current and switches voltages accurately by means of external devices, such as an oscilloscope.

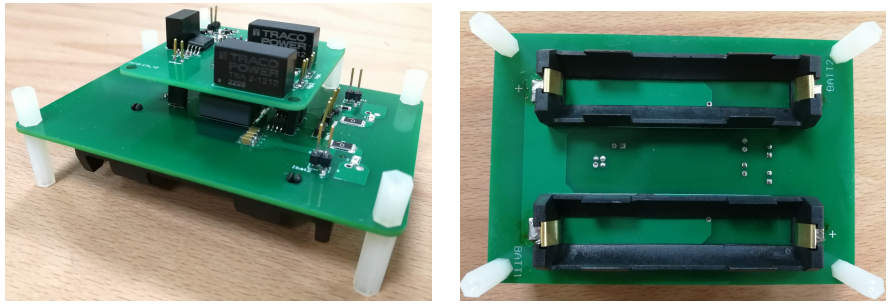

(a) (b)

Figure 5.8: Experimental prototype of the simplified-architecture multi-inductor cell equalizer: (a) side view and (b) bottom view.

Further details about the components selected for the experimental pro-

Table 5.3: Parameters of the Experimental Prototype.

Internal resistance of the cells	$R_0 = 20m\Omega$
Series resistance of the inductor	$R_L = 10m\Omega$
Drain-source on-state resistance for the switches	$R_{ds} = 2.6m\Omega$
Rise time	$t_{rise} = 42ns$
Fall time	$t_{fall} = 78ns$
Dead time	$\rho = 250ns$
Forward voltage of the internal body diode	$V_d = 0.4V$

totype are reported as follows:

- MOSFETs by Vishay, model Si4186DY, have been selected for their low drain-to-source on-state resistance and fast dynamic response.
- Two single-channel gate drivers by Infineon, model 1EDI20N12AF, with a proper isolated power supply have been adopted for the driver section.
- 3-Ah SONY VTC6 cylindrical cells have been selected with the aim of verifying the correct behavior of the prototype and validating the design methodology. Several experimental tests have been performed in order to calibrate the parameters of the zero-order equivalent circuit model as a function of both charging/discharging C-rates and temperatures. In this way, the typical value of the internal resistance of the cell has been determined experimentally, resulting equal to 20 mΩ.
- The power board has been designed to allow for multiple experimental tests in various combinations of L and f_s, therefore the Bourns series model SRP1770TA has been selected for the inductors, which is also characterized by a low series DC-resistance.

The main parameters of the components selected for the experimental prototype are summarized in Table 5.3.

Considering the components selected for the experimental prototype, the design methodology described in section 5.3.4 has been numerically implemented with the aim of defining the inductor size for achieving a desired balancing current $\bar{I}_{2,r} = 2A$ when a maximum voltage imbalance of 200 mV is considered when $V_{B1} = 4.2V$ and $V_{B2} = 4V$. The design methodology has been operated for several values of the switching frequency, ranging from 10kHz to 100 kHz, in order to achieve different sizing solutions for the inductor and consequently evaluate the efficiency for each design condition.

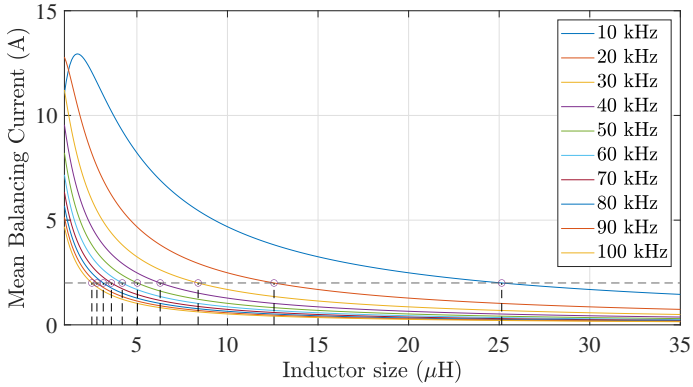

Figure 5.9: Numerical results: dependency of inductor size with the mean balancing current and frequency.

figure 5.9 shows the results of the design methodology applied to the experimental prototype developed, which highlight the variability of the mean balancing current $\bar{I}_{2,r}$ with respect to L and f_s. In this way, the possible combinations L-f_s that allow for satisfying the design requirements are obtained by interpolating the function graphs illustrated in figure 5.9 with the desired $\bar{I}_{2,r}$.

Table 5.4: Design Results for Different Combinations of Inductor and Switching Frequency with $\bar{I}_{2,r} = 2A$.

L (μH)	fs (kHz)	η (%)	P_{sw} (mW)	D_L (%)
25.14	10	91.35	41.65	50.42
12.57	20	90.97	83.44	50.44
8.38	30	90.58	125.38	50.45
6.28	40	90.19	167.45	50.47
5.03	50	89.80	209.67	50.49
4.19	60	89.42	252.04	50.51
3.59	70	89.03	294.55	50.53
3.14	80	88.64	337.15	50.55
2.79	90	88.26	380.00	50.57
2.51	100	87.87	422.90	50.59

Numerical results have been reported in table 5.4, which also highlight the efficiency (η), the switching losses (P_{sw}) and the duty cycle that ensures LCCM (D_L) for each design pair (L,f_s). As result, considering the specific set of parameters selected for performing the design methodology, higher

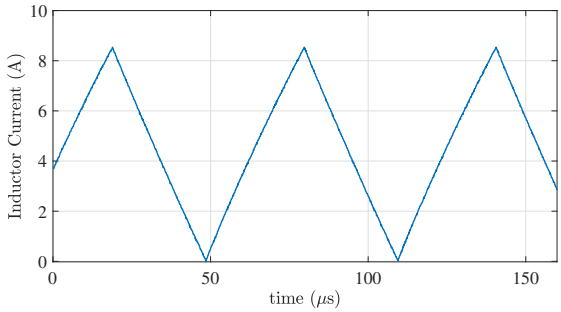

Figure 5.10: Experimental test considering L=15 μH, f_s = 16.443 kHz, V_{B1} = 4.2 V and ΔV = 200 mV.

L and lower f_s allow for achieving higher efficiency for the inductor-based balancing process. This is mainly due to the impact of the switching losses, which strongly increase as the f_s rises. Moreover, devices with better performances have to be selected in order to increase the efficiency with respect to the f_s rise.

In order to experimentally validate the results achieved by performing the proposed design methodology, different operating conditions in terms of L and f_s have been investigated within the sizing results reported in Table 5.4. Since commercially available inductor sizes are limited among the manufacturers, values close to the ones achieved from the design methodology have been selected and the correct switching frequency for ensuring the desired $\bar{I}_{2,r}$ in LCCM operations has been calculated accordingly. In particular, three inductors by Bourns, model SRP1770TA, are considered for the experimental validation tests: 3.3μH, 5.6μH and 15μH having a series resistances of 3.9$m\Omega$, 7.05$m\Omega$ and 20.5$m\Omega$, respectively. The switching frequencies achieved by the proposed methodology are reported in Table 5.5 and the correct functionalities are demonstrated in Fig 5.10 for a single sizing case scenario ($L = 15\mu$H).

For each test, the mean balancing current $\bar{I}_{1,r}$ and efficiency (η) have been numerically calculated considering the series resistances of the commercial inductors, whereas the mean balancing current $\bar{I}_{2,r}$ is equal to 2A as for design requirements. As result, a higher efficiency is observed for a lower inductor size and a higher switching frequency, with a maximum value of 91.24%. The efficiency reduction with the switching frequency increases differs from the sizing results reported in Table 5.4, however it is related to the increased series resistance of the commercial inductors.

Table 5.5 also reports the mean balancing currents and the efficiency obtained experimentally. In this case, the efficiency for each experimental

Table 5.5: Comparison between Numerical and Experimental Results.

		NUMERICAL			EXPERIMENTAL		
L (μH)	f_s (kHz)	$\bar{I}_{1,r}$ (A)	$\bar{I}_{2,r}$ (A)	η (%)	$\bar{I}_{1,r}$ (A)	$\bar{I}_{2,r}$ (A)	η (%)
3.3	78.037	2.01	2.00	91.24	1.96	1.81	88.04
5.6	45.436	2.04	2.00	91.07	2.11	1.92	86.80
15	16.443	2.16	2.00	87.36	2.28	2.01	83.65

test has been directly evaluated by measuring the cell voltages and currents, thus calculating the discharging and charging powers for the most and the least charged cells, respectively. The experimental results confirm the goodness of the design methodology, demonstrating the capability of the proposed approach in capturing the non-ideality of the equalization circuit. Indeed, by comparing the experimental and the numerical results, maximum relative errors expressed in percentage and absolute value of 5.6% and 9.5% are respectively achieved for $\bar{I}_{1,r}$, $\bar{I}_{2,r}$, whereas a maximum absolute error of 4.27% is obtained for η. These results validate the proposed design methodology since the errors are compatible with the uncertainty ranges of the components adopted for the experimental prototype. Moreover, they highlight the need of high-precision components for accurately achieving the desired performances from the inductor-based equalization circuit.

5.3.6 Control strategy

This section presents two model-based control strategies for optimally managing the functionality of inductor-based cell equalizers in terms of efficiency and equalization time. In particular, two different approaches have been proposed, both oriented to adjust control parameters, such as the duty cycle (D_L) and the frequency of the switching signals (f_s), depending on the severity of the voltage imbalance among the cells during the balancing operation. The proposed approaches are named Constant-Frequency Control (CFC) and Variable-Frequency Control (VFC).

5.3.6.1 Constant Frequency Control

The first control strategy, named as Constant-Frequency Control (CFC), aims at varying the duty cycle for leading the equalization circuit to always operate at LCCM, thus maximizing the mean balancing current for each imbalance condition. However, according to (5.21) and (5.27), the mean balancing current decreases as the voltage imbalance among the cells low-

Table 5.6: Design parameters based on the inductor-based cell equalizer prototype

Desired mean balancing current	$\bar{I}_{2,r} = 2A$
Terminal voltage of the most charged cell	$V_{B1} = 4.2V$
Terminal voltage of the least charged cell	$V_{B2} = 4V$
Switching frequency	50 kHz
Series resistance of the inductor	$R_L = 25m\Omega$
Drain-source on-state resistance for the switches	$R_{ds} = 2.6m\Omega$
Rise time	$t_{rise} = 42ns$
Fall time	$t_{fall} = 78ns$
Dead time	$\rho = 250ns$
Forward voltage of the internal body diode	$V_d = 0.4V$

ers for a fixed design of the cell equalizer in terms of inductor size, static and dynamic parameters of the circuit components. Therefore, the CFC does not allow for achieving a constant balancing current over different imbalance conditions. However, it allows for reaching the best performance achievable without modifying the switching frequency.

In order to quantitatively evaluate the performance of this control strategy, the mean balancing current is defined as metric. A case scenario for the design of the inductor-based cell equalizer has been considered. In detail, the design parameters of the experimental prototype developed have been taken into account and summarized in Table 5.6. Note that a maximum balancing current $\bar{I}_{2,r}$ of $2A$ is achievable with this prototype only when a maximum voltage imbalance of $200mV$ occurs among the cells.

Figures 5.11a and 5.11b respectively show the variation of the duty cycle to be imposed to the switches for allowing the equalization circuit to operate at LCCM ($D_{L,r}$) and the maximum balancing current $\bar{I}_{2,r}$ achievable with respect to the terminal voltages of the most and the least charged cells (V_{B1}, V_{B2}). For each voltage imbalance, the model equations in real conditions and the design parameters reported in Table 5.6 are considered for determining both $D_{L,r}$ and $\bar{I}_{2,r}$. The contour lines represent the collection of the operating points characterized by the same $D_{L,r}$ or $\bar{I}_{2,r}$, whereas the black straight lines highlight the operating points at zero voltage imbalance, thus resulting as a balancing target when the cell transients are extinguished (e.g. relaxation and voltage drop on the internal resistance). Note that, assuming $V_{B1} > V_{B2}$, all the operating conditions achievable during the balancing process are contained in the area below the balancing target. In particular, as shown in figures 5.11a and 5.11b, starting from the voltage imbalance highlighted with a red dot, the balancing target is reached by transferring the energy between the most charged cell and the least charged one, resulting the cells' terminal voltages following the direc-

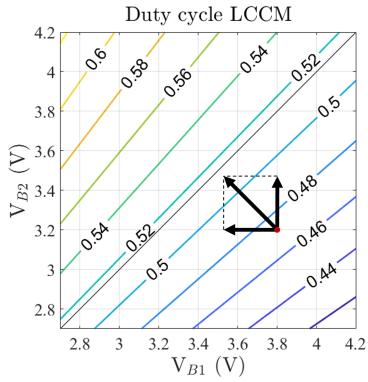

(a)

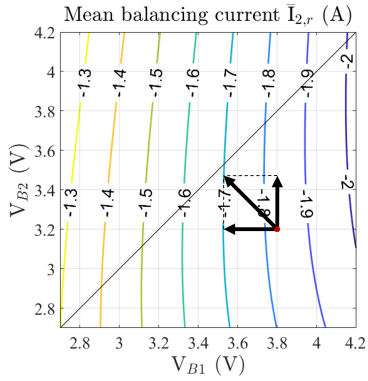

(b)

Figure 5.11: Contour lines of the duty cycle (a) and balancing current (b) under the cell voltage operating range of V_{B1} and V_{B2}, for constant-frequency control.

tions indicated by the arrows. Moreover, the contour lines show that $D_{L,r}$ strongly depends on the voltage imbalance, whereas the amplitude of $\bar{I}_{2,r}$ is mainly impacted by the voltage of the most charged cell V_{B1}. However, figure 5.11b also illustrates quantitatively the reduction of the amplitude of $\bar{I}_{2,r}$, highlighting the limitation of the CFC in terms of energy transfer and the need of additional control variables for achieving a constant balancing current regardless the specific imbalance condition, which would result in a lower equalization time.

5.3.6.2 Variable Frequency Control

With the aim of improving the performance of the inductor-based cell equalizers, a Variable-Frequency Control (VFC) strategy has been pro-

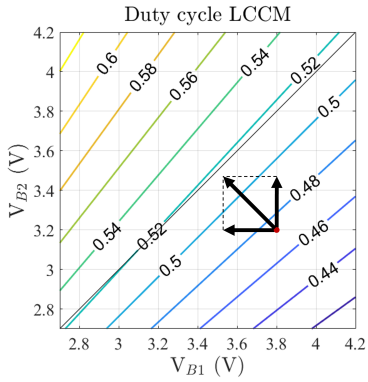

(a)

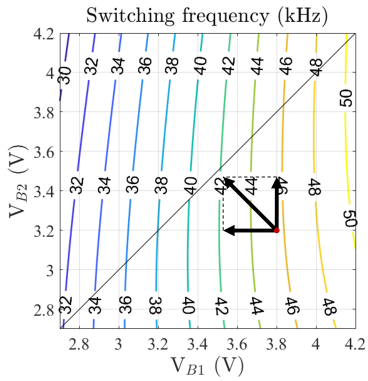

(b)

Figure 5.12: (a) Contour lines of the duty cycle and (b) balancing current under the cell voltage operating range of V_{B1} and V_{B2}, for variable-frequency control when $\bar{I}_{2,r} = 2A$.

posed, which includes the possibility to adjust the switching frequency. In this way, two control variables (duty cycle and switching frequency) are managed over time depending on the different imbalance conditions. In detail, according to the model equations in real conditions, the following steps are continuously operated by the VFC:

1. the duty cycle is adjusted in order to ensure the LCCM operations for the equalization circuit;

2. the switching frequency is adjusted in order to ensure the desired mean balancing current $\bar{I}_{2,r}$.

Figures 5.12a and 5.12b illustrate the contour lines representing the im-

pact of the terminal voltages of the most/least charged cells on both the duty cycle and the switching frequency to be imposed to the switches for allowing the equalization circuit to operate at LCCM ($D_{L,r}$) with the maximum mean balancing current $\bar{I}_{2,r} = 2A$. The same components' parameters reported in Table 5.6 have been adopted for evaluating the performance of the VFC. As possible to notice in Figs. 5.12(a) and 5.12(b), an increasing switching frequency is required for achieving a constant maximum mean balancing current $\bar{I}_{2,r}$ as the terminal voltage of the most charged cell increases.

5.3.7 Performance analysis

Numerical analyses have been conducted to study the performance of the proposed control strategies, CFC and VFC, under different initial imbalance conditions defined by the initial state of charge of the most charged cell (SoC_{B1}) and the initial voltage imbalance (ΔV_0). In particular, 5 different SoC_{B1} $(10\%, 30\%, 50\%, 70\%, 90\%)$ and 4 different ΔV_0 $(50mV, 100mV, 150mV, 200mV)$ have been considered, for a total of 20 different combinations.

The end balancing condition specifies when the balancing procedure should be terminated because the cells are balanced. Two different approaches can be used to determine the end balancing condition [69]:

1. *Voltage*: the balancing process is ended when the voltage imbalance among the cells becomes lower than a designed threshold;
2. *State of Charge (SoC)*: the balancing process is terminated when the difference between the SoCs of the most charged cell and the least charged one becomes lower than a designed threshold.

Voltage-based end-balancing condition is often adopted due to the simplicity of implementation. However, with this method it is usually difficult to reach an accurate balancing condition because of the voltage drop across the internal resistance. Indeed, once the balancing action is stopped, the current becomes zero and the voltage imbalance is still present, often resulting higher than the desired threshold. On the other hand, the SoC-based end condition overcomes the drawback of the voltage-based and results more accurate. However, the calculation of the SoC is required, which is typically affected by the accuracy of this estimation. For the scope of this analysis and to properly compare the proposed control strategies, the SoC-based end-balancing condition has been implemented.

To account for real cell voltage behavior, the 3-Ah SONY VTC6 18650 cylindrical cell has been experimentally tested and the related zero-order

Table 5.7: Main characteristics of the SONY VTC6 cylindrical cell.

Parameter	Value
Chemistry	NMC
Nominal Capacity	3 Ah
Nominal Voltage	3.6 V
Cut-Off Voltage	2.5 V
Max. Charging Current	6 A (@2C)
Max. Discharging Current	30 A (@10C)
Temp. Range Charge	0 - 60°C
Temp. Range Discharge	-20 - 60°C
Internal resistance @1C, $SoC = 50\%$	24 mΩ

equivalent circuit model has been calibrated considering different operating conditions in terms of charging/discharging currents (C-rates). Higher order equivalent circuit models can be considered for this analysis. However, the results will not be impacted since the control of the balancing action is defined by the SoC evolution and not the voltage itself. The main characteristics of the 3-Ah SONY VTC6 are illustrated in Table 5.7.

A specific imbalance condition ($SoC_{B1} = 60\%$, $\Delta V_0 = 200mV$) has been reported as example to validate the functionalities of the cell equalizer and highlight the different behavior of the balancing process between CFC and VFC. In particular, figure 5.14 illustrates the evolution over time of the terminal voltages, the currents and the SoCs of the cells as well as the duty cycle and switching frequency during the balancing process for both constant-frequency and variable-frequency control strategies. Several aspects need to be highlighted:

- considering Figs. 5.13a and 5.13c, despite the terminal voltage of the least charged cell becomes higher than the voltage of the most charged one, the balancing process continues until the states of charge of both cells becomes equal.

- The VFC balancing process is faster than the CFC one because the mean balancing current is higher (figure 5.13b).

- Figures 5.13d and 5.13e show the behavior of the two different control strategies, therefore respectively the variations of the duty cycle needed for ensuring LCCM and the adjustments of the switching frequency in the VFC required for achieving a constant balancing current for the least charged cell.

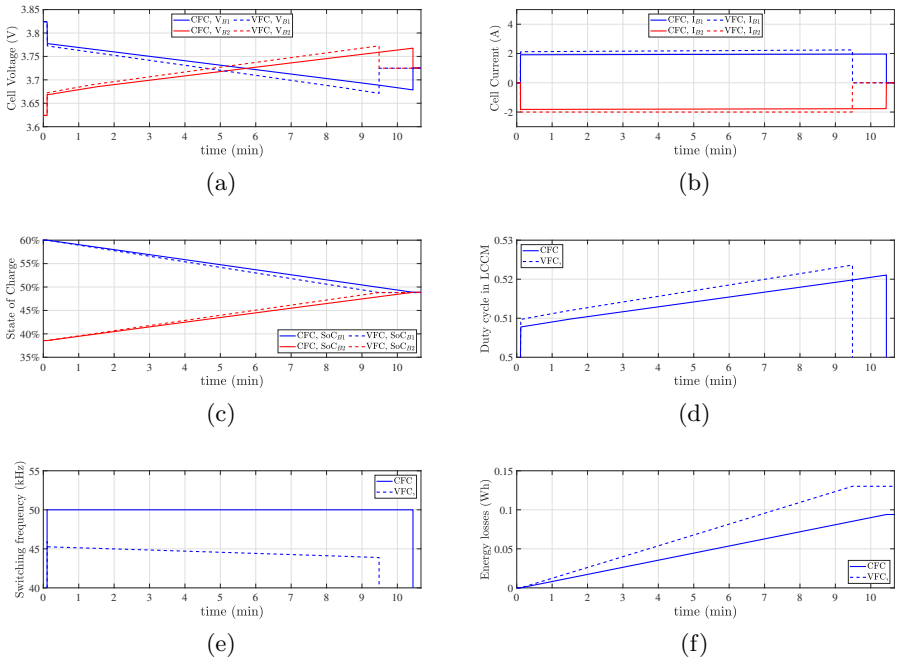

Figure 5.13: Balancing process with $SoC_{B1} = 60\%$ and $\Delta V_0 = 200mV$ as initial imbalance condition. The plots show the different behavior between the two control strategies (CFC in straight line and VFC in dashed line): (a) cell voltages, (b) cell currents, (c) cell SoCs, (d) duty cycle for LCCM, (e) switching frequency and (f) total energy losses.

Moreover, two performance parameters have been considered to better compare the behavior of the balancing process with respect to the control strategy adopted under different initial imbalance conditions: energy efficiency and equalization time.

Since the efficiency of the equalization process cannot be uniquely defined for each imbalance condition in terms of power, the energy efficiency is defined as an indicator of the amount of energy exchanged among the cells and the related losses.

In detail, assuming cell 1 and cell 2 to be respectively the most and the least charged cells, this factor is defined as the ratio between the absolute value of energy charged to cell 2 (E_{B2}), purged of the energies lost to switching (E_{sw}), and the energy discharged from cell 1 (E_{B1}):

$$\eta = \frac{E_{out}}{E_{in}} = \frac{|E_{B2}| - E_{sw}}{E_{B1}} \tag{5.32}$$

Numerical results of the energy efficiency for the balancing process with respect to the initial imbalance conditions (SoC_{B1}, ΔV_0) are reported in Figs. 5.14a and 5.14b for CFC and VFC, respectively. It is possible to observe that the energy efficiency of CFC is around 90% for a wide range of operating conditions. At low initial SoC (SoC_{B1}<30%) and ΔV_0>50mV, the energy efficiency varies in a wide range from 75% to 90%. VFC performs well at low initial SoC conditions having efficiency higher than 88%. However, under the other operating conditions, the energy efficiency in CFC is slightly higher than that in VFC, as illustrated in Table 5.8. In this case, the energy efficiency increases from about 88.5% (for 10%≤ SoC_{B1}<90%) to around 90% (SoC_{B1}=90%), however the effect of voltage imbalance is minimal.

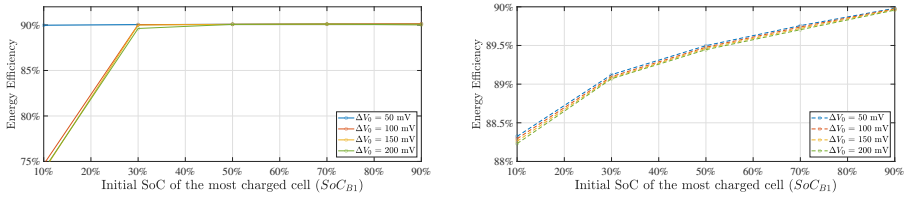

(a) (b)

Figure 5.14: Numerical results for energy efficiency in both (a) constant-frequency and (b) variable-frequency controls.

Table 5.8: Energy efficiency for CVC and VFC for different initial states of charge of the most charged cell (SoC_{B1}) and initial voltage imbalances (ΔV_0).

ΔV_0	SoC_{B1}									
	10%		30%		50%		70%		90%	
	CFC	VFC	CFC	VFC	CFC	VFC	CFC	VFC	CFC	VFC
50mV	89.97	88.32	90.04	89.12	90.08	89.50	90.11	89.76	90.13	89.98
100mV	74.68	88.29	90.04	89.10	90.08	89.48	90.10	89.74	90.13	89.97
150mV	73.98	88.26	90.00	89.08	90.07	89.46	90.10	89.72	90.10	89.97
200mV	74.11	88.23	89.62	89.07	90.07	89.44	90.10	89.70	90.02	89.96

The evaluation of the time interval needed for equalizing the SoCs of the cells starting from a specific initial imbalance condition (SoC_{B1}, ΔV_0) is reported in Fig 5.15a for both CFC and VFC strategies. The same color represents the same initial conditions in terms of voltage imbalance,

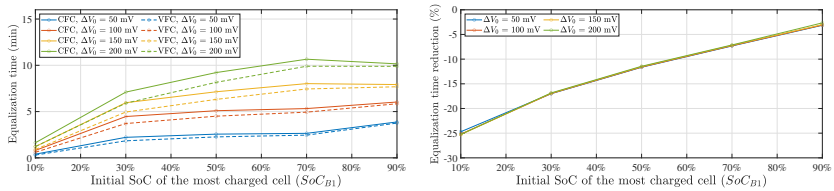

(a) (b)

Figure 5.15: Numerical results for equalization time in both constant-frequency and variable-frequency controls (a) and time reduction in VFC with respect to the CFC (b) .

Table 5.9: Equalization time for CVC and VFC for different initial states of charge of the most charged cell (SoC_{B1}) and initial voltage imbalance (ΔV_0).

ΔV_0	SoC_{B1}									
	10%		30%		50%		70%		90%	
	CFC	VFC	CFC	VFC	CFC	VFC	CFC	VFC	CFC	VFC
50mV	0.40	0.30	2.22	1.84	2.56	2.26	2.65	2.45	3.88	3.76
100mV	0.80	0.60	4.46	3.71	5.09	4.50	5.32	4.94	6.03	5.85
150mV	1.21	0.91	5.96	4.95	7.14	6.32	8.02	7.44	7.92	7.68
200mV	1.63	1.22	7.10	5.91	9.22	8.16	10.66	9.90	10.16	9.89

whereas straight and dashed lines represent the results achieved by performing CVC and VFC, respectively. The equalization time with VFC is always shorter than the one achieved with CFC, and the lower the initial SoC of the most charged cell, the greater the difference between the equalization times of CFC and VFC, due to the difference in balancing current. Moreover, the equalization time is lower when the cells are close to the minimum SoC in all voltage imbalance conditions investigated, highlighting the possibility to perform the equalization process in specific operating conditions that minimize the time required by the balancing process. However, this phenomenon strictly depends on the internal characteristics of the considered cell. According to the results shown in figure 5.15a and depicted in Table 5.9, the maximum equalization time registered is equal to 10.66 minutes with CFC and 9.9 minutes with VFC for the balancing process started with $SoC_{B1} = 70\%$ and $\Delta V_0 = 200mV$, however the minimum equalization time results equal to 0.4 minutes with CFC and 0.3 minutes with VFC for the balancing process started with $SoC_{B1} = 10\%$ and ΔV_0

$= 50mV$. It is also straightforward to notice in figure that VFC allows for reducing the equalization time in every imbalance condition, and this difference is much higher when the balancing process is performed at low SoC levels.

Conclusions

In this dissertation, two relevant aspects in battery management system design are addressed. Regarding the task of SoP estimation, this research activity was carried out in order to identify a methodology to compare and validate the algorithms currently proposed in the literature or adopted commercially. Numerical simulations and experimental tests were performed to compare the classical map-based estimation methods with one of the model-based methods. The results showed a substantial difference in the predicted value, which was related to the fact that the map-based methods do not take into account the current internal dynamics of the cell, since the offline power estimation is derived from an impulsive experimental test in which the starting condition for estimation is always a prolonged resting condition. Another factor that has a strong influence on battery power capacity is the temperature evolution over time. Temperature rise cannot be a phenomenon to be neglected in the estimation of power limits, since it is necessary to consider that the battery is allowed to experience a current of extreme value continuously for a time specified by the requirements of the individual application. The possible sudden increase in temperature offers causes an increase in the dischargeable capacity over time, so the maximum power estimate is inaccurate, but still conservative.

On the other hand, the research activity presented by this thesis is focused on the optimization of active balancing systems. From a thorough literature review, it has been observed that the proposed architectures for balancing cells in battery packs are not designed considering the different unbalancing operating conditions nor the actual parameters of the components used. Therefore, the original contribution of the research activity presented in this thesis is the derivation of analytical models for the purpose of developing a design methodology for active balancing circuits. Two architectures were analyzed that differ in both the method of energy transmission between cells and the component means of transfer.

The first architecture uses a multi-winding transformer in which each cell is connected to a single winding through an H-bridge. This architecture

is also referred to as multiple-active bridge (MAB) because it refers to the same isolated converter architecture realized by only two ports.

The large number of components used, augmented by the electronic circuitry that provides isolation between the different windings is certainly the biggest disadvantage. However, this type of architecture allows cell-to-cell energy transfer through simple, open-loop control. Analytical demonstration proves that this occurs because the average current of each cell is directly proportional to the difference between the voltage of the individual cell and the average voltage between cells. Actually, there is no direct proportionality because a correction factor appears in the averaging current formula that takes into account the parasitic parameters of the components. Given this, the system is self-balancing in that cells that are more charged than the average are discharged and vice versa, the voltages converge to the average and the currents tend to cancel. In order to develop the design methodology for the MAB architecture, the condition in which a cell experiences the maximum allowable current has been analytically derived. The methodology was then validated through the creation of an experimental prototype, confirming the effectiveness of the methodological approach. Furthermore, the performance provided by this prototype was assessed under various imbalance conditions. Moreover, the original contribution of this work rely on the HIL approach to emulate the batteries. The experimental results have shown that the energy efficiency of this method results very high, especially considering large imbalance conditions, while the self-balancing energy transfer results slow.

The same systematic approach have been used in the second active balancing architecture that allows the energy transfer by means an inductor. This architecture realize the adjacent-cell-to cell balancing and need a feedback control loop to achieve the best performances in balancing process. The analytical model have been developed for design purposes. In this case, some consideration have been proposed about the duty cycle and the control strategy, which impact on the calculation of the mean balancing current and the inductor design. As for the MAB architecture, the proposed design methodology has been validated through several experimental tests.

Moreover, in his case, an optimized control mode has been proposed and validated numerically. The research activity reported in this dissertation offer the possibility of future improvement such as:

- The MAB architecture can be suitable for performing equalization process at module level, instead of the cell level, because the voltage between modules become higher and less winding are needed for the integration within a large battery pack.

- Comparison analysis between different active balancing circuits over different imbalance conditions.
- Performance enhancement of hybrid battery packs by using active balancing systems.

List of Figures

List of Tables

Bibliography

[1] T. Chen, Y. Jin, H. Lv, A. Yang, M. Liu, B. Chen, Y. Xie, and Q. Chen, "Applications of lithium-ion batteries in grid-scale energy storage systems," *Transactions of Tianjin University*, vol. 26, no. 3, pp. 208–217, 2020.

[2] K. Xu, "Nonaqueous liquid electrolytes for lithium-based rechargeable batteries," *Chemical reviews*, vol. 104, no. 10, pp. 4303–4418, 2004.

[3] N. Nitta, F. Wu, J. T. Lee, and G. Yushin, "Li-ion battery materials: present and future," *Materials Today*, vol. 18, no. 5, pp. 252–264, 2015. [Online]. Available: https://www.sciencedirect.com/science/article/pii/S1369702114004118

[4] K. Mizushima, P. Jones, P. Wiseman, and J. Goodenough, "Lixcoo2 (0¡x¡-1): A new cathode material for batteries of high energy density," *Materials Research Bulletin*, vol. 15, no. 6, pp. 783–789, 1980.

[5] K. Pan, F. Zou, M. Canova, Y. Zhu, and J.-H. Kim, "Systematic electrochemical characterizations of si and sio anodes for high-capacity li-ion batteries," *Journal of Power Sources*, vol. 413, pp. 20–28, 2019. [Online]. Available: https://www.sciencedirect.com/science/article/pii/S0378775318313612

[6] C. Linse and R. Kuhn, "10 - design of high-voltage battery packs for electric vehicles," in *Advances in Battery Technologies for Electric Vehicles*, ser. Woodhead Publishing Series in Energy, B. Scrosati, J. Garche, and W. Tillmetz, Eds. Woodhead Publishing, 2015, pp. 245–263.

[7] A. Pesaran, M. Keyser, G. H. Kim, S. Santhanagopalan, and K. Smith, "Tools for designing thermal management of batteries in electric drive vehicles (presentation)," 2 2013. [Online]. Available: https://www.osti.gov/biblio/1064502

[8] Q. Wang, B. Jiang, B. Li, and Y. Yan, "A critical review of thermal management models and solutions of lithium-ion batteries for the development of pure electric vehicles," *Renewable & Sustainable Energy Reviews*, vol. 64, pp. 106–128, 2016. [Online]. Available: https://api.semanticscholar.org/CorpusID:56270954

[9] G. Plett, *Battery Management Systems, Volume I: Battery Modeling.* Artech, 2015.

[10] M. Doyle, T. F. Fuller, and J. Newman, "Modeling of galvanostatic charge and discharge of the lithium/polymer/insertion cell," *Journal of The Electrochemical Society*, vol. 140, no. 6, p. 1526, jun 1993. [Online]. Available: https://dx.doi.org/10.1149/1.2221597

[11] J. Marcicki, M. Canova, A. T. Conlisk, and G. Rizzoni, "Design and parametrization analysis of a reduced-order electrochemical model of graphite/lifepo4 cells for soc/soh estimation," *Journal of Power Sources*, vol. 237, pp. 310–324, 2013.

[12] C. R. Birkl, M. R. Roberts, E. McTurk, P. G. Bruce, and D. A. Howey, "Degradation diagnostics for lithium ion cells," *Journal of Power Sources*, vol. 341, pp. 373–386, 2017.

[13] G. Zubi, R. Dufo-Lòpez, M. Carvalho, and G. Pasaoglu, "The lithium-ion battery: State of the art and future perspectives," *Renewable and Sustainable Energy Reviews*, vol. 89, pp. 292–308, 2018. [Online]. Available: https://www.sciencedirect.com/science/article/pii/S1364032118300728

[14] L. Lu, X. Han, J. Li, J. Hua, and M. Ouyang, "A review on the key issues for lithium-ion battery management in electric vehicles," *Journal of Power Sources*, vol. 226, pp. 272–288, 2013.

[15] M. Lelie, T. Braun, M. Knips, H. Nordmann, F. Ringbeck, H. Zappen, and D. U. Sauer, "Battery management system hardware concepts: An overview," *Applied Sciences*, vol. 8, no. 4, 2018. [Online]. Available: https://www.mdpi.com/2076-3417/8/4/534

[16] G. Plett, *Battery Management Systems, Volume II: Equivalent-Circuit Methods.* Artech, 2015.

[17] L. Jiang, Y. Li, Y. Huang, J. Yu, X. Qiao, Y. Wang, C. Huang, and Y. Cao, "Optimization of multi-stage constant current charging pattern based on taguchi method for li-ion battery," *Applied*

Energy, vol. 259, p. 114148, 2020. [Online]. Available: https://www.sciencedirect.com/science/article/pii/S0306261919318355

[18] P. Keil and A. Jossen, "Charging protocols for lithium-ion batteries and their impact on cycle life-an experimental study with different 18650 high-power cells," *Journal of Energy Storage*, vol. 6, pp. 125–141, 2016. [Online]. Available: https://www.sciencedirect.com/science/article/pii/S2352152X16300147

[19] Y. Gao, X. Zhang, Q. Cheng, B. Guo, and J. Yang, "Classification and review of the charging strategies for commercial lithium-ion batteries," *IEEE Access*, vol. 7, pp. 43 511–43 524, 2019.

[20] R. Klein, N. A. Chaturvedi, J. Christensen, J. Ahmed, R. Findeisen, and A. Kojic, "Optimal charging strategies in lithium-ion battery," in *Proceedings of the 2011 American Control Conference*, 2011, pp. 382–387.

[21] M. Mastali, J. Vazquez-Arenas, R. Fraser, M. Fowler, S. Afshar, and M. Stevens, "Battery state of the charge estimation using kalman filtering," *Journal of Power Sources*, vol. 239, pp. 294–307, 2013. [Online]. Available: https://www.sciencedirect.com/science/article/pii/S0378775313005259

[22] Z. Yu, R. Huai, and L. Xiao, "State-of-charge estimation for lithium-ion batteries using a kalman filter based on local linearization," *Energies*, vol. 8, no. 8, pp. 7854–7873, 2015. [Online]. Available: https://www.mdpi.com/1996-1073/8/8/7854

[23] P. Weicker, *A systems approach to lithium-ion battery management.* Artech house, 2013.

[24] D. Luenberger, "An introduction to observers," *IEEE Transactions on Automatic Control*, vol. 16, no. 6, pp. 596–602, 1971.

[25] X. Hu, F. Sun, and Y. Zou, "Estimation of state of charge of a lithium-ion battery pack for electric vehicles using an adaptive luenberger observer," *Energies*, vol. 3, no. 9, pp. 1586–1603, 2010. [Online]. Available: https://www.mdpi.com/1996-1073/3/9/1586

[26] B. Wang, Z. Liu, S. E. Li, S. J. Moura, and H. Peng, "State-of-charge estimation for lithium-ion batteries based on a nonlinear fractional model," *IEEE Transactions on Control Systems Technology*, vol. 25, no. 1, pp. 3–11, 2017.

[27] D. Kim, K. Koo, J. J. Jeong, T. Goh, and S. W. Kim, "Second-order discrete-time sliding mode observer for state of charge determination based on a dynamic resistance li-ion battery model," *Energies*, vol. 6, no. 10, pp. 5538–5551, 2013. [Online]. Available: https://www.mdpi.com/1996-1073/6/10/5538

[28] X. Chen, W. Shen, Z. Cao, and A. Kapoor, "Adaptive gain sliding mode observer for state of charge estimation based on combined battery equivalent circuit model," *Computers & Chemical Engineering*, vol. 64, pp. 114–123, 2014. [Online]. Available: https://www.sciencedirect.com/science/article/pii/S0098135414000477

[29] ——, "A novel approach for state of charge estimation based on adaptive switching gain sliding mode observer in electric vehicles," *Journal of Power Sources*, vol. 246, pp. 667–678, 2014. [Online]. Available: https://www.sciencedirect.com/science/article/pii/S0378775313013797

[30] D. Kim, T. Goh, M. Park, and S. W. Kim, "Fuzzy sliding mode observer with grey prediction for the estimation of the state-of-charge of a lithium-ion battery," *Energies*, vol. 8, no. 11, pp. 12 409–12 428, 2015. [Online]. Available: https://www.mdpi.com/1996-1073/8/11/12327

[31] X. Chen, W. Shen, M. Dai, Z. Cao, J. Jin, and A. Kapoor, "Robust adaptive sliding-mode observer using rbf neural network for lithium-ion battery state of charge estimation in electric vehicles," *IEEE Transactions on Vehicular Technology*, vol. 65, no. 4, pp. 1936–1947, 2015.

[32] X. Tang, Y. Wang, and Z. Chen, "A method for state-of-charge estimation of lifepo4 batteries based on a dual-circuit state observer," *Journal of Power Sources*, vol. 296, pp. 23–29, 2015. [Online]. Available: https://www.sciencedirect.com/science/article/pii/S0378775315300756

[33] J. Xie, J. Ma, Y. Sun, and Z. Li, "Estimating the state-of-charge of lithium-ion batteries using an h-infinity observer with consideration of the hysteresis characteristic," *Journal of Power Electronics*, vol. 16, no. 2, pp. 643–653, 2016.

[34] S. Tong, J. H. Lacap, and J. W. Park, "Battery state of charge estimation using a load-classifying neural network," *Journal of Energy Storage*, vol. 7, pp. 236–243, 2016. [Online]. Available: https://www.sciencedirect.com/science/article/pii/S2352152X16300949

[35] S. Hosseininasab, Z. Wan, T. Bender, G. Vagnoni, and L. Bauer, "State-of-charge estimation of lithium-ion battery based on a combined method of neural network and unscented kalman filter," in *2020 IEEE Vehicle Power and Propulsion Conference (VPPC)*, 2020, pp. 1–7.

[36] J. Tian, R. Xiong, W. Shen, and J. Lu, "State-of-charge estimation of lifepo4 batteries in electric vehicles: A deep-learning enabled approach," *Applied Energy*, vol. 291, p. 116812, 2021. [Online]. Available: https://www.sciencedirect.com/science/article/pii/S0306261921003147

[37] H. Zhang, W. Na, and J. Kim, "State-of-charge estimation of the lithium-ion battery using neural network based on an improved thevenin circuit model," in *2018 IEEE Transportation Electrification Conference and Expo (ITEC)*, 2018, pp. 342–346.

[38] G. Nuroldayeva, Y. Serik, D. Adair, B. Uzakbaiuly, Z. Bakenov *et al.*, "State of health estimation methods for lithium-ion batteries," *International Journal of Energy Research*, vol. 2023, 2023.

[39] Z. Wang, G. Feng, D. Zhen, F. Gu, and A. Ball, "A review on online state of charge and state of health estimation for lithium-ion batteries in electric vehicles," *Energy Reports*, vol. 7, pp. 5141–5161, 2021. [Online]. Available: https://www.sciencedirect.com/science/article/pii/S2352484721007150

[40] E. Karden, *Using low frequency impedance spectroscopy for characterization, monitoring, and modeling of industrial batteries.* Shaker, 2002.

[41] U. Westerhoff, T. Kroker, K. Kurbach, and M. Kurrat, "Electrochemical impedance spectroscopy based estimation of the state of charge of lithium-ion batteries," *Journal of Energy Storage*, vol. 8, pp. 244–256, 2016.

[42] Y. Li, M. Abdel-Monem, R. Gopalakrishnan, M. Berecibar, E. Nanini-Maury, N. Omar, P. van den Bossche, and J. Van Mierlo, "A quick on-line state of health estimation method for li-ion battery with incremental capacity curves processed by gaussian filter," *Journal of Power Sources*, vol. 373, pp. 40–53, 2018. [Online]. Available: https://www.sciencedirect.com/science/article/pii/S0378775317314532

[43] X. Li, Z. Wang, L. Zhang, C. Zou, and D. D. Dorrell, "State-of-health estimation for li-ion batteries by combing the incremental capacity

analysis method with grey relational analysis," *Journal of Power Sources*, vol. 410-411, pp. 106–114, 2019. [Online]. Available: https://www.sciencedirect.com/science/article/pii/S0378775318311777

[44] L. Song, K. Zhang, T. Liang, X. Han, and Y. Zhang, "Intelligent state of health estimation for lithium-ion battery pack based on big data analysis," *Journal of Energy Storage*, vol. 32, p. 101836, 2020.

[45] USABC, "Battery test manual for electric vehicles," 2020.

[46] M. D'Arpino, N. Regmi, and P. Ketineni, "Impact of battery pack power limits on vehicle performance," in *2023 IEEE Transportation Electrification Conference & Expo (ITEC)*, 2023, pp. 1–8.

[47] P. Malysz, J. Ye, R. Gu, H. Yang, and A. Emadi, "Battery state-of-power peak current calculation and verification using an asymmetric parameter equivalent circuit model," *IEEE Transactions on Vehicular Technology*, vol. 65, no. 6, pp. 4512–4522, 2016.

[48] R. D. Anderson, Y. Zhao, X. Wang, X. G. Yang, and Y. Li, "Real time battery power capability estimation," in *2012 American Control Conference (ACC)*, 2012, pp. 592–597.

[49] L. H. Saw, Y. Ye, and A. A. O. Tay, "Integration issues of lithium-ion battery into electric vehicles battery pack," *Journal of Cleaner Production*, vol. 113, pp. 1032–1045, 2016. [Online]. Available: https://api.semanticscholar.org/CorpusID:111346916

[50] U. Abronzini, C. Attaianese, M. D. Monaco, F. Porpora, G. Tomasso, M. Granato, and G. Frattini, "Optimal modular bms for high performances nmc battery pack," in *2018 IEEE International Conference on Electrical Systems for Aircraft, Railway, Ship Propulsion and Road Vehicles & International Transportation Electrification Conference (ESARS-ITEC)*, 2018, pp. 1–6.

[51] F. Porpora, U. Abronzini, C. Attaianese, M. Di Monaco, and G. Tomasso, "Real time balancing for modular passive battery management system," in *PCIM Europe 2019; International Exhibition and Conference for Power Electronics, Intelligent Motion, Renewable Energy and Energy Management*, 2019, pp. 1–6.

[52] U. Abronzini, M. Di Monaco, F. Porpora, G. Tomasso, M. D'Arpino, and C. Attaianese, "Thermal management optimization of a passive bms for automotive applications," in *2019 AEIT International Conference of Electrical and Electronic Technologies for Automotive (AEIT AUTOMOTIVE)*, 2019, pp. 1–6.

[53] M. D. Monaco, F. Porpora, G. Tomasso, M. D'Arpino, and C. Attaianese, "Design methodology for passive balancing circuit including real battery operating conditions," in *2020 IEEE Transportation Electrification Conference & Expo (ITEC)*, 2020, pp. 467–471.

[54] M. Caspar, T. Eiler, and S. Hohmann, "Systematic comparison of active balancing: A model-based quantitative analysis," *IEEE Transactions on Vehicular Technology*, vol. 67, no. 2, pp. 920–934, 2018.

[55] M. Daowd, N. Omar, P. Van Den Bossche, and J. Van Mierlo, "Passive and active battery balancing comparison based on matlab simulation," in *2011 IEEE Vehicle Power and Propulsion Conference*, 2011, pp. 1–7.

[56] M. Hoque, M. Hannan, A. Mohamed, and A. Ayob, "Battery charge equalization controller in electric vehicle applications: A review," *Renewable and Sustainable Energy Reviews*, vol. 75, pp. 1363–1385, 2017. [Online]. Available: https://www.sciencedirect.com/science/article/pii/S1364032116308681

[57] J. Gallardo-Lozano, E. Romero-Cadaval, M. I. Milanes-Montero, and M. A. Guerrero-Martinez, "Battery equalization active methods," *Journal of Power Sources*, vol. 246, pp. 934–949, 2014.

[58] F. Porpora, M. D. Monaco, G. Tomasso, and M. D'Arpino, "Model-based design methodology for capacitor-based equalization circuits," in *2021 IEEE Energy Conversion Congress and Exposition (ECCE)*, 2021, pp. 1482–1489.

[59] Y. Shang, C. Zhang, N. Cui, and C. C. Mi, "A delta-structured switched-capacitor equalizer for series-connected battery strings," *IEEE Transactions on Power Electronics*, vol. 34, no. 1, pp. 452–461, 2019.

[60] A. Farzan Moghaddam and A. Van den Bossche, "An efficient equalizing method for lithium-ion batteries based on coupled inductor balancing," *Electronics*, vol. 8, no. 2, 2019. [Online]. Available: https://www.mdpi.com/2079-9292/8/2/136

[61] S.-H. Park, K.-B. Park, H.-S. Kim, G.-W. Moon, and M.-J. Youn, "Single-magnetic cell-to-cell charge equalization converter with reduced number of transformer windings," *IEEE Transactions on Power Electronics*, vol. 27, no. 6, pp. 2900–2911, 2012.

[62] S. Li, C. C. Mi, and M. Zhang, "A high-efficiency active battery-balancing circuit using multiwinding transformer," *IEEE Transactions on Industry Applications*, vol. 49, no. 1, pp. 198–207, 2013.

[63] U. Abronzini, M. D. Monaco, F. Porpora, G. Tomasso, M. D'Arpino, and C. Attaianese, "High performance active battery management system with multi-winding transformer," in *2019 IEEE Energy Conversion Congress and Exposition (ECCE)*, 2019, pp. 1231–1236.

[64] L. F. Costa, F. Hoffmann, G. Buticchi, and M. Liserre, "Comparative analysis of multiple active bridge converters configurations in modular smart transformer," *IEEE Transactions on Industrial Electronics*, vol. 66, no. 1, pp. 191–202, 2019.

[65] S. Yarlagadda, T. T. Hartley, and I. Husain, "A battery management system using an active charge equalization technique based on a dc/dc converter topology," *IEEE Transactions on Industry Applications*, vol. 49, no. 6, pp. 2720–2729, 2013.

[66] A. Farzan Moghaddam and A. Van den Bossche, "An efficient equalizing method for lithium-ion batteries based on coupled inductor balancing," *Electronics*, vol. 8, no. 2, 2019.

[67] U. Abronzini, C. Attaianese, M. D'Arpino, M. Di Monaco, and G. Tomasso, "Steady-state dead-time compensation in vsi," *IEEE Transactions on Industrial Electronics*, vol. 63, no. 9, pp. 5858–5866, 2016.

[68] S. Bolognani, M. Ceschia, P. Mattavelli, A. Paccagnella, and M. Zigliotto, "Improved fpga-based dead time compensation for svm inverters," in *Second International Conference on Power Electronics, Machines and Drives (PEMD 2004).*, vol. 2, 2004, pp. 662–667 Vol.2.

[69] M. Caspar, T. Eiler, and S. Hohmann, "Systematic comparison of active balancing: A model-based quantitative analysis," *IEEE Transactions on Vehicular Technology*, vol. 67, no. 2, pp. 920–934, 2018.